8-4-2001

Evaluating Data Averaging Techniques for High Gradient Flow Fields through Uncertainty Analysis

Boon Liang Heng

EVALUATING DATA AVERAGING TECHNIQUES FOR HIGH GRADIENT FLOW FIELDS THROUGH UNCERTAINTY ANALYSIS

By

Boon Liang Heng

A Thesis
Submitted to the Faculty of
Mississippi State University
in Partial Fulfillment of the Requirements
for the Degree of Master of Science
in Mechanical Engineering
in the Department of Mechanical Engineering

Mississippi State, Mississippi

August 2001

EVALUATING DATA AVERAGING TECHNIQUES FOR HIGH GRADIENT FLOW FIELDS THROUGH UNCERTAINTY ANALYSIS

By

Boon Liang Heng

Approved:

Susan T. Hudson Assistant Professor of Mechanical Engineering (Director of Thesis)	Rogelio Luck Graduate Coordinator Department of Mechanical Engineering
B. K. Hodge Professor of Mechanical Engineering (Committee Member)	W. Glenn Steele Professor of Mechanical Engineering (Committee Member)
A. Wayne Bennett Dean of the College of Engineering	

Name: Boon Liang Heng

Date of Degree: August 4, 2001

Institution: Mississippi State University

Major Field: Mechanical Engineering

Major Professor: Dr. Susan T. Hudson

Title of Study: EVALUATING DATA AVERAGING TECHNIQUES FOR HIGH GRADIENT FLOW FIELDS THROUGH UNCERTAINTY ANALYSIS

Pages in Study: 153

Candidate for Degree of Master of Science

Experimental data from two cold airflow turbine tests were evaluated. The two tests had different, relatively high gradient flow fields at the turbine exit. The objective of the research was to evaluate data requirements, including the averaging techniques, the number of measurements, and the types of measurements needed, for high gradient flow fields. Guidelines could then be established for future tests that could allow reduction in test time and costs. An enormous amount of data was collected for both tests. These test data were then manipulated in various ways to study the effects of the averaging techniques, the number of measurements, and the types of measurements on the turbine efficiency. The effects were evaluated relative to maintaining a specific accuracy (1%) for the turbine efficiency. Mass and area averaging were applied to each case. A detailed uncertainty analysis of each case was done to evaluate the uncertainty of the efficiency calculations. A new uncertainty analysis technique was developed to include conceptual

bias estimates for the spatially averaged values required in the efficiency equations. Conceptual bias estimates were made for each test case, and these estimates can be used as guidelines for similar turbine tests in the future. The evaluations proved that mass averaging and taking measurements around the full 360° was crucial for obtaining accurate efficiency calculations in high gradient flow fields. In addition, circumferential averaging of wall-static pressure measurements could be used rather than measuring static pressures across the annulus of the high gradient flow field while still maintaining highly accurate efficiency calculations. These are an important finding in that considerable time and cost savings may be realized due to the decreased test time, probe measurements, and calibration requirements.

ACKNOWLEDGEMENTS

The completed research work and thesis was successful thanks to the guidance and advise from my major professor, Dr. Susan T. Hudson. I would like to thank Dr. Hudson for giving me the opportunity to excel in research work and for supporting me throughout the graduate program. In addition, I would like to add that Dr. Hudson is a great teacher, a generous person, and a good mentor. Also, I would like to thank the faculty and staff members of the Department of Mechanical Engineering for providing me the motivation and education to complete my graduate level work. I would like to give special thanks to Dr. B. K. Hodge for teaching me to think like an engineer. In addition, I deeply appreciate the help provided by Dr. Glenn W. Steele.

Finally, I would like to thank my parents for allowing me to pursue my higher education at Mississippi State University. Even though I have been away from them for more than 3 years, their guidance and love were never forgotten.

TABLE OF CONTENTS

CHAPTER Page

LIST OF TABLES

TABLE Page

TABLE Page

TABLE Page

LIST OF FIGURES

FIGURE Page

FIGURE Page

FIGURE Page

LIST OF SYMBOLS

Symbol	Definition
A	Area
B	Bias limit estimate
B_{XY}	Bias covariance estimate
C_p	Specific heat at constant pressure
h	Enthalpy
J	Conversion constant (778.3 ft-lb_f /BTU)
K	Conversion constant (p / 30 rad*min/rev*sec)
M	Mach number
N	Speed
P	Precision limit estimate
P	Static pressure
P_0	Total pressure
P_{01}	Turbine inlet total pressure
P_{02}	Turbine exit total pressure
P_{01C}	Turbine inlet total pressure dummy value
P_{02C}	Turbine exit total pressure dummy value
Pr	Pressure ratio

r	Result
R	Specific gas constant
S	Sample standard deviation
T_0	Total temperature or reference temperature
T_{01}	Turbine inlet total temperature
T_{02}	Turbine exit total temperature
T_{01C}	Turbine inlet total temperature dummy value
T_{02C}	Turbine exit total temperature dummy value
Tq	Torque
U	Uncertainty estimate
W	Weighting factor
$\dot{W}$	Mass flow rate
X	Measured variable
z	Compressibility factor
a_2	Turbine exit flow or yaw angle
g	Ratio of specific heat
m	Viscosity
h_{me}	Mechanical method turbine efficiency
h_{th}	Thermodynamic method turbine efficiency

CHAPTER I

INTRODUCTION

Experimental data from two cold airflow turbine tests were evaluated. The first turbine test setup was a technology turbine with a square exit volute. The second test setup was the same technology turbine with a circular exit volute. These two different exit volutes created different and relatively high gradient flow fields at the exit of the turbine. The objective of the research was to evaluate data requirements, including the averaging techniques, the number of measurements, and the types of measurements needed, for high gradients flow fields. This study could then establish guidelines for future turbine test requirements. These guidelines could reduce test time and analysis time, thereby saving money while meeting the test goals. Uncertainty analysis techniques developed to evaluate the data also allow a better understanding of the measurements and analysis techniques required to meet the test goals.

1.1 Background

Understanding the turbine flow field is an important aspect in characterizing the aerodynamic performance of the machine. The turbine flow field can be visualized by proper experimental measurements. Therefore, component testing is useful for new

turbine designs that incorporate new technology. Component testing is often done under scaled conditions, which allows a broader test envelope [1].

The research work discussed in this thesis involves experimental data obtained from the Oxidizer Technology Turbine Rig (OTTR) [2]. The OTTR was designed to support the development of advanced turbines for future liquid rocket engines. The results from the experimental work were used to validate Computational Fluid Dynamics (CFD) codes used for design and performance prediction. Therefore, the accuracy of the performance evaluation was strict, and the uncertainty goal for the turbine efficiency was 1% ($U_h / h * 100 = \pm 1\%$). The normal operation of the OTTR created high pressure and temperature gradients. The high turning, high speed, and high loading flow of the OTTR made it difficult to measure the turbine flow field. In addition, probe interference, rake blockage, and measurement averaging were important. In this work, the experimental data were evaluated relative to the uncertainty goal.

1.2 Turbine Efficiency Methods

In order to develop test guidelines to meet specific uncertainty goals, the turbine flow fields and data analysis methods were studied. Two equations used to calculate turbine efficiency from measured test variables were evaluated during this study [3]. Both equations are derived from the basic definition of turbine efficiency: actual enthalpy change over ideal or isentropic enthalpy change. Both methods are used for “cold” air flow turbine testing where the temperature is relatively low so that an ideal gas may be assumed and γ and C_p are considered constant.

For the first method, the thermodynamic method, the temperature drop across the turbine is measured to determine the actual enthalpy change ($\Delta h = C_p \Delta T$). Isentropic relations are used to relate the ideal enthalpy change in terms of the turbine inlet and exit total pressures rather than the temperatures. With the above assumptions, the equation for thermodynamic efficiency becomes

$$h_{th} = \frac{T_{01} - T_{02}}{T_{01}\left[1 - \left(\frac{P_{02}}{P_{01}}\right)^{\frac{g-1}{g}}\right]} \tag{1.1}$$

For the second method, the mechanical method, the ideal enthalpy change is calculated the same as before. However, the mechanical measurements of torque and speed are used along with the measured mass flow rate to determine the actual enthalpy change. The efficiency equation is

$$h_{me} = \frac{K \cdot Tq \cdot N}{J \cdot C_p \cdot \dot{W} \cdot T_{01}\left[1 - \left(\frac{P_{02}}{P_{01}}\right)^{\frac{g-1}{g}}\right]} \tag{1.2}$$

The units used in this thesis for the above equations are psia for pressure, °R for temperature, ft-lb_f for torque, RPM for speed, lb_m/sec for mass flow rate, and BTU/lb_m°R for C_p. The conversion constants, J and K, are needed for these units. These constants are defined in the list of symbols.

Note that the temperatures and pressures in Equations 1.1 and 1.2 are average values at a cross section. Two averaging techniques and a new uncertainty analysis technique were employed for evaluating the turbine efficiency calculations. Mass and area averaging methods were used to compare the experimental data from both cold

airflow turbine tests. The two averaging methods were used to calculate properties needed for the turbine efficiency calculation. The number of data points and the types of measurements required to meet specific data accuracy requirements were also studied. A new uncertainty analysis technique was developed to properly account for conceptual bias errors that arise when the cross-sectional average value required in the data reduction equation is approximated by an average of multiple point measurements. The results of this work along with relevant conclusions are presented in this thesis.

The experimental data were obtained from two different tests: the OTTR with a square exit volute and the OTTR with a circular exit volute. The two volutes generated different gradients in the turbine exit flow field. Data obtained from those tests were evaluated and compared using uncertainty analysis techniques. Test data were manipulated in different ways to verify minimum test requirements while maintaining the 1% accuracy. Three cases of data manipulation were done: reduction of the number of measurements, eliminating measurements at specific quadrants, and wall-static pressure averaging. Different averaging techniques were applied to each case above. The results obtained were compared against one another. The enhanced uncertainty analysis technique developed by Hudson was employed to calculate the uncertainty of the efficiency for the various conditions [1, 4]. Further work was done to modify the uncertainty analysis technique to incorporate the conceptual bias error. The new detailed uncertainty analysis results show the dramatic effects of the correlated bias terms on the uncertainty and the impact of reduced measurements. The new uncertainty analysis helped to verify the guidelines for future turbine testing requirements.

1.3 Overview

Before evaluating the experimental data, a literature survey was conducted. Information on testing of similar turbine designs and on data averaging techniques was sought. The survey yielded little information since the OTTR design was very different from other turbine systems. The majority of the information was obtained from journal articles that were published for the OTTR testing [4, 5, 6, 7, 8, 9, 10, 11, 12, and 13]. Information on data averaging techniques was also limited. The information available in the literature involved time averaging rather than spatial averaging for high gradient systems [1]. Uncertainty analysis literature on conceptual bias application for this situation was not productive either. Conceptual bias is "bias that arises when a symbol in the data reduction equation is replaced by a measured value" [14]. Generally, conceptual bias is one of the elemental systematic error sources for a point measurement. In this work, the concern is estimating the difference between the "true" average value at a cross-section and the average value obtained from averaging some finite number of measurements. No technique for properly incorporating this error into the uncertainty was found in the literature.

This thesis shows an evaluation of data averaging and uncertainty calculation requirements for a turbine system that generates high gradient flow fields. The test data were manipulated to better understand the minimum requirements needed to run the experiments with sufficient accuracy. The different techniques used to manipulate the experimental data included reducing the number of measured data points in the turbine exit section, eliminating specific quadrants of data measurements due to probe access restrictions, and using wall-static pressure measurements rather than static pressure

measurements obtained across the annulus with 3-hole probes. The different test settings above were chosen to help simplify probe access restriction issues for the turbine sections. The data were both mass averaged and area averaged for the various test settings. The different averaging methods and test settings created different uncertainty in the efficiency calculations. The new uncertainty analysis technique developed was used to define and prove the validity of the testing methods. The major background information about the experiment, including a facility description, model description, instrumentation, and test conditions, are presented in Chapter 2. The turbine flow field analysis methodology, turbine flow field mappings and efficiency results are discussed in Chapter 3. The efficiency results help to determine the preliminary conclusion for the turbine testing guidelines. The uncertainty analysis methodology and the new conceptual bias implementation are described in Chapter 4. Chapter 5 then shows the initial uncertainty analysis results, and the results are used to reinforce the preliminary conclusions made in Chapter 3. Finally, Chapter 6 summarizes the conclusions made with the uncertainty analyses and averaging techniques in the previous chapters. A generalized guideline for future turbine test requirements is provided in accordance with the results of the analyses in previous chapters.

CHAPTER II

DESCRIPTION OF EXPERIMENT

2.1 Background

The turbine model was designed to support the development of advanced turbines for future liquid rocket engines. The design was known as the Gas Generator Oxidizer Turbine (GGOT). The GGOT was developed by the Turbine Technology Team within the Consortium for Computational Fluid Dynamics Application in Propulsion Technology [15,16]. The GGOT gas path was incorporated into a turbine test rig at Marshall Space Flight Center (MSFC). The test rig was named the Oxidizer Technology Turbine Rig (OTTR), which was tested in the cold airflow Turbine Test Equipment (TTE) at MSFC. The OTTR was heavily instrumented to carefully measure the flow field at the turbine inlet (Plane 1104) and exit (Plane 1202). The measurements were used to evaluate turbine performance and to validate Computational Fluid Dynamics (CFD) codes developed during the turbine design phase. The uncertainty goal for the turbine efficiency was $\pm 1\%$ ($U_h / h * 100 = \pm 1\%$). The results of the evaluation would prove the benefits of CFD application to turbine design. The OTTR test program goals and plans are documented in references 1 and 2.

The OTTR performance evaluation included two different exit volutes. The first was an oversized square exit volute designed to evaluate a broad off-design envelope for the turbine. The oversized volute prevented the flow from choking at the exit volute before choking in the turbine at off-design points. The second exit volute was a circular exit volute. The circular exit volute was aerodynamically designed to match the turbine exit flow field and to minimize gradients. The two different volutes caused different gradients in pressure and temperature at the turbine exit. The flow fields generated had high Mach number and high swirl flow at the turbine exit. The average temperature and average pressure at the turbine inlet and exit were required to calculate the performance of the turbine. Accurate measurements had to be obtained, and these measurements had to be properly averaged to meet the uncertainty goal of the test. The task was accomplished by maximizing the number of measurements at the turbine inlet and exit, properly calibrating the probes used for the measurements, and properly averaging the measurements. The data from both the square and the circular volute tests will be the focus of this thesis. The data evaluation discussed in this thesis will help develop future turbine test guidelines for obtaining the data necessary to meet specific uncertainty requirements.

2.2 Facility Description

The OTTR baseline test was conducted in the MSFC Turbine Test Equipment (TTE) [1, 17]. The TTE (Figure 2.1) is a blowdown facility, which operates by expanding high pressure air (420 psig) from one or two 6000 cubic feet air tanks to atmospheric conditions. Air flows from the storage tanks through a heater section, quiet

trim control valve, and a calibrated subsonic mass flow venturi. Flow then continues through the test model, backpressure valve, and exhausts to atmosphere. Flow straighteners are used in the piping upstream of the test model. Two sections containing four bosses (2–inch diameter) each are also included for facility measurements and seeding for LDV measurements. The facility can accommodate axial flow, radial inflow, and radial outflow turbines.

This equipment can deliver up to 220 psia air for run times from 30 seconds to over one hour, depending on inlet pressure and mass flow rate. The heater allows a blowdown controlled temperature between $530^{\circ}R$ and $830^{\circ}R$. The TTE has manual set point closed-loop control of the model inlet total pressure, inlet total temperature, shaft rotational speed, and pressure ratio. In addition to these control parameters, the facility can accurately measure mass flow rate, torque, and horsepower. The associated data acquisition system is capable of measuring 512 pressures, 120 temperatures, and several model health monitoring variables [1].

2.3 Model Description

The OTTR model was a 50% scale model of the GGOT turbine design (Figures 2.2, 2.3, 2.4, 2.5) [1, 18]. The model was divided into the inlet volute, turbine stage, exit volute, and diffuser [1, 2, 18]. The inlet volute allowed the conditioned air from the TTE to flow through the turbine section. The turbine section was a single stage configuration with 20 vanes and 42 blades rotating clockwise (viewed from aft looking upstream). The turbine blades (Figure 2.2) had a turning angle of 157°. After the turbine section, flow was guided through the exit volute and the diffuser. Two exit volutes configurations

were used, and data were obtained for both systems. The first configuration was an oversized square exit volute designed to prevent the flow from choking at the exit volute. The second was a circular exit volute aerodynamically designed to match the turbine exit flow field and minimize gradients. Both exit volutes were configured to be 139° away from the inlet volute (Figure 2.4). Details of the configuration of the OTTR are in references 2 and 18.

2.4 Instrumentation

Both the square exit volute and circular exit volute tests had similar instrumentation. The instrumentation was planned so that the performance of each section (inlet volute, turbine, exit volute, diffuser) could be evaluated. An overview of the model instrumentation is given in Table 2.1. The instrumentation will help achieve three purposes:

i). Measurements for performance evaluation.

ii). CFD code validation.

iii). Health monitoring to ensure safe model operation.

The details of all the instrumentation were included in references 1 and 17.

The inlet and exit planes of the turbine section were the greatest emphasis in this thesis. The required data measurements at the inlet and exit of the turbine were recorded using total pressure and total temperature rakes, cobra probes on radial traverse actuators (Figure 2.6), and a three-hole modified prism (YC) probe (Figure 2.7). This instrumentation was installed on a rotating ring. Each ring held eight rakes and two probes with radial actuators. An automatic traverse gear moved the ring through 90°

circumferentially at the turbine inlet and exit (Figure 2.4 along the direction of rotation). The ring rotation along with the number of rakes allowed the entire 360° of the turbine inlet and exit plane to be covered (Figure 2.8). The rakes contained five probes positioned on centers of equal area within the turbine inlet and exit (Figure 2.8). The yaw angles of the rakes were adjusted manually. Measurements taken every 2.5° created 720-point measurements along the turbine inlet or exit.

The three-hole probes were carefully calibrated to obtain yaw angle, total pressure, and static pressure. The cobra probes also contained a thermocouple for total temperature measurements. These probes were mounted on radial traverse actuators so that the radial position could be automatically set and adjusted during test runs. The cobra probes also operated in an "auto-nulling" mode meaning that they automatically adjusted to the angle of the incoming flow. Therefore, the only calibration necessary to obtain flow angle with the cobra probes was to obtain the "offset" for the particular probe at 0°. For static pressure, the cobra probes were calibrated at 0° over a Mach number range. The cobra probes were used to map two 90° quadrants of the turbine inlet and exit planes. This was because the casings had to be open to accommodate the radial actuators. Obviously, the entire 360° could not be open. The two 90° quadrants were the largest openings allowed by the structural guidelines. The two quadrants at the turbine exit were from 167° to 257° and from 347° turning clockwise through 0° to 77° (all angles measured from top-dead-center, TDC, of Figure 2.4 and Figure 2.9). The remaining two quadrants of the turbine exit plane were mapped using the YC probe. The YC probe stem was short so that it could be mounted in a holder similar to those for the pressure and temperature rakes. With the design, it could move under the closed sections

of the casing; therefore, it could be used at any rake position and could cover the entire 360°. However, since the YC probe had to be manually set for both radial position and yaw angle, it was much more difficult to use and consumed much more test time. The YC probe required the calibrations mentioned above for the cobra probes as well as additional calibration data over a yaw angle range since it could not "auto-null." The YC probe covered the two quadrants from 54.5° to 144.5° and from 234.5° to 324.5° (all angles measured from top-dead-center, TDC, of Figure 2.4 and Figure 2.9). The YC and cobra probe measurements overlapped through two 22.5° sections. Hence, two 22.5° sections of the turbine exit were not measured (Figure 2.9). These two sections were filled using linear regressions.

All of the rakes and probes used at the turbine inlet and exit were carefully calibrated. The calibration information will not be repeated here but can be found in reference 1.

2.5 OTTR Test Conditions

The OTTR was tested at the turbine aerodynamic design point (ADP) and over a broad off-design operating range. The ADP test conditions are the emphasis of this thesis. The set point parameters for the tests were the turbine inlet total pressure, inlet total temperature, speed, and total-to-total pressure ratio (inlet total pressure to exit total pressure) [1]. The ADP set point parameters for both volute tests were: $P_{01} = 100\,psia$, $T_{01} = 560^{\circ}R$, $N = 3710\,RPM$, and $\mathrm{Pr}_{t-t} = 1.60$ [16]. The test facility set point for pressure ratio was different from the model set point $\mathrm{Pr}_{t-t} = 1.60$ due to the facility

piping. The facility pressure ratio was 1.85 for the square exit volute test and 1.95 for the circular volute test to achieve $\mathrm{Pr}_{t-t} = 1.60$ across the model.

Table 2.1 OTTR Instrumentation Overview

Inlet Volute:
Inlet–2 bosses 90° off. Circumferential wall statics–10 planes. 2 laser window locations at 4 planes.
Turbine Inlet and Exit (Plane 1104 and Plane 1202):
4 total pressure rakes (5 probes each). 4 total temperature rakes (5 probes each). 2 auto-nulling cobra probes with radial actuators. Each can traverse 90° circumferentially 1 three-hole modified prism (YC) probe that can be mounted in any exit rake position. Maximum of 8 rakes and 2 cobras can be inserted at once. Automatic circumferential traverse.
Turbine:
Inner and outer wall statics–7 planes. Vane surface statics: 4 circumferential locations at 50% span, 1 circumferential location at 10% span, 1 circumferential location at 90% span. Disk cavity static pressures: 4 front, 4 rear. Disk cavity total temperatures: 2 front, 2 rear.
Exit Volute:
Circumferential wall statics–10 planes. Exit total pressure rake (9 probes). Can be mounted in two positions (90° off). 2 laser window locations at 4 planes.
Diffuser:
Statics–7 axially and 4 exit. Exit total pressure rake (9 probes). Can be mounted in two positions (90° off). (Square Exit Volute) Exit total pressure rake (9 probes) on automatic circumferential traverse. (Circular Exit Volute)
Miscellaneous
2 speed pick-ups. Accelerometers: 2 horizontal, 2 vertical. Contoured blank plugs for all bosses. Health monitoring instrumentation.

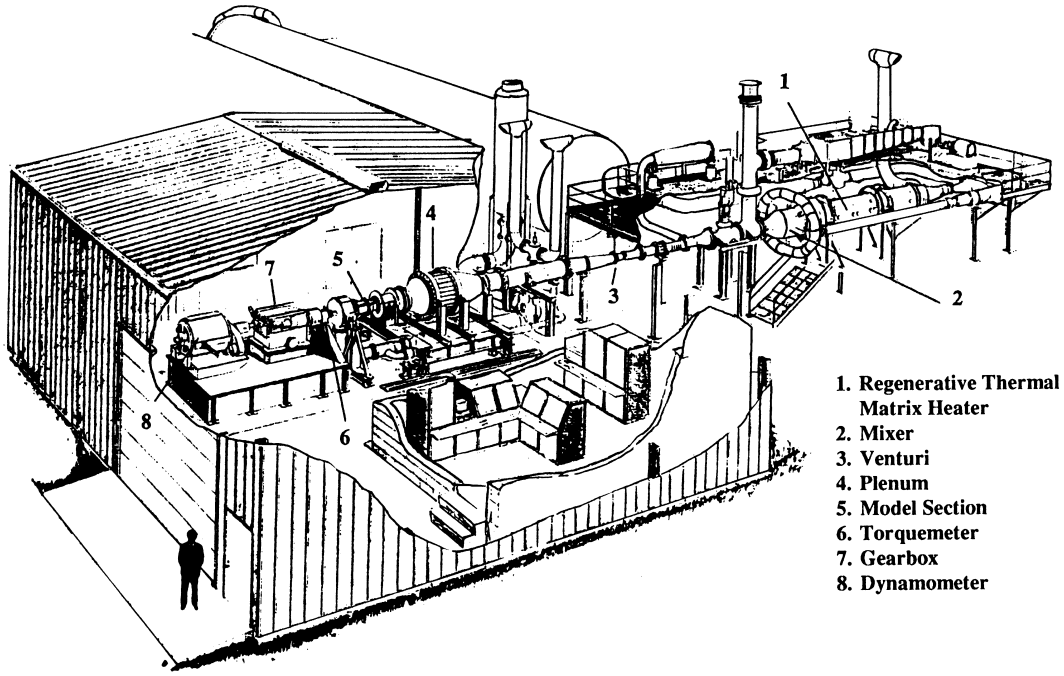

Figure 2.1 TTE Schematic

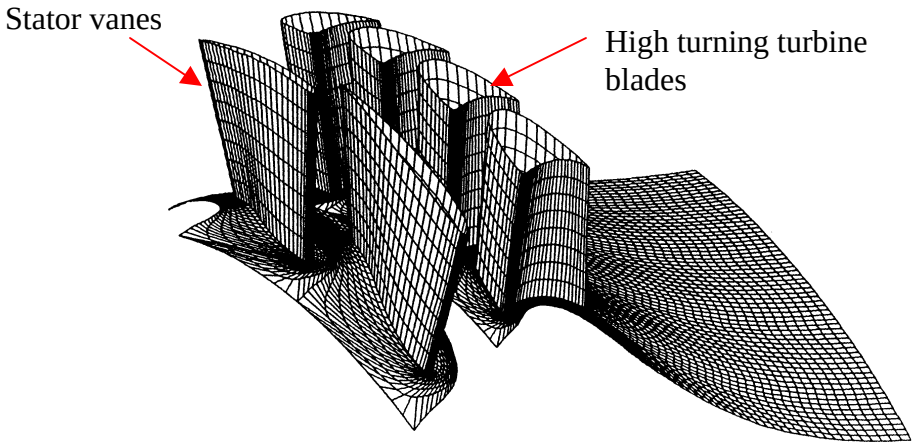

Figure 2.2 OTTR Vanes and Blades

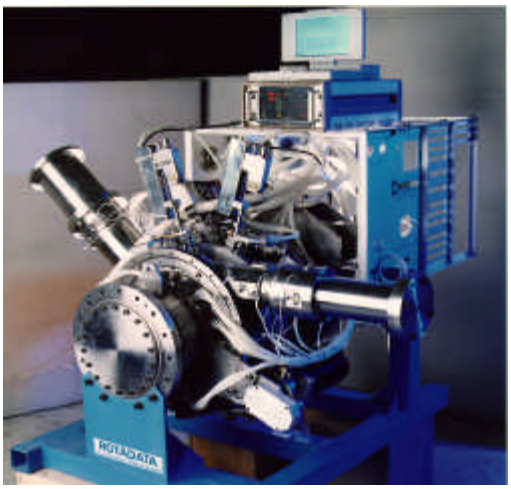

Figure 2.3 (a) OTTR with Square Exit Volute

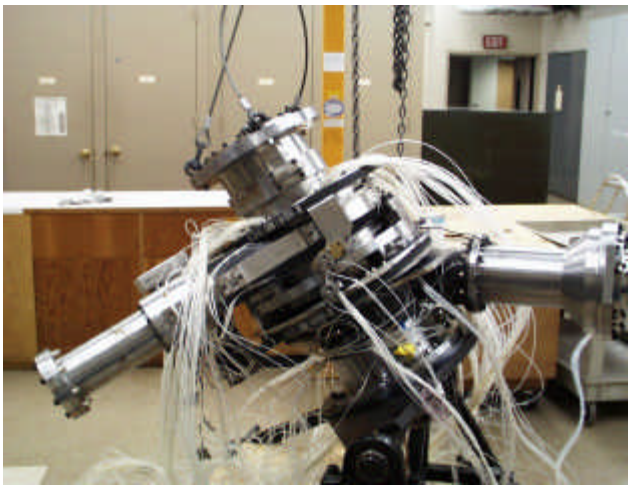

Figure 2.3 (b) OTTR with Circular Exit Volute

Figure 2.3 OTTR

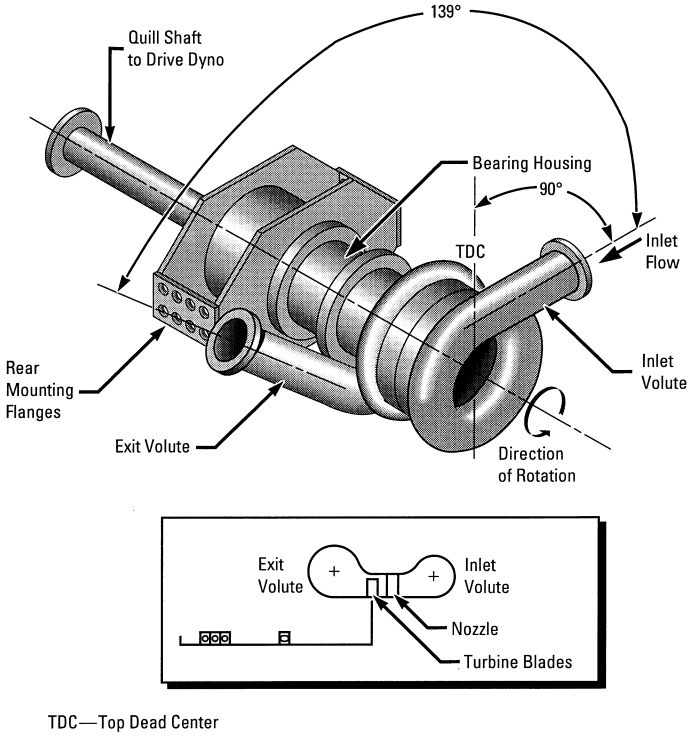

Figure 2.4 OTTR Schematic

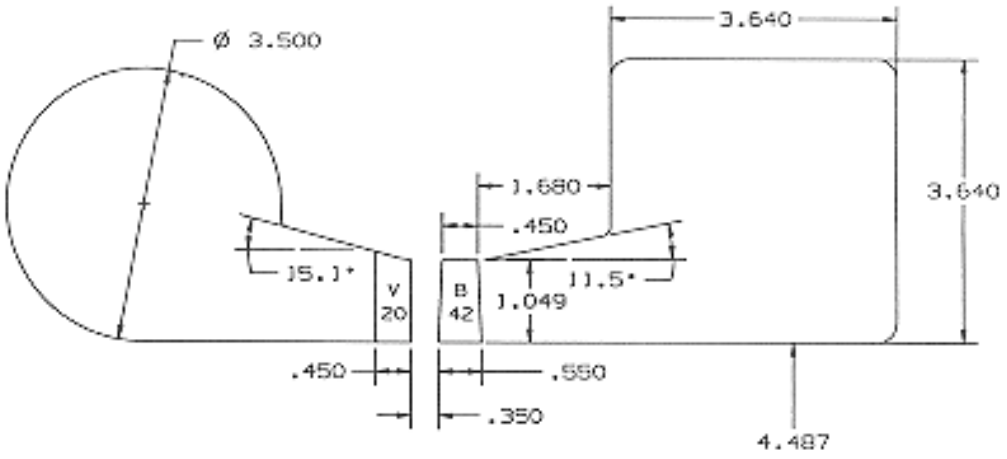

Figure 2.5 OTTR Flowpath for Square Exit Volute

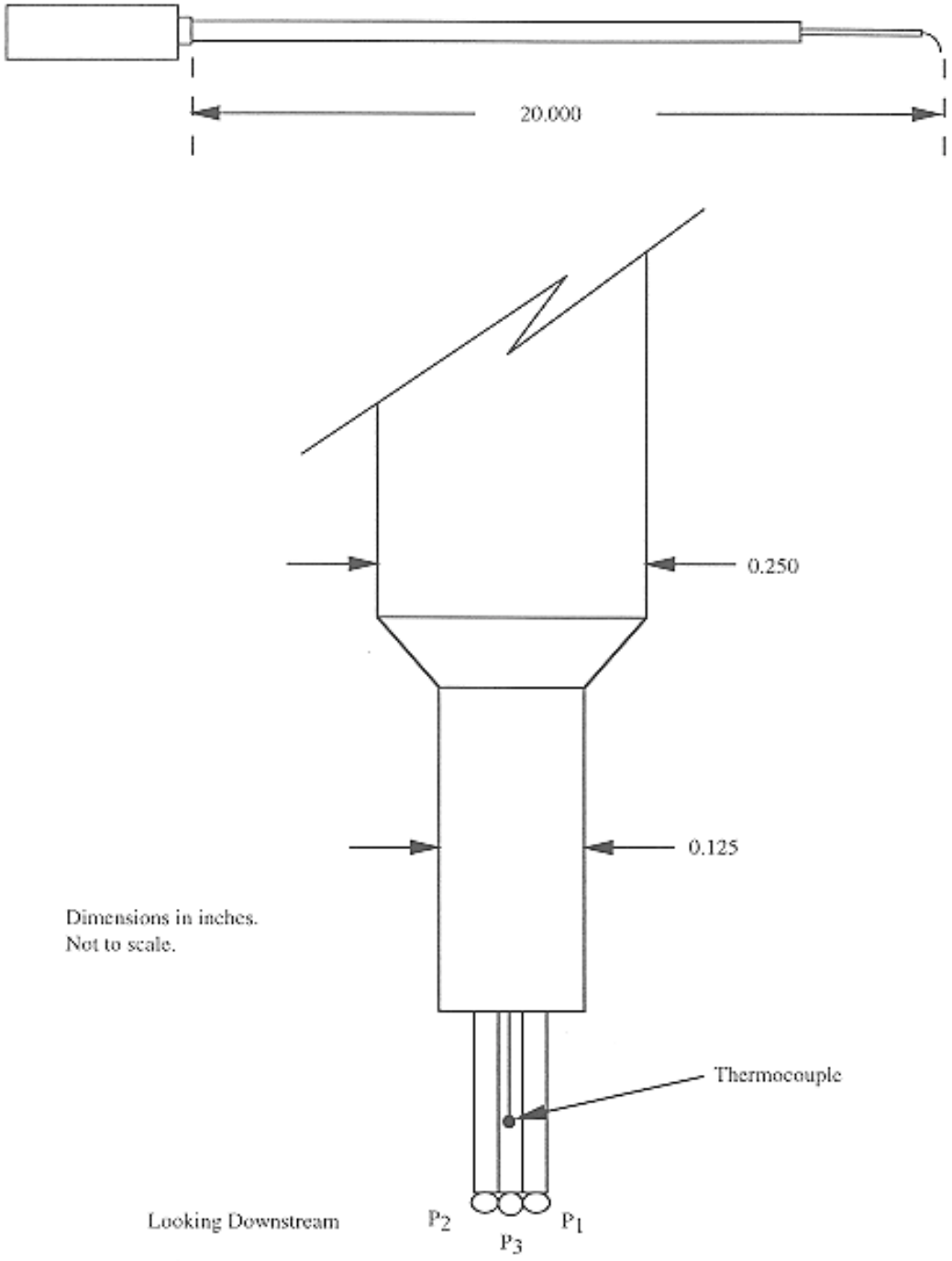

Figure 2.6 Cobra Probe Schematic

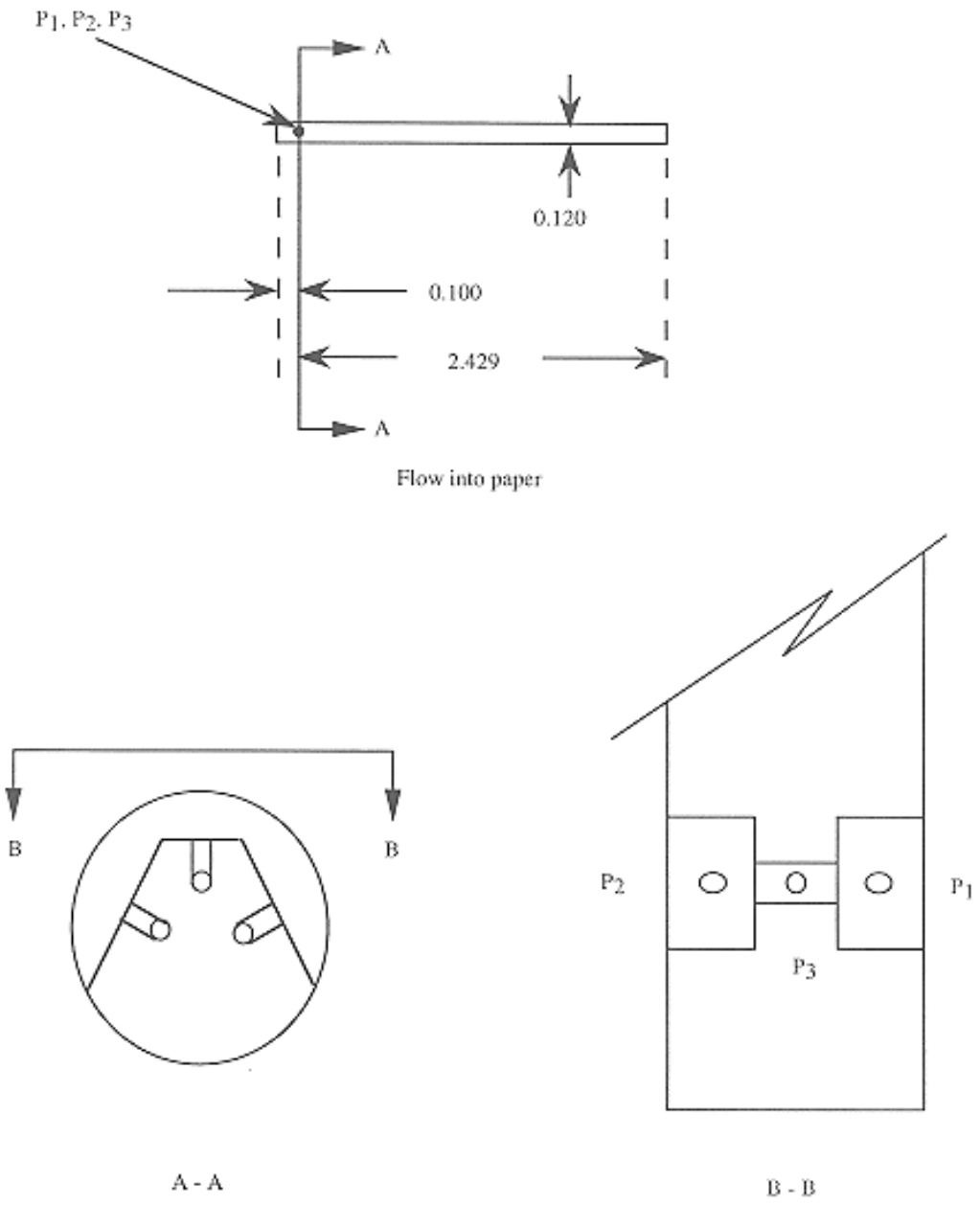

Figure 2.7 Modified Prism (YC) Probe Schematic

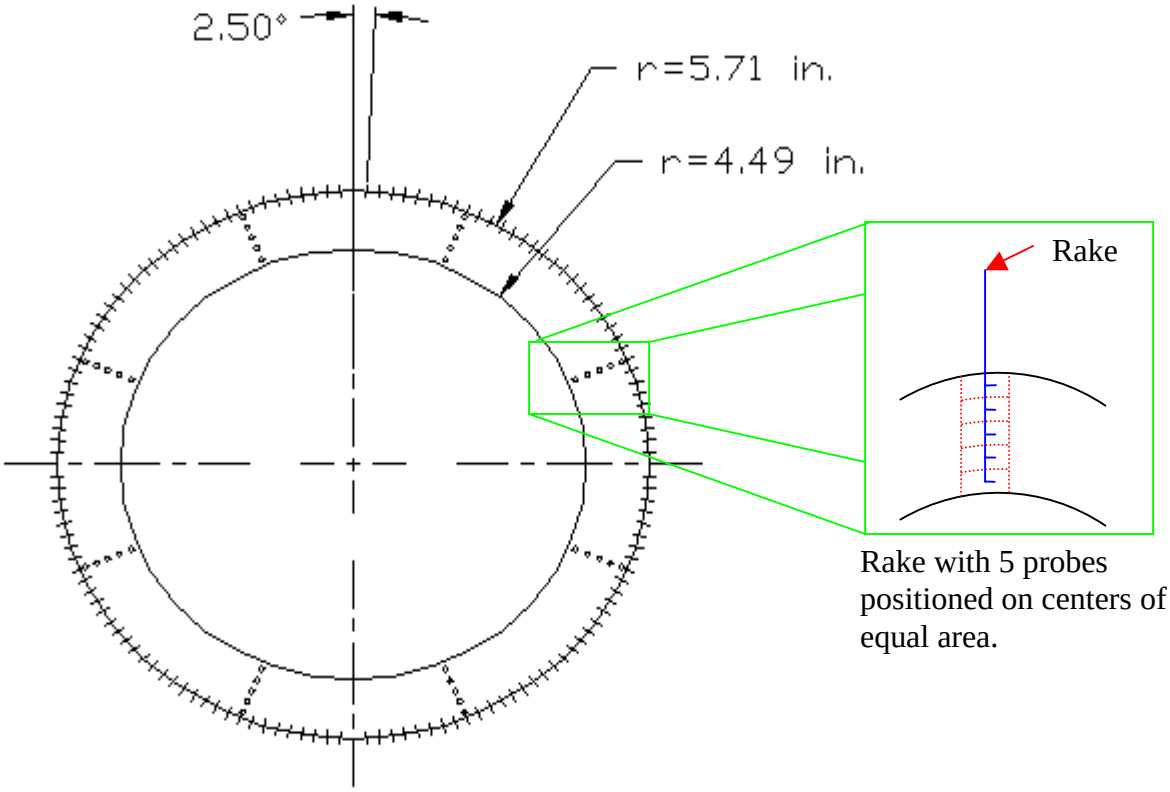

Figure 2.8 OTTR Inlet and Exit Instrumentation

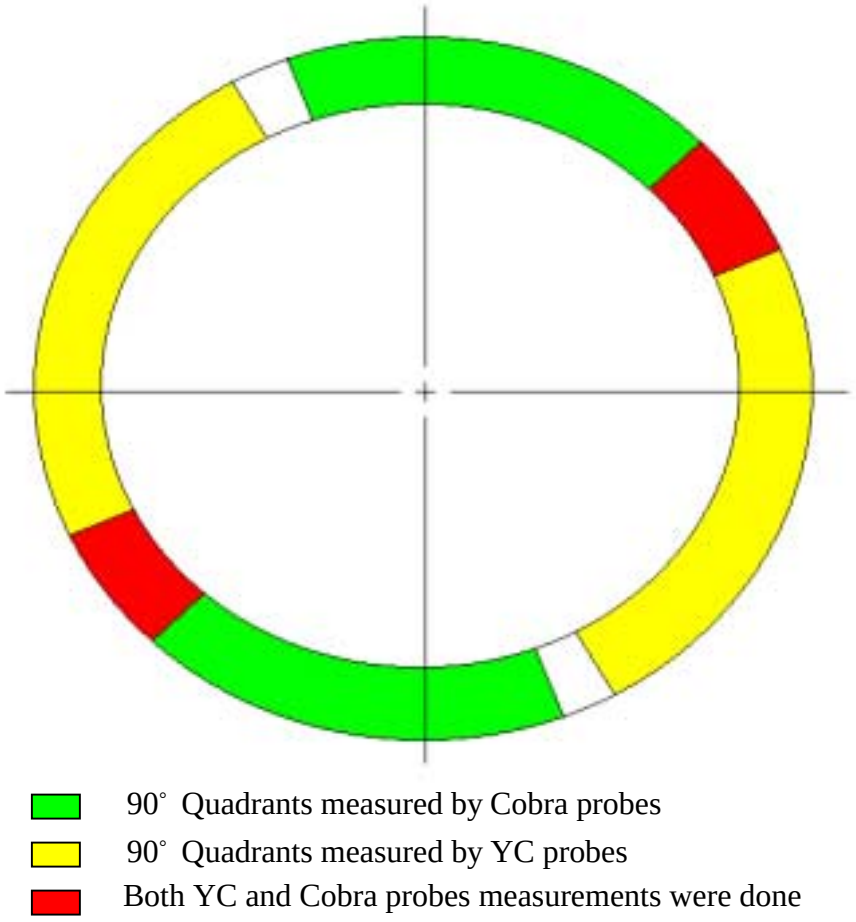

Figure 2.9 Cobra and YC probes Coverage of the Turbine Exit Plane

CHAPTER III

EXPERIMENTAL DATA ANALYSIS

3.1 Analysis Methodology

Experimental data from two different tests were analyzed–the OTTR with a square exit volute and the OTTR with a circular exit volute. The two different volutes generated different flow fields at the turbine exit. Comparisons between the two different volutes were made to help establish guidelines for future turbine testing requirements. The comparisons included evaluating averaging techniques, the number of measurements needed to maintain a specific accuracy, and the types of measurements needed for performance calculations. The analysis procedures used for each of these comparisons are described in this section. The results of the various analyses are then given in the remaining sections of this chapter.

3.1.1 Averaging Techniques

The properties needed for the turbine efficiency calculations (Equation 1.1 and Equation 1.2) were averaged values of the turbine inlet and exit cross-sections. The OTTR had volutes that generated high pressure and temperature gradients; therefore, proper averaging of the pressure and temperature measurements at the turbine inlet and

exit was critical. Two averaging techniques were used to analyze the OTTR experimental data [1]. The first averaging technique was area averaging

$$Q = \sum \frac{Q_i \Delta A_i}{A} \tag{3.1}$$

(where $Q = P_0, P, T_0, a$). The second averaging technique was mass averaging

$$Q = \sum \frac{Q_i \Delta \dot{W}_i}{\dot{W}} \tag{3.2}$$

Both area averaging and mass averaging were used to evaluate the turbine flow fields in the square exit volute system and the circular exit volute system. Comparisons between the two different tests were needed to establish a broader overview of averaging effects on high gradient turbine systems. The effects of area and mass averaging on the turbine efficiency calculations were analyzed.

3.1.1.1 Area Averaging

For the OTTR, area averaging was the same as numerical averaging because all measurements were made on centers of equal areas. Area averaging did not consider the mass flow through the control area. This assumption defines Equation 3.1 as the summation of the magnitude of the property measurements from the inlet or exit divided by the total number of measurements. As will be shown in the next section, the turbine inlet plane was relatively uniform with low gradients; therefore, the turbine inlet measurements were always area averaged. However, high pressure and temperature gradients existed in the turbine exit plane. Area averaging treated each measurement equally, neglecting the actual mass flow through the control area (Figure 2.8). A low

mass flow rate at a particular point suggested that the measurements at that point contributed little to the overall average (cross-sectional average of the inlet or exit). Therefore, a correction value must be added to the calculation to account for mass flow at the turbine exit plane. The correction value would be added to the conceptual bias estimate of the measurements. The conceptual bias estimate will be discussed in detail in Chapter 4.

3.1.1.2 Mass Averaging

Large gradients existed in the exit flow field of the OTTR suggesting the need to mass average the experimental data. The mass averaging procedure required four measurements (P_0, P, T_0, a). Since no information was available prior to the test on the number of measurements needed to meet the efficiency uncertainty goal of 1%, the number of measurements to be taken was determined based on the size of the probes and the flow area. The measurements were made every 2.5° at each of the five radial locations, resulting in 720-point measurements of P_0, P, T_0, and a . The Mach number was calculated from the total and static pressures at each point as follows:

$$M = \sqrt{\frac{2}{g-1}\left(\left(\frac{P_0}{\mathrm{P}}\right)^{\frac{g-1}{g}} - 1\right)} \tag{3.3}$$

The weighting factor, W_i, for each measurement within a control area of 0.0545 in^2 was then calculated according to the following equation:

$$W_i = 0.0545\cos(a)\sqrt{\frac{g}{zR}}\frac{P_{0_i}}{\sqrt{T_{0_i}}}\frac{M_i}{\left[1+\left(\frac{g-1}{2}\right)M_i^2\right]^{\frac{g+1}{2(g-1)}}} \quad (3.4)$$

The sum of the product of the measured value time its weighting factor was then calculated at each radial location for all quantities to be mass averaged (P_0, P, T_0, and a). The property measurements at each location were multiplied by the weighting factor calculated at each location. Those values were then summed together and divided by the total mass flow rate ($\sum W_i$) [1]. The mass averaging technique accounted for the mass flow rate through the turbine section. Therefore, the mass averaged values of the 720-point measurements were assumed to be the "true" property values for the turbine exit (both square and circular volute tests). The differences between the mass and area averaged quantities will be explained by the uncertainty analysis results. The uncertainty results will be given in Chapter 5.

3.1.2 Reducing Number of Measurements

Further analysis of the OTTR test rig experimental data involved reducing the number of point measurements used for calculating the average values at the turbine exit plane. Initially, 720-point measurements were taken at the turbine inlet and exit planes. The averages of those point measurements were used to calculate the efficiency (Equation 1.1 and 1.2). The instrumentation used to obtain those 720-point measurements was complex, and obtaining the measurements required a large amount of test time resulting in high costs. Therefore, reducing the number of measurements was studied to determine the impact on the efficiency calculation and the uncertainty of the

efficiency. The OTTR test goal was to obtain sufficient measurements from the turbine inlet and exit so that the uncertainty of the efficiency remained below 1%; therefore, the measurement reduction study evaluated the minimum number of measurements needed to achieve that goal. Note that since the turbine inlet plane had low gradients, the number of measurements made would have much less impact on the calculations than at the exit plane. Therefore, it was assumed that the number of inlet plane measurements could be reduced at least as much as the number of exit plane measurements and the reduction of the number of measurements was not studied explicitly.

The data measurement procedures for total pressure, total temperature, static pressure, and yaw angle were explained in Section 2.4. Rakes and probes were inserted in a rotating ring, which moved through 90° circumferentially along the turbine inlet and exit resulting in 360° coverage. Measurements were made at 5 radial positions (Figure 2.8). The measurements were taken every 2.5° creating 720-point measurements of each quantity along the turbine inlet or exit. If the data had been taken every 5°, the total number of measurement would have been 360-points for each quantity at a plane. Hence, the total number of measurements required would be reduced by half. Measurements taken every 10° would give a total of 180-point measurements for each quantity, and measurements taken every 20° would give a total of 90-point measurements for each quantity. These four different numbers of measurements for the turbine exit will be discussed in this thesis (720-point, 360-point, 180-point, and 90-point measurements). Mass averaging and area averaging of each case were analyzed. The control areas of each case are listed in Table 3.1.

The measurement reduction processes above maintained the 360° coverage of the turbine exit. Another technique studied was to measure two 90° quadrants of the turbine exit. This process was studied since the probes mounted on radial actuators could not access the full 360°. The casings had to be "closed" over certain areas to hold the unit together. For the OTTR, the radial actuators could be used in two 90° quadrants; therefore, cobra probes that automatically adjusted to the correct yaw angle and radial position could be used. Measurements made in the "closed" area had to be done with a probe (the YC probe) that was manually moved to each radial position and yaw angle position. This greatly increased the test time.

The quadrants analysis utilized the measurements made by the cobra probes and the YC probes. The quadrant measurements were described in Section 2.4 (Figure 2.9). Averaging was performed on two case studies. The first case study was to mass and area average measurements made by the cobra probes. Two 90° quadrants were not measured by the cobra probes; therefore, the empty quadrants were filled with linear regressions with the measured values (cobra probes measurements) as reference. The same comparisons of mass versus area averaging, reducing the number of measurements, and square volute versus circular volute stated previously were performed. The second case study was to mass and area average measurements made by the YC probe. The same comparisons made in the first case were repeated in the YC probe case study.

3.1.3 Evaluation of Measurement Types

Static pressure measurements collected using the cobra probes and YC probe across the annulus at the turbine exit were elaborate and difficult. Extensive calibration

and test time were necessary to obtain these measurements. Wall-static pressures are much easier to obtain. Therefore, the effect on turbine efficiency of using an average of the wall-static pressure measurements rather than the static pressure measurements across the annulus at the turbine exit was studied. These static pressure measurements were needed to calculate the weighting factor for mass averaging; therefore, the choice of the type of static pressure measurements to use will affect the mass averaged efficiency calculations. Note that the same three-hole probes (cobra and YC probes) used to measure static pressure across the annulus were also used to obtain flow angle. Eliminating the need to use cobra and YC probes for static pressure while still requiring their use for flow angle measurements would save time and money relative to calibration requirements—calibration for flow angle is much simpler than calibration for static pressure. However, relaxing the requirements for flow angle measurements could provide further benefits in terms of test time. Therefore, a sensitivity study was done, and this study showed that the effects of flow angle measurements on efficiency calculations were negligible. Hence, it was assumed that the flow angles measured by the cobra probes covering 180° would be adequate, and this thesis concentrates on the effects of wall-static pressure averaging on turbine efficiency.

Two case studies for static pressure averaging were done. The first method was to numerically average all wall-static measurements (NWA). The second method was to average the turbine outer wall-static pressure with the inner wall-static pressure at specified circumferential locations (CWA). Wall-static pressure measurements were taken at the turbine inner wall (Figure 2.8, r = 4.49 in) and turbine outer wall (Figure 2.8, r = 5.71 in). The eight outer wall-static pressure taps were located on the rotating ring.

As the rotating ring moved to measure total pressure and total temperature using the rakes, the outer wall-static pressures were recorded as well. The inner wall-static pressure taps were stationary and were placed at eight circumferential locations on the turbine inner wall ($41^{\circ}, 86^{\circ}, 131^{\circ}, 176^{\circ}, 221^{\circ}, 266^{\circ}, 311^{\circ}$, and 356°). The turbine inner wall was divided into eight sections. Each section spanned 45° circumferentially along the turbine inner wall. The eight wall-static pressure positions were assumed as the centers of each of the 45° sections. Every point within each section was assumed to be equal to the wall-static pressure measurement at the center of that section. With these assumptions, averages at every 2.5° circumferentially were calculated (point average of inner wall value and outer wall value). Thus, a circumferential average of wall-static pressure (CWA) was obtained.

Uncertainty analyses for all the cases were needed to determine the accuracy of the efficiency calculations and to make valid comparisons. The uncertainty results would prove the usefulness of each case study and reinforce the validity of the turbine testing guidelines developed in Chapters 5 and 6. Uncertainty analysis procedures will be presented in Chapter 4, and the results will be shown in Chapter 5.

3.2 Turbine Flow Field Mappings

The results of the averaging technique comparisons, measurement reduction analyses, and evaluation of the types of measurements required for the different volutes are presented in the following sections. The turbine mapping figures are all presented with reference to the circumferential locations and radial positions of the probes across the turbine inlet and exit planes. The X-axis of all of the figures represents the

circumferential coverage of the turbine inlet and exit. The Y-axis shows the magnitude of the turbine probe measurements. The nomenclature listed in all the figures is PT-1104, PT-1202, TC-1104, TC-1202, Pstatic, YAW, W1200, PS-1202, PS-1200, and PSYC. The first one to the letters represents the measured properties (PT is total pressure, Pstatic and PS are exit static pressures, TC is a total temperature, YAW is flow angle, and W is a mass flow rate). A dash followed by four numbers after the letters denotes turbine plane specifications. Plane 1104 is the turbine inlet and plane 1202 is the turbine exit for the rake measurements and static pressure measurements, as described in Section 2.1. The number 1200 also represents the turbine exit plane for the cobra probe measurements. Finally, the numbering presented in the legends of each figure represents percent spans of the probes placed radially across the turbine inlet and exit cross-sections. The percent span was calculated with the inner radius (0% Span) set as the base and the outer radius set as the maximum radius (100% Span). The number (1) or 01 in the legends is the 10.7% span from the inner radius of the turbine. Similarly, the number (2) or 02 is 32.4%; the number (3) or 03 is 52.8%; the number (4) or 04 is 72.1%; and the number (5) or 05 is the 90.6% span from the inner radius of the turbine. The inner diameter (ID) and outer diameter (OD) of the turbine exit wall-static measurements are listed clearly in the legends of the figures.

3.2.1 Square Exit Volute Test

The flow field mapping of the OTTR with the square exit volute included turbine inlet and exit total pressure distributions, inlet and exit total temperature distributions, exit static pressure distribution, and exit mass flow distribution. The turbine inlet and

exit mappings for the 720-point measurements case study are illustrated in Figures 3.1, 3.2, 3.3, 3.4, and 3.5. The next set of figures (3.6 through 3.11) shows the effect of reducing the number of measurements while maintaining 360° coverage of the exit plane (Section 3.1.2). Figures 3.6 and 3.7 are the total and static pressure mappings for the 360-point measurements. Next, Figures 3.8 and 3.9 are similar mappings for the 180-point measurements. Lastly, Figures 3.10 and 3.11 are similar mappings for the 90-point measurements.

The cobra probe measurement reduction analysis (Section 3.1.2) maps for exit total and static pressure with the maximum (720-points) and minimum (90-points) number of points are given in Figures 3.12 through 3.15. Recall from Section 3.1.2 that only two quadrants were actually measured with the cobra probes, and linear regressions were used for the remaining points (Figure 2.9). The cobra probe measurements and the linear regression are presented in Figures 3.12 and 3.13 (refer to Figure 2.9 details of cobra probes measurements). There were 360-point measurements taken with cobra probes, and 360-points were generated with linear regression. Similar plots for the YC probe analysis are shown in Figures 3.16 through 3.19. The mapping comparisons will be used to explain the effects of mass versus area averaging and reducing the number of measured points on the turbine efficiency.

Figures 3.20 and 3.21 will be used to explain the impact of using the wall-static pressure measurements for the turbine efficiency calculations (Section 3.1.3). Note that, at the turbine inlet (Figure 3.20), there were only wall-static pressure measurements. No probes were used to measure the static pressure across the annulus of the turbine inlet because the flow field had low gradients. At the turbine exit (Figure 3.21), there were ID

and OD wall-static pressure measurements as well as cobra probe (PS1200) and YC probe (PSYC) static pressure measurements across the annulus. The PS1200 and PSYC measurements were average static pressures across the annulus–average values of 5 radial measurements at each circumferential location.

3.2.2 Circular Exit Volute Test

The mappings for the OTTR with the circular exit volute are similar to those in the previous section. The maps of this setup will be compared with the maps given in Section 3.2.1. Figures 3.22 through 3.26 are for the 720-point measurements case study, Figures 3.27 and 3.28 are for the 360-point measurements, Figures 3.29 and 3.30 are for the 180-point measurements, and Figures 3.31 and 3.32 are for the 90-point measurements. The cobra and YC probe mappings are in Figures 3.33 through 3.40. Lastly, Figures 3.41 and 3.42 will be used to explain the wall-static pressure averaging technique. Refer to Section 3.1 for details of each case study.

3.2.3 Comparisons

The mappings were used to help understand the relative gradients present in the turbine inlet and exit flow fields for the square and circular exit volute tests, the effects of these gradients on the average values calculated at the turbine inlet and exit planes, and the effects of these average values on turbine efficiency. An effort was made to quantify the gradient for each flow field to provide a feel for the relative differences in the gradients. To do this, the gradient was defined as follows

$$Gradient(\%) = \frac{MaximumMeasuredValue - MinimumMeasureValue}{AverageValue} \qquad (3.5)$$

The gradients are given in Table 3.2. The results show that the gradients are very low at the turbine inlet relative to the turbine exit. Also, the gradients were larger at the turbine exit with the square volute than they were for the circular volute, as expected (Note that % values were much lower for temperature than they were for pressure and flow angle. This was because that the temperature was in $^{\circ}R$; therefore, the denominator in Equation 3.5 was in the 505 and 560 range whereas the average values for both pressure and flow angle reached maximums of less than 100).

The results of the mappings showed that the turbine inlet total pressure and total temperature measurements were uniform and relatively flat for both the square and circular volutes; therefore, the use of area averaging at the turbine inlet was sufficient (Figures 3.1 and 3.22). The turbine exit plane, however, had high pressure and temperature gradients for both volutes (Figures 3.1 through 3.3 and 3.22 through 3.24). Therefore, the mass flow at the turbine exit had large variations (Figures 3.5 and 3.26). These data showed that mass averaging at the turbine exit plane was more suitable since the weighting factor of each measurement was determined by the amount of mass flow through the specified control area (Section 3.1). Mass averaging the turbine exit plane was suitable for both volutes. The mass averaged values of the 720-point measurements for each quantity were assumed to be the "true" property values for both the square and the circular volute tests.

Comparisons of Figures 3.1, 3.6, 3.8, and 3.10 show the effect of reducing the number of measurements on the total pressure distribution. The average value of Figure 3.10 was very different compared to the average value of Figure 3.1. The difference

exists because Figure 3.10 did not measure many of the high gradient points, and the percentage of uniform measurements dominated the high gradient points. The assumption above will be verified by efficiency calculations in Section 3.2. The trend described above is illustrated in Figures 3.1 through 3.11. The mappings of the circular volute showed similar trends, but the circular volute mappings showed smaller gradients (Figures 3.22 through 3.32). Therefore, the average values for each measurement reduction test case were quite close. The results of averaging will be provided in Section 3.3.

The exit total and static pressure mappings of the different quadrants for the OTTR with the square exit volute are in Figures 3.12 through 3.19, while Figures 3.33 through 3.40 are similar mapping for the circular volute. The cobra probe measurements covered two quadrants (from 167° to 257° and from 347° to 77°). The two quadrants not measured were filled by linear regression. Figures 3.12, 3.13, 3.33 and 3.34 show the cobra measurements taken every 2.5° circumferentially (720-points); whereas, Figures 3.14, 3.15, 3.35, and 3.36 depict cobra measurements taken every 20° circumferentially (90-points). The YC probe measurements covered from 54.5° to 144.5° and from 234.5° to 324.5°. Figures 3.16, 3.17, 3.37, and 3.38 present the YC probe measurements taken every 2.5° circumferentially. The remaining Figures 3.18, 3.19, 3.39, and 3.40 illustrate YC probe measurements taken every 20° circumferentially.

The highest gradient section was between 225° and 315° for the square exit volute test turbine exit plane (Figures 3.1 through 3.5). The YC probe mappings covered 64.4% of this highest gradient section, while the cobra probe mappings covered 35.6% of the highest gradient section. The regression for the cobra probe mappings (Figure 3.12)

created a different total pressure profile from the original 720-point data (Figure 3.1). A comparison of the static pressure profiles (Figures 3.3 and 3.13) shows that the high gradient portion was extended to the circumferential location of 357° for the reduced number of measurements. Compared to the mappings with 360° circumferential coverage (Figures 3.1 through 3.11), the cobra probe mappings (Figures 3.12 through 3.15) were very different. The YC probe, however, mapped more of the highest gradient section and had a profile that was nearly the same as the original 720-point data (Figures 3.1, 3.3, and 3.16 through 3.19); hence, the mappings with regression were very similar to those with full 360° circumferential coverage. These cases demonstrate that mapping different quadrants rather than covering the full 360° can significantly alter the results. The number of cobra probe point measurements was reduced to 90-points in Figures 3.14 and 3.15. Figures 3.14 and 3.15 had profiles that closely to the profiles in Figures 3.12 and 3.13. Similar results are seen in Figures 3.16 through 3.19.

The highest gradient section for the OTTR with the circular exit volute was between 180° and 270° at the turbine exit plane. Hence, the cobra probe mappings covered 85.5% of the high gradient portion, whereas the YC probe mappings only covered 14.5% of the highest gradient portion (Figures 3.22 through 3.26 and 3.33 through 3.40). The effects of using regressions were similar to those noted for the square volute quadrant mappings. In addition, the cobra probe total pressure mapping (Figure 3.33) were nearly the same as the original 720-point data (Figure 3.22). Comparisons of Figures 3.34 and 3.24 show that the static pressure profile of the cobra probe mapping was nearly the same as the original 720-point static pressure mapping. The YC probe mappings (Figures 3.37 through 3.40) had different total pressure and static pressure

profiles comparing with the original 720-point mappings (Figures 3.22 and 3.24). The results generated by reducing the quadrant measurements were very close to the results with 720-point quadrant measurements (Figures 3.33 and 3.34 for cobra probes, and 3.37 and 3.38 for YC probes).

Using wall-static pressure measurements could reduce the use of the cobra and YC probes. Figures 3.20 and 3.41 depict the inlet wall-static pressure distributions for the square and circular volute tests, respectively. Figures 3.21 and 3.42 illustrate the static pressure profiles at the turbine exit plane. The pressure profiles at the exit for both volutes were quite similar; however, the gradient was larger at the turbine exit for the square volute test. The wall-static pressure measurements were compared with the measurements made by the cobra and YC probes in the annulus at the turbine exit. The three-hole probe measurements in the annulus and the wall-static pressure measurements gave very similar circumferential trends for both volutes. The differences between the sets of measurements were used to develop conceptual bias error estimates for wall-static averaging. The conceptual bias estimates are discussed in Chapter 4. The efficiency uncertainty calculations using wall-static pressure averaging (Chapter 5) will yield more insight about the usefulness of this measurement method.

3.3 Efficiency Results

Efficiency calculations were done for the square and circular volute tests using both area and mass averaging at the turbine exit for the following cases:

i). 720 point measurements.

ii). 360 point measurements.

iii). 180 point measurements.

iv). 90 point measurements.

v). Using cobra probe measurements only (with and without regression).

vi). Using YC probe measurements only (with and without regression).

vii). Wall-static pressure averaging.

The efficiency was calculated using the thermodynamic method and the mechanical method (Equation 1.1 and 1.2) given in Chapter 1. Note that the equations given in Chapter 1 use the total-to-total pressure ratio to calculate efficiency. The same equations were also used with the total-to-static pressure ratio. The total-to-total efficiency calculations used the inlet total pressure and the exit total pressure of the turbine (the total-to-total pressure ratio) while the total-to-static efficiency calculations used the inlet total pressure and the exit static pressure of the turbine (the total-to-static pressure ratio). The choice of the total-to-total or total-to-static pressure ratio depends on the application; therefore, both cases were evaluated.

3.3.1 Square Exit Volute Test

The first part of the analysis involved the averaging comparisons. The former section states the importance of weighting a measurement based on the mass flow in high gradient regions. Hence, the efficiency calculations using mass averaged turbine exit quantities were considered the best or closest to the "true" value for the OTTR. Therefore, the mass averaged efficiency was considered the "true" value for the analyses in this thesis. Remember that the turbine inlet had very low gradients; therefore, all quantities were area averaged at the inlet.

The turbine inlet (Figures 3.1 and 3.2) had low gradients, hence area averaging the inlet properties was applicable. The OTTR ADP inlet values are given in Table 3.3. The area averaged inlet properties given were used for all efficiency calculation cases. The turbine exit had high gradients; therefore, mass averaging was used. The mass and area averaged properties are given in Tables 3.4, 3.5, and 3.6. Note that the mass averaged properties of P_{02}, P_2, T_{02}, and M_2 are higher than the area averaged properties, whereas the area averaged a_2 is higher than the mass averaged a_2. Similar trends were noted in Tables 3.5 and 3.6 (cobra and YC average values).

The impact of the various average values on the efficiency calculations was not obvious from the values in Tables 3.4, 3.5, and 3.6. Hence, the difference between the average properties and the "true" average properties for each case were tabulated. The differences are given in Tables 3.7, 3.8, and 3.9. In general, the differences between the average values and the "true" values with 360° circumferential coverage increased as the number of measurements decreased (Table 3.7). On the other hand, these differences seemed to be random with quadrant coverage (Tables 3.8 and 3.9). The impact of those differences was not obvious; hence, the turbine efficiency was calculated to further the study. Note that the efficiency calculated with mass averaging 720-point measurements was assumed to be the "true" efficiency value.

The area averaged efficiency results were lower than the "true" efficiency values (Table 3.10, 3.11, and 3.12). There were no large changes in efficiency as the number of points was reduced for any case (Tables 3.10, 3.11, and 3.12). Reducing the number of point measurements was not expected to significantly influence the area averaged calculations. Reducing the number of measurements alters the gradient profile of the

flow field. These changes should give different mass averaged property values, hence generating different efficiency results as the number of measurements decreases. However, the area averaged values do not use these gradients to "weight" each measurement and change the average values. Therefore, reducing the number of measurements should not affect the area averaged values as significantly as the mass averaged values. The fact that the mass averaged calculations were not affected as significantly as expected cannot be fully explained without uncertainty analysis results (Chapter 5).

To help understand why the mass averaged efficiency calculations did not change significantly when the number of measurements was reduced, comparisons between the average property values of the 720-point measurements and the average property values generated from the 360-point, 180-point, and 90-point measurements and their impact on efficiency calculations was studied (Tables 3.4, 3.5 and 3.6). The task was to prove that the difference in average values influences the changes in efficiency calculations. MathCad simulation showed that the thermal efficiency formula was driven by two major properties: the exit total pressure and exit total temperature. These two properties change the efficiency in opposite directions. The differences in average values were quite inconsistent as the number of measurements was reduced (Tables 3.7, 3.8, and 3.9). The impact of those differences of average values on the efficiency calculations was analyzed (Tables 3.10, 3.11, and 3.12). The opposite effects of the different averaged property values for the efficiency equations could have caused the unexpected results. The uncertainty contribution of each property must be analyzed to fully explain the impact of

averaging technique on the efficiency calculations. The uncertainty analysis methodology will be presented in Chapter 4 and the results in Chapter 5.

The analysis showed that measuring only portions of the highest gradient section of the turbine exit flow field had unpredictable effects on the calculation of the efficiency. There were significant differences between the efficiency calculations using only the cobra probe measurements and the "true" values (Table 3.11). There were small differences between the efficiency calculations using only the YC probe measurements and the "true" values (Table 3.12). The differences may have been smaller for the YC probe quadrants coverage because more of the highest gradient region was covered by these measurements, as noted earlier. The YC probe mapping covered 64.4% of the highest gradient section of the turbine exit while the cobra probes mapping covered 35.6% of the highest gradient section. This would imply that the cobra averaging should have a greater efficiency deviation from the "true" value.

The cobra analysis showed that the efficiencies calculated with regression deviated more from the "true" value than the efficiencies calculated without regression (The deviation was small for calculations with and without regression). The regression generated two 90° quadrants of "guess" measurements (Figures 3.12 and 3.13); hence, the averaging of the properties was biased and inaccurate. The results proved the importance of mapping the entire circumferential area of the turbine exit, in order to reduce error. The uncertainty analysis results will be used to substantiate this conclusion.

Table 3.13 shows the efficiency results of CWA and NWA for the square exit volute case. The results are similar to the efficiency results in Table 3.10. The efficiency results of CWA and NWA do not appear to be affected until the number of measurements

is reduced to 90-points, but the impact of wall-static averaging was not obvious based on efficiency calculations alone. The uncertainty analysis of wall-static averaging will give better insight for the averaging results.

3.3.2 Circular Exit Volute Test

The turbine inlet mapping (Figures 3.22 and 3.23) again had low gradients as expected. The OTTR ADP inlet values for the circular volute test are given in Table 3.14. The area averaged inlet properties given were used for all efficiency calculation cases for the turbine with the circular exit volute. The mass and area averaged properties of the turbine exit are given in Tables 3.15, 3.16, and 3.17. Note that the cobra and YC measurement reduction analyses without regression were not repeated for the circular volute test since no significant differences were noted for the square volute test. Again, the mass averaged properties of P_{02}, P_2, T_{02}, and M_2 were higher than the area averaged properties, whereas the area averaged a_2 was higher than the mass averaged a_2. Tables 3.16 and 3.17 show the cobra and YC average values. An analysis of the differences between the average properties and the "true" average properties for each case, similar to that done for the square exit volute, was done for the circular exit volute. The differences are given in Tables 3.18, 3.19, and 3.20. The trends of the circular volute average values were the same as those presented for the square volute. Hence, the impact that each average property had on the efficiency calculations based on the differences of values alone was not obvious. Therefore, the efficiency calculations were again studied. Note that the efficiency calculated with mass averaging 720-point measurements was assumed to be the "true" efficiency value.

The turbine efficiency with the circular exit volute was higher than the turbine efficiency with the square exit volute. The circular exit volute was designed to match the turbine exit flow field; hence, a better efficiency was expected. The conclusions made for mass versus area averaging were similar to those for the square exit volute test. In addition, uncertainty analysis of mass versus area averaging will give more insight.

The efficiency calculations did not vary significantly from the "true" value for any of the cobra or YC cases (Tables 3.22 and 3.23). The cobra and YC mass averaged values were unpredictable (Tables 3.19 and 3.20). The assumption made in Section 3.2.1 concerning the highest gradient coverage could be the reason for the unpredictable variations of the averaged values for the cobra and YC measurements. The opposite effects of the averaged properties on the efficiency calculations could explain why the calculated efficiencies are so close to the same number. For the circular volute test, the cobra probes covered more of the highest gradient section of the exit plane. The cobra probe mapping covered 85.5% of the highest gradient section while the YC only covered 14.5%, yet the results from both showed little change in efficiency. The small differences in the efficiency calculations may be attributed to the lower gradients in the circular exit volute compared to that of the square exit volute. All of these ideas will be addressed in Chapter 5.

The major observation made for the efficiency comparisons for the circular volute test was that the difference between each case and the "true" values were small. The turbine exit flow field with the circular volute had smaller gradients than that of the square volute test. This may have caused the averaged values to be closer to the "true" values. Again, uncertainty analyses will better explain the efficiency results.

Table 3.24 shows the efficiency results of CWA and NWA for the square exit volute case. The results are similar to the efficiency results in Table 3.21. Again, the efficiency results of CWA and NWA do not appear to be affected, and the impact of wall-static averaging was not obvious based on efficiency calculations alone. The wall-static averaging will be analyzed using uncertainty analysis in Chapter 5.

Table 3.1 Control Area for each Turbine Test Case

Number of Point Measurements	**Control Area**
720-point measurements	0.0545 in^2
360-point measurements	0.1090 in^2
180-point measurements	0.2180 in^2
90-point measurements	0.4360 in^2

Table 3.2 Flow Field Gradients

Variables	**Gradient (%)**	
	Square	**Circular**
Inlet Total Pressure	7.0	7.2
Inlet Total Temperature	0.6	0.6
Exit Total Pressure	37.6	29.6
Exit Total Temperature	4.0	3.6
Exit Static Pressure	58.1	35.9
Exit Flow Angle	52.3	37.3

Table 3.3 OTTR ADP Inlet Values (Square Volute)

Inlet Conditions	
P_{01} (psia)	99.80
T_{01} ($^{\circ}R$)	559.03
N (RPM)	3754.36
Pr	1.84
$\dot{W}$	11.47
Tq	243.87
Power (Hp)	174.32

Table 3.4 OTTR ADP Average Values (Square Volute with 360° Circumferential Coverage)

OTTR with Square Exit Volute Data Reduction		**720 Points**	**360 Points**	**180 Points**	**90 Points**
Mass Avg.	P_{02} (psia)	59.72	59.73	59.74	59.83
	P_2 (psia)	43.36	43.47	43.44	43.39
	T_{02} ($^{\circ}R$)	507.61	507.57	507.58	507.48
	a_2 ($^{\circ}$)	68.96	68.24	68.35	68.36
	M_2	0.6879	0.6852	0.6861	0.6892
Area Avg.	P_{02} (psia)	57.53	57.52	57.51	57.54
	P_2 (psia)	43.11	43.17	43.17	43.18
	T_{02} ($^{\circ}R$)	505.40	505.37	505.35	505.18
	a_2 ($^{\circ}$)	72.28	71.79	71.91	71.96
	M_2	0.6393	0.6371	0.6364	0.6360

Table 3.5 OTTR ADP Average Values (Square Volute with Cobra Quadrants Coverage)

OTTR with Square Exit Volute Data Reduction (Cobra Probes)		**720 Points**	**w/ Cobra Only**	**Cobra 720 Pt (Reg.)**	**Cobra 360 Pt (Reg.)**	**Cobra 180 Pt (Reg.)**	**Cobra 90 Pt (Reg.)**
Mass Avg.	P_{02} (psia)	59.72	60.46	60.46	60.49	60.46	60.47
	P_2 (psia)	43.36	43.61	43.61	43.61	43.62	43.62
	T_{02} ($^{\circ}R$)	507.61	508.30	508.30	508.31	508.30	508.14
	a_2 ($^{\circ}$)	68.96	68.63	68.63	68.68	68.64	68.62
	M_2	0.6879	0.6961	0.6961	0.6966	0.6958	0.6962
Area Avg.	P_{02} (psia)	57.53	57.99	57.99	57.99	57.99	57.98
	P_2 (psia)	43.11	43.14	43.14	43.15	43.15	43.16
	T_{02} ($^{\circ}R$)	505.40	505.59	505.59	505.59	505.60	505.42
	a_2 ($^{\circ}$)	72.28	72.83	72.83	72.83	72.85	72.87
	M_2	0.6393	0.6207	0.6507	0.6507	0.6506	0.6502

Table 3.6 OTTR ADP Average Values (Square Volute with YC Quadrants Coverage)

OTTR with Square Exit Volute Data Reduction (YC Probes)		**720 Points**	**w/ YC Only**	**YC 720 Pt (Reg.)**	**YC 360 Pt (Reg.)**	**YC 180 Pt (Reg.)**	**YC 90 Pt (Reg.)**
Mass Avg.	P_{02} (psia)	59.72	59.31	59.80	59.82	59.80	59.78
	P_2 (psia)	43.36	41.47	42.96	42.97	42.93	42.80
	T_{02} ($^\circ R$)	507.61	507.20	507.74	507.76	507.74	507.70
	a_2 ($^\circ$)	68.96	69.85	69.61	69.65	69.61	69.44
	M_2	0.6879	0.7285	0.6999	0.6998	0.7006	0.7040
Area Avg.	P_{02} (psia)	57.53	57.54	57.69	57.69	57.68	57.69
	P_2 (psia)	43.11	41.44	42.67	42.69	42.66	42.58
	T_{02} ($^\circ R$)	505.40	505.52	505.67	505.67	505.67	505.62
	a_2 ($^\circ$)	72.28	72.29	72.82	72.82	72.82	72.65
	M_2	0.6393	0.6896	0.6573	0.6567	0.6575	0.6594

Table 3.7 Difference of Average Values (Square Volute with 360° Circumferential Coverage)

Difference of Properties (OTTR with Square Exit Volute)		**720 Points**	**360 Points**	**180 Points**	**90 Points**
Mass Avg.	P_{02} (psia)	0.0000	-0.0063	-0.0205	-0.1017
	P_2 (psia)	0.0000	-0.1087	-0.0876	-0.0372
	T_{02} ($^\circ R$)	0.0000	0.0383	0.0322	0.1335
	a_2 ($^\circ$)	0.0000	0.7262	0.6146	0.6004
	M_2	0.0000	0.0027	0.0018	-0.0014
Area Avg.	P_{02} (psia)	2.1941	2.2043	2.2186	2.1834
	P_2 (psia)	0.2471	0.1890	0.1911	0.1807
	T_{02} ($^\circ R$)	2.2121	2.2390	2.2619	2.4239
	a_2 ($^\circ$)	-3.3220	-2.8323	-2.9459	-3.0017
	M_2	0.0486	0.0508	0.0515	0.0519

Table 3.8 Difference of Average Values (Square Volute with Cobra Quadrants Coverage)

Difference of Properties (OTTR with Square Exit Volute, Cobra Probes)		**w/ Cobra Only**	**Cobra 720 Pt (Reg.)**	**Cobra 360 Pt (Reg.)**	**Cobra 180 Pt (Reg.)**	**Cobra 90 Pt (Reg.)**
Mass Avg.	P_{02} (psia)	-0.6554	-0.7370	-0.7616	-0.7362	-0.7439
	P_2 (psia)	-1.4015	-0.2545	-0.2534	-0.2667	-0.2581
	T_{02} ($^\circ R$)	-0.9676	-0.6870	-0.7049	-0.6939	-0.5286
	a_2 ($^\circ$)	0.1177	0.3301	0.2835	0.3183	0.3465
	M_2	0.0238	-0.0082	-0.0088	-0.0079	-0.0083
Area Avg.	P_{02} (psia)	1.7710	1.7359	1.7358	1.7372	1.7454
	P_2 (psia)	-0.7461	0.2135	0.2118	0.2087	0.1968
	T_{02} ($^\circ R$)	1.8057	2.0151	2.0177	2.0064	2.1873
	a_2 ($^\circ$)	-4.0506	-3.8730	-3.8699	-3.8886	-3.9097
	M_2	0.0654	0.0371	0.0372	0.0372	0.0377

Table 3.9 Difference of Average Values (Square Volute with YC Quadrants Coverage)

Difference of Properties (OTTR with Square Exit Volute, YC Probes)		**w/ YC Only**	**YC 720 Pt (Reg.)**	**YC 360 Pt (Reg.)**	**YC 180 Pt (Reg.)**	**YC 90 Pt (Reg.)**
Mass Avg.	P_{02} (psia)	0.4128	-0.0797	-0.0911	-0.0748	-0.0600
	P_2 (psia)	1.8852	0.3988	0.3835	0.4235	0.5598
	T_{02} ($^\circ R$)	0.4134	-0.1360	-0.1472	-0.1319	-0.0864
	a_2 ($^\circ$)	-0.8880	-0.6485	-0.6865	-0.6445	-0.4816
	M_2	-0.0407	-0.0121	-0.0119	-0.0127	-0.0161
Area Avg.	P_{02} (psia)	2.1808	2.0346	2.0353	2.0431	2.0391
	P_2 (psia)	1.9204	0.6828	0.6629	0.6996	0.7770
	T_{02} ($^\circ R$)	2.0870	1.9357	1.9382	1.9427	1.9874
	a_2 ($^\circ$)	-3.3305	-3.8574	-3.8618	-3.8577	-3.6835
	M_2	-0.0017	0.0306	0.0311	0.0304	0.0284

Table 3.10 OTTR ADP Performance Results (Square Volute with 360° Circumferential Coverage)

Efficiency Calculation (Square Exit Volute)		720 Points	360 Points	180 Points	90 Points
Mass Avg. 1104-1202	η Thermo t-t	0.646	0.646	0.647	0.650
	η Mech t-t	0.604	0.604	0.604	0.606
	η Thermo t-s	0.412	0.413	0.413	0.414
	η Mech t-s	0.385	0.386	0.386	0.385
Area Avg. 1104-1202	η Thermo t-t	0.632	0.632	0.632	0.635
	η Mech t-t	0.565	0.564	0.564	0.565
	η Thermo t-s	0.428	0.429	0.429	0.431
	η Mech t-s	0.383	0.383	0.383	0.383

Table 3.11 OTTR ADP Performance Results (Square Volute with Cobra Quadrants Coverage)

Efficiency Calculation (Square Exit Volute)		720 Points	w/ Cobra Only	Cobra 720 Pt (Reg.)	Cobra 360 Pt (Reg.)	Cobra 180 Pt (Reg.)	Cobra 90 Pt (Reg.)
Mass Avg. 1104-1202	η Thermo t-t	0.646	0.646	0.651	0.652	0.651	0.654
	η Mech t-t	0.604	0.616	0.618	0.618	0.618	0.618
	η Thermo t-s	0.412	0.418	0.409	0.408	0.409	0.410
	η Mech t-s	0.385	0.399	0.387	0.387	0.388	0.388
Area Avg. 1104-1202	η Thermo t-t	0.632	0.635	0.638	0.638	0.638	0.640
	η Mech t-t	0.565	0.572	0.572	0.572	0.572	0.572
	η Thermo t-s	0.428	0.436	0.427	0.427	0.427	0.429
	η Mech t-s	0.383	0.392	0.383	0.383	0.383	0.383

Table 3.12 OTTR ADP Performance Results (Square Volute with YC Quadrants Coverage)

Efficiency Calculation (Square Exit Volute)		**720 Points**	**W/ YC Only**	**YC 720 Pt (Reg.)**	**YC 360 Pt (Reg.)**	**YC 180 Pt (Reg.)**	**YC 90 Pt (Reg.)**
Mass Avg. 1104-1202	η Thermo t-t	0.646	0.643	0.645	0.646	0.645	0.646
	η Mech t-t	0.604	0.596	0.605	0.605	0.605	0.605
	η Thermo t-s	0.412	0.396	0.407	0.407	0.406	0.405
	η Mech t-s	0.385	0.368	0.381	0.381	0.381	0.380
Area Avg. 1104-1202	η Thermo t-t	0.632	0.631	0.632	0.632	0.632	0.632
	η Mech t-t	0.565	0.565	0.567	0.567	0.567	0.567
	η Thermo t-s	0.428	0.410	0.421	0.422	0.421	0.421
	η Mech t-s	0.383	0.367	0.379	0.379	0.378	0.378

Table 3.13 OTTR ADP Performance Results (Square Volute NWA and CWA)

Efficiency Calculation (Square Exit Volute)		**720 Pt**	**360 Pt**	**180 Pt**	**90 Pt**
Mass Avg.	h_{th} (True)	0.646	0.646	0.647	0.650
	h_{me} (True)	0.604	0.604	0.604	0.606
	h_{th} (CWA)	0.649	0.645	0.649	0.652
	h_{me} (CWA)	0.606	0.605	0.606	0.607
	h_{th} (NWA)	0.648	0.646	0.648	0.651
	h_{me} (NWA)	0.604	0.604	0.604	0.605

Table 3.14 OTTR ADP Inlet Values (Circular Volute)

Inlet Conditions	
P_{01} (psia)	99.97
T_{01} ($^{\circ}R$)	557.36
N (RPM)	3755.22
Pr	1.93
$\dot{W}$	11.54
Tq	242.85
Power (Hp)	173.64

Table 3.15 OTTR ADP Average Values (Circular Volute with 360° Circumferential Coverage)

OTTR with Circular Exit Volute Data Reduction		**720 Points**	**360 Points**	**180 Points**	**90 Points**
Mass Avg.	P_{02} (psia)	60.79	60.79	60.79	60.85
	P_2 (psia)	42.37	42.38	42.35	42.38
	T_{02} ($^{\circ}R$)	506.74	506.77	506.77	506.78
	a_2 ($^{\circ}$)	71.12	71.13	71.11	71.04
	M_2	0.7341	0.7338	0.7347	0.7348
Area Avg.	P_{02} (psia)	58.96	58.96	58.96	59.02
	P_2 (psia)	42.18	42.18	42.16	42.16
	T_{02} ($^{\circ}R$)	504.90	504.93	504.92	504.91
	a_2 ($^{\circ}$)	73.56	73.57	73.55	73.52
	M_2	0.7007	0.7006	0.7013	0.7024

Table 3.16 OTTR ADP Average Values (Circular Volute with Cobra Quadrants Coverage)

OTTR with Circular Exit Volute Data Reduction (Cobra Probes)		**720 Points**	**Cobra 720 Pt (Reg.)**	**Cobra 360 Pt (Reg.)**	**Cobra 180 Pt (Reg.)**	**Cobra 90 Pt (Reg.)**
Mass Avg.	P_{02} (psia)	60.79	60.81	60.81	60.82	60.85
	P_2 (psia)	42.37	42.60	42.59	42.58	42.62
	T_{02} ($^\circ R$)	506.74	506.77	506.79	506.79	506.79
	a_2 ($^\circ$)	71.12	71.50	71.54	71.49	71.50
	M_2	0.7341	0.7289	0.7291	0.7297	0.7293
Area Avg.	P_{02} (psia)	58.96	58.91	58.91	58.92	58.95
	P_2 (psia)	42.18	42.27	42.27	42.25	42.26
	T_{02} ($^\circ R$)	504.90	504.81	504.82	504.83	504.81
	a_2 ($^\circ$)	73.56	73.97	73.98	73.97	74.04
	M_2	0.7007	0.6985	0.6986	0.6993	0.6996

Table 3.17 OTTR ADP Average Values (Circular Volute with YC Quadrants Coverage)

OTTR with Circular Exit Volute Data Reduction (YC Probes)		**720 Points**	**YC 720 Pt (Reg.)**	**YC 360 Pt (Reg.)**	**YC 180 Pt (Reg.)**	**YC 90 Pt (Reg.)**
Mass Avg.	P_{02} (psia)	60.79	60.72	60.72	60.71	60.71
	P_2 (psia)	42.37	41.36	41.37	41.36	41.37
	T_{02} ($^\circ R$)	506.74	506.78	506.79	506.79	506.75
	a_2 ($^\circ$)	71.12	71.03	71.05	71.02	70.96
	M_2	0.7341	0.7580	0.7578	0.7579	0.7578
Area Avg.	P_{02} (psia)	58.96	58.92	58.92	58.91	58.93
	P_2 (psia)	42.18	41.29	41.30	41.29	41.29
	T_{02} ($^\circ R$)	504.90	504.90	504.92	504.91	504.87
	a_2 ($^\circ$)	73.56	73.26	73.26	73.24	73.16
	M_2	0.7007	0.7224	0.7223	0.7223	0.7225

Table 3.18 Difference of Average Values (Circular Volute with 360° Circumferential Coverage)

Difference of Properties (OTTR with Circular Exit Volute)		**720 Points**	**360 Points**	**180 Points**	**90 Points**
Mass Avg.	P_{02} (psia)	0.0000	-0.0003	0.0006	-0.0586
	P_2 (psia)	0.0000	-0.0107	0.0227	-0.0110
	T_{02} ($^\circ R$)	0.0000	-0.0231	-0.0229	-0.0339
	a_2 ($^\circ$)	0.0000	-0.0150	0.0118	0.0818
	M_2	0.0000	0.0003	-0.0006	-0.0007
Area Avg.	P_{02} (psia)	1.8349	1.8347	1.8330	1.7708
	P_2 (psia)	0.1939	0.1898	0.2149	0.2113
	T_{02} ($^\circ R$)	1.8393	1.8165	1.8218	1.8326
	a_2 ($^\circ$)	-2.4425	-2.4534	-2.4294	-2.4050
	M_2	0.0334	0.0335	0.0328	0.0317

Table 3.19 Difference of Average Values (Circular Volute with Cobra Quadrants Coverage)

Difference of Properties (OTTR with Circular Exit Volute, Cobra Probes)		**Cobra 720 Pt (Reg.)**	**Cobra 360 Pt (Reg.)**	**Cobra 180 Pt (Reg.)**	**Cobra 90 Pt (Reg.)**
Mass Avg.	P_{02} (psia)	-0.0197	-0.0208	-0.0296	-0.0605
	P_2 (psia)	-0.2294	-0.2219	-0.2038	-0.2455
	T_{02} ($^\circ R$)	-0.0319	-0.0492	-0.0499	-0.0454
	a_2 ($^\circ$)	-0.3780	-0.4187	-0.3725	-0.3820
	M_2	0.0052	0.0050	0.0044	0.0048
Area Avg.	P_{02} (psia)	1.8786	1.8785	1.8710	1.8452
	P_2 (psia)	0.0987	0.1016	0.1233	0.1148
	T_{02} ($^\circ R$)	1.9317	1.9208	1.9161	1.9299
	a_2 ($^\circ$)	-2.8564	-2.8638	-2.8527	-2.9196
	M_2	0.0356	0.0355	0.0348	0.0345

Table 3.20 Difference of Average Values (Circular Volute with YC Quadrants Coverage)

Difference of Properties (OTTR with Circular Exit Volute, YC Probes)		**YC 720 Pt (Reg.)**	**YC 360 Pt (Reg.)**	**YC 180 Pt (Reg.)**	**YC 90 Pt (Reg.)**
Mass Avg.	P_{02} (psia)	0.0755	0.0759	0.0835	0.0797
	P_2 (psia)	1.0091	1.0019	1.0105	1.0076
	T_{02} ($^\circ R$)	-0.0413	-0.0510	-0.0483	-0.0112
	a_2 ($^\circ$)	0.0862	0.0696	0.0986	0.1529
	M_2	-0.0239	-0.0237	-0.0238	-0.0237
Area Avg.	P_{02} (psia)	1.8761	1.8731	1.8800	1.8643
	P_2 (psia)	1.0842	1.0746	1.0823	1.0785
	T_{02} ($^\circ R$)	1.8393	1.8260	1.8368	1.8708
	a_2 ($^\circ$)	-2.1373	-2.1442	-2.1238	-2.0465
	M_2	0.0117	0.0118	0.0118	0.0116

Table 3.21 OTTR ADP Performance Results (Circular Volute with 360° Circumferential Coverage)

Efficiency Calculation (Circular Exit Volute)		**720 Points**	**360 Points**	**180 Points**	**90 Points**
Mass Avg. 1104-1202	η Thermo t-t	0.662	0.662	0.662	0.663
	η Mech t-t	0.620	0.620	0.620	0.621
	η Thermo t-s	0.399	0.399	0.398	0.398
	η Mech t-s	0.373	0.373	0.373	0.373
Area Avg. 1104-1202	η Thermo t-t	0.650	0.650	0.650	0.651
	η Mech t-t	0.585	0.585	0.585	0.587
	η Thermo t-s	0.412	0.412	0.412	0.412
	η Mech t-s	0.371	0.371	0.371	0.371

Table 3.22 OTTR ADP Performance Results (Circular Volute with Cobra Quadrants Coverage)

Efficiency Calculation (Circular Exit Volute)		**720 Points**	**Cobra 720 Pt (Reg.)**	**Cobra 360 Pt (Reg.)**	**Cobra 180 Pt (Reg.)**	**Cobra 90 Pt (Reg.)**
Mass Avg. 1104-1202	η Thermo t-t	0.662	0.662	0.662	0.662	0.663
	η Mech t-t	0.620	0.620	0.620	0.620	0.621
	η Thermo t-s	0.399	0.401	0.400	0.400	0.401
	η Mech t-s	0.373	0.375	0.375	0.375	0.375
Area Avg. 1104-1202	η Thermo t-t	0.650	0.650	0.650	0.650	0.651
	η Mech t-t	0.585	0.585	0.585	0.585	0.585
	η Thermo t-s	0.412	0.414	0.414	0.414	0.414
	η Mech t-s	0.371	0.372	0.372	0.372	0.372

Table 3.23 OTTR ADP Performance Results (Circular Volute with YC Quadrants Coverage)

Efficiency Calculation (Circular Exit Volute)		**720 Points**	**YC 720 Pt (Reg.)**	**YC 360 Pt (Reg.)**	**YC 180 Pt (Reg.)**	**YC 90 Pt (Reg.)**
Mass Avg. 1104-1202	η Thermo t-t	0.662	0.660	0.660	0.660	0.661
	η Mech t-t	0.620	0.618	0.618	0.618	0.618
	η Thermo t-s	0.399	0.388	0.388	0.388	0.389
	η Mech t-s	0.373	0.364	0.364	0.364	0.364
Area Avg. 1104-1202	η Thermo t-t	0.650	0.649	0.649	0.649	0.650
	η Mech t-t	0.585	0.585	0.585	0.585	0.585
	η Thermo t-s	0.412	0.403	0.403	0.403	0.404
	η Mech t-s	0.371	0.363	0.363	0.363	0.363

Table 3.24 OTTR ADP Performance Results (Circular Volute NWA and CWA)

Efficiency Calculation (Circular Exit Volute)		**720 Pt**	**360 Pt**	**180 Pt**	**90 Pt**
Mass Avg.	h_{th} (True)	0.662	0.662	0.662	0.663
	h_{me} (True)	0.620	0.620	0.620	0.621
	h_{th} (CWA)	0.664	0.664	0.664	0.665
	h_{me} (CWA)	0.630	0.630	0.630	0.631
	h_{th} (NWA)	0.663	0.663	0.663	0.664
	h_{me} (NWA)	0.629	0.629	0.629	0.630

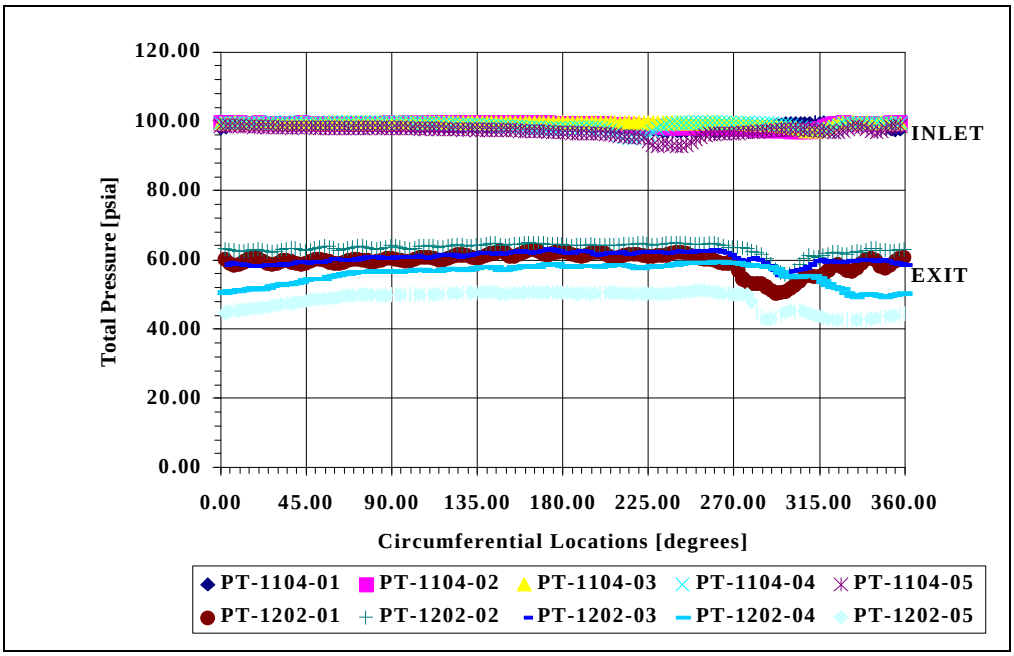

Figure 3.1 Turbine Inlet and Exit Total Pressure Distributions (Square Volute with 720-Points Circumferential Coverage)

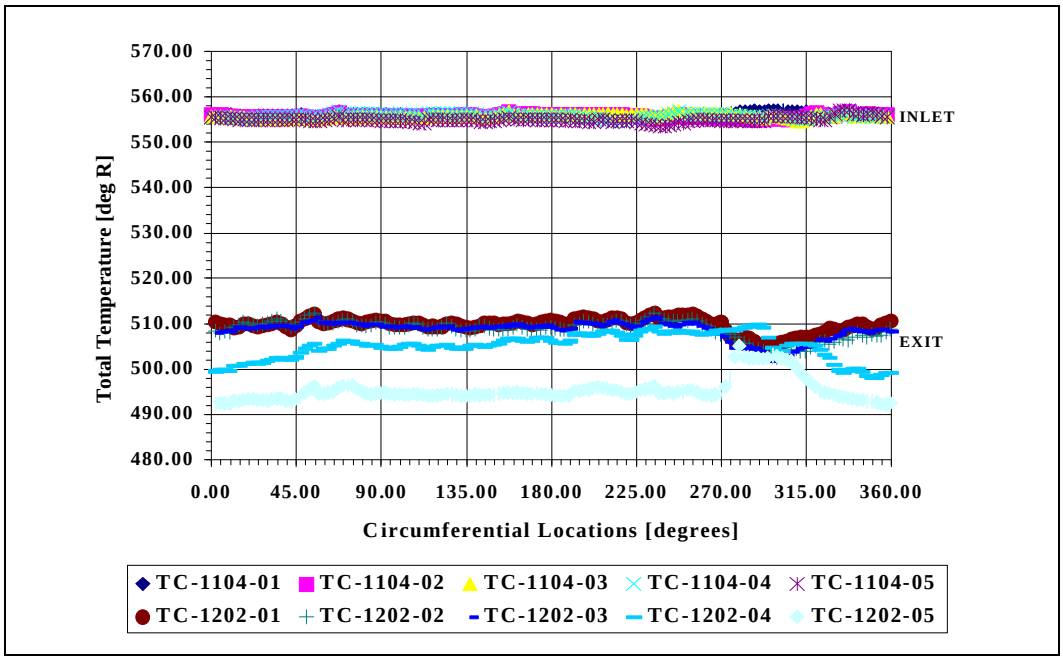

Figure 3.2 Turbine Inlet and Exit Total Temperature Distributions (Square Volute with 720-Points Circumferential Coverage)

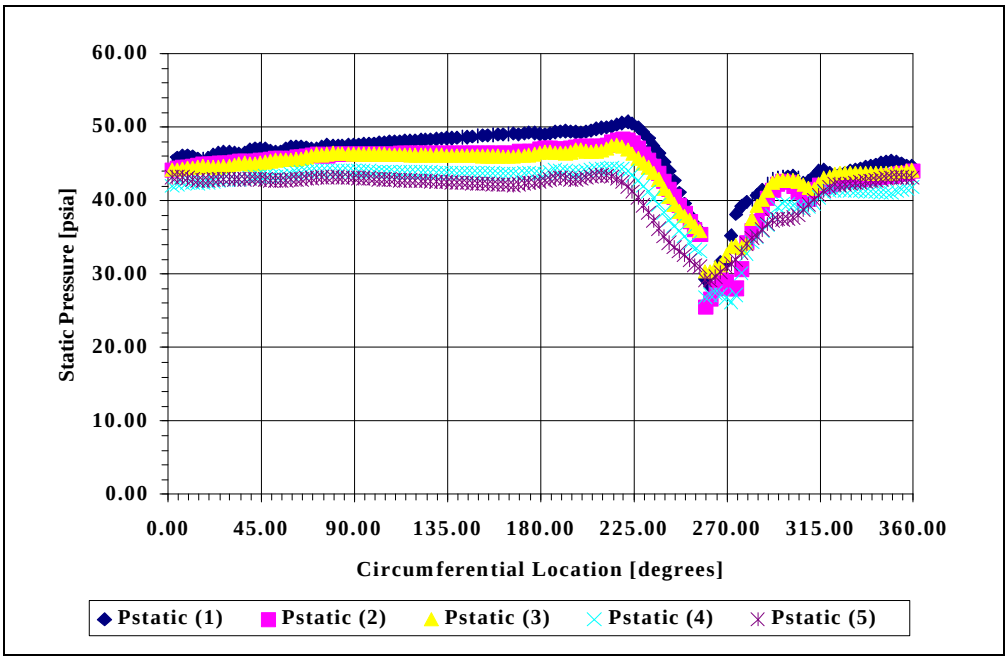

Figure 3.3 Turbine Exit Static Pressure Distribution (Square Volute with 720-Points Circumferential Coverage)

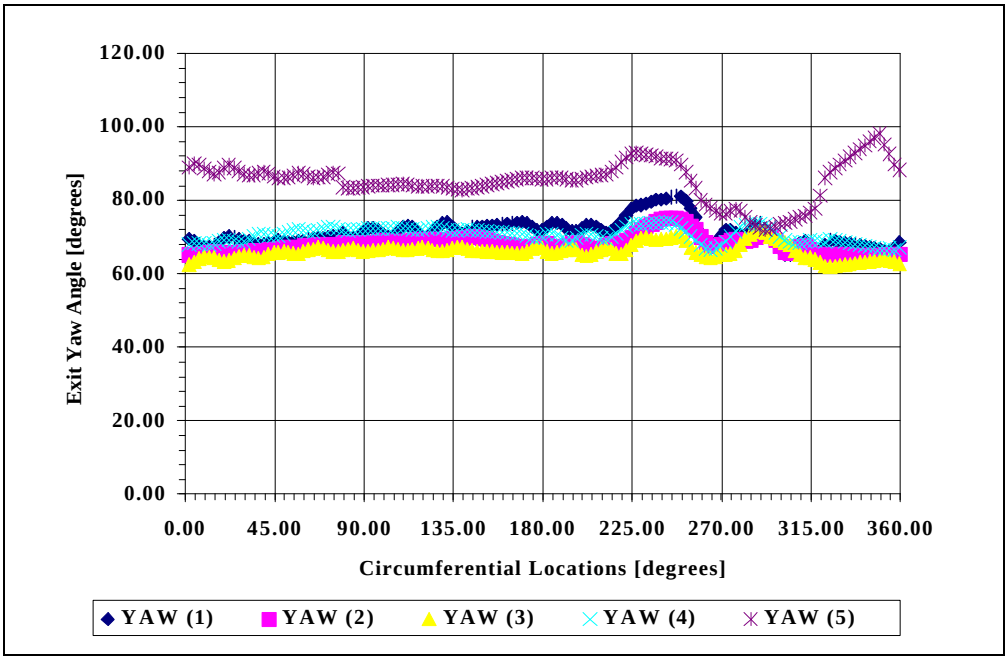

Figure 3.4 Turbine Exit Yaw Angle Distribution (Square Volute with 720-Points Circumferential Coverage)

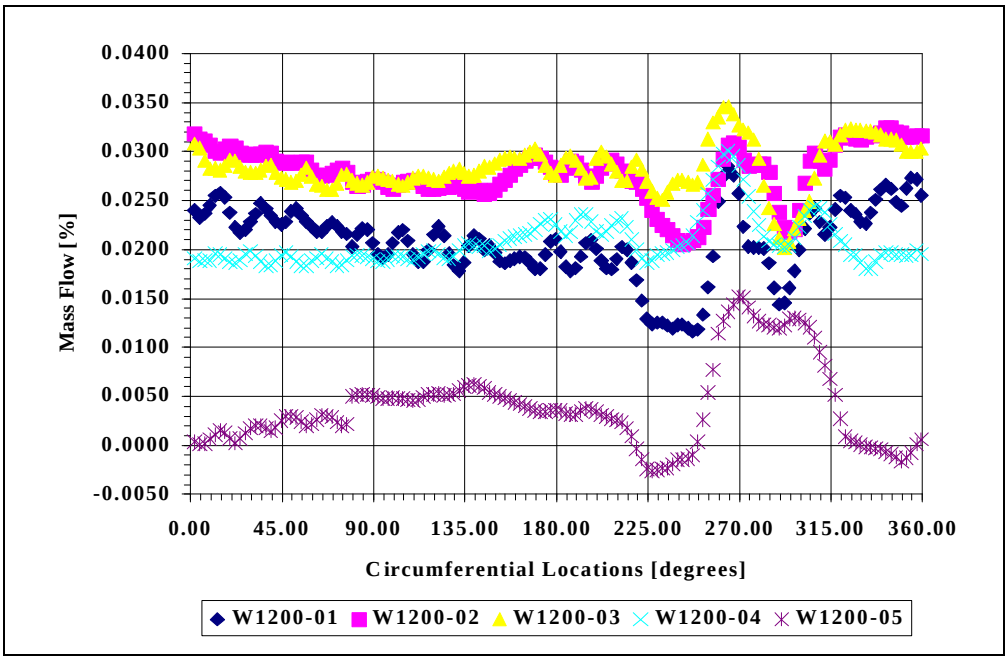

Figure 3.5 Turbine Exit Mass Flow Distribution (Square Volute with 720-Points Circumferential Coverage)

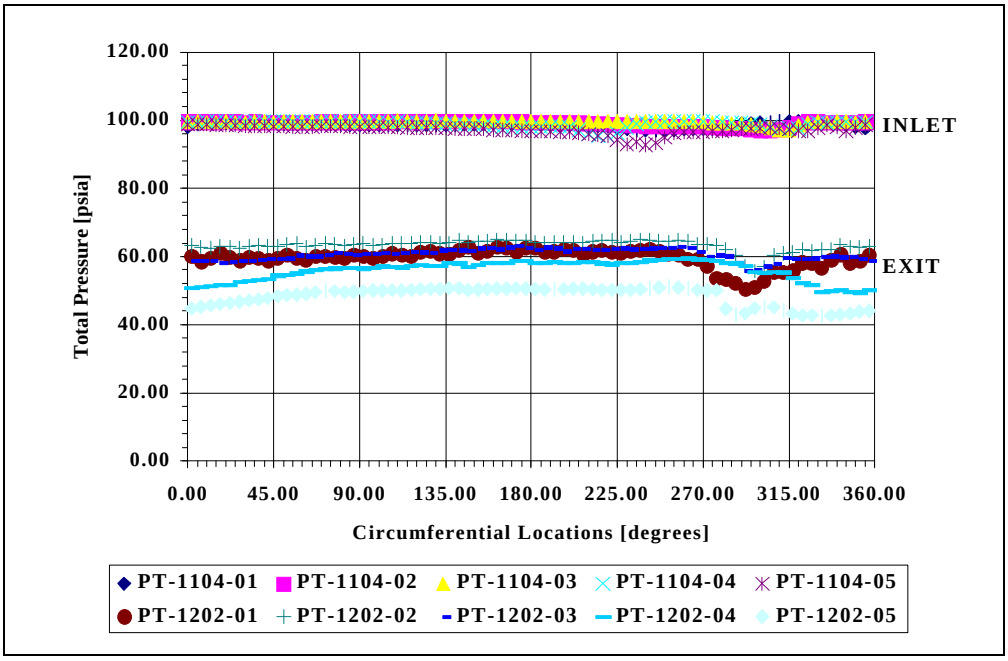

Figure 3.6 Turbine Inlet and Exit Total Pressure Distributions (Square Volute with 360-Points Circumferential Coverage)

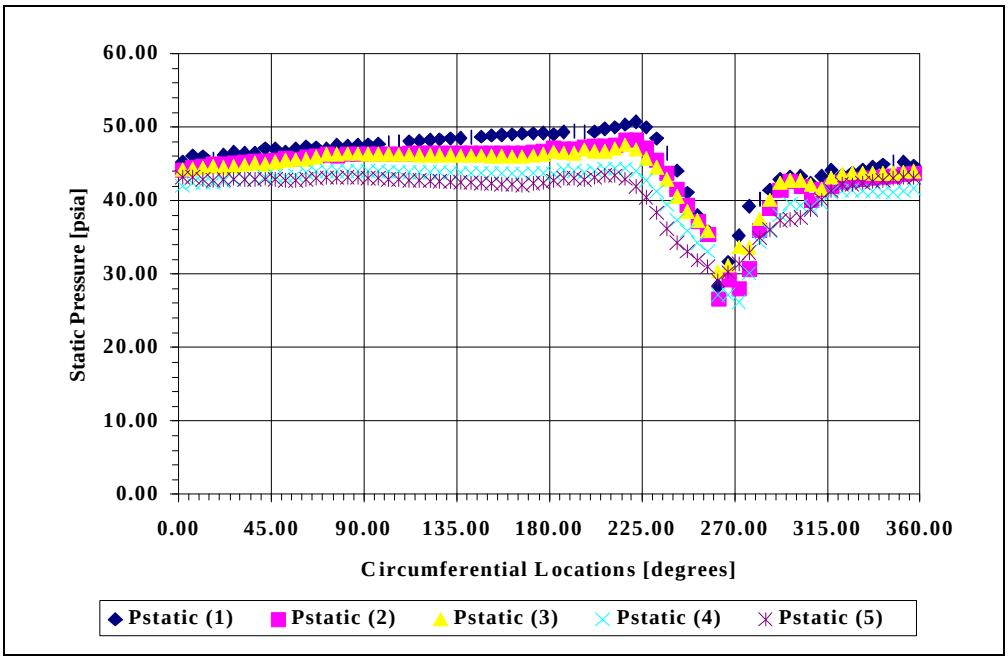

Figure 3.7 Turbine Exit Static Pressure Distribution (Square Volute with 360-Points Circumferential Coverage)

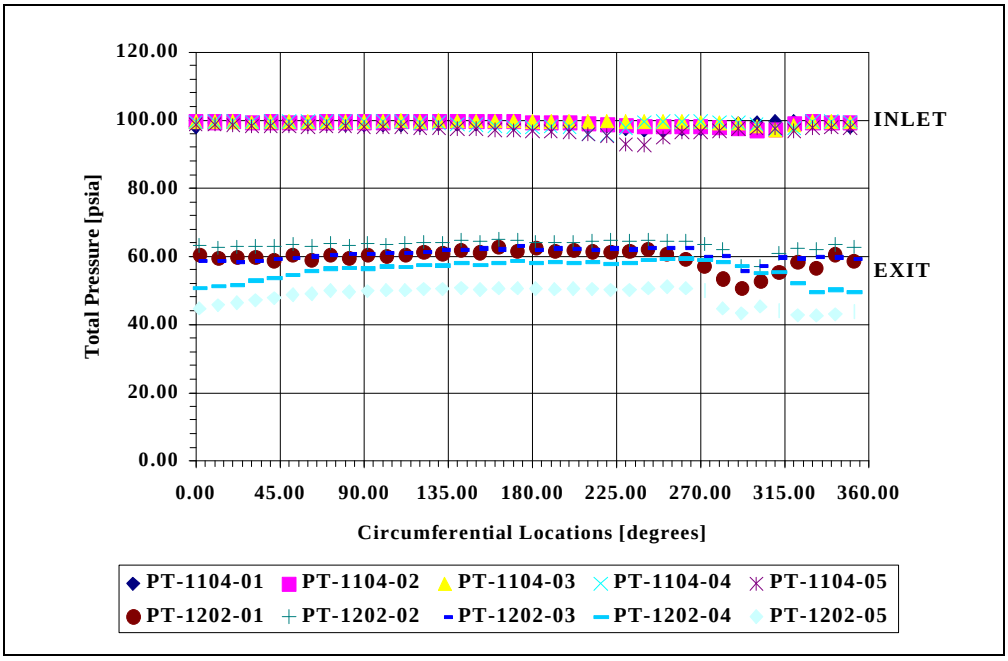

Figure 3.8 Turbine Inlet and Exit Total Pressure Distributions (Square Volute with 180-Points Circumferential Coverage)

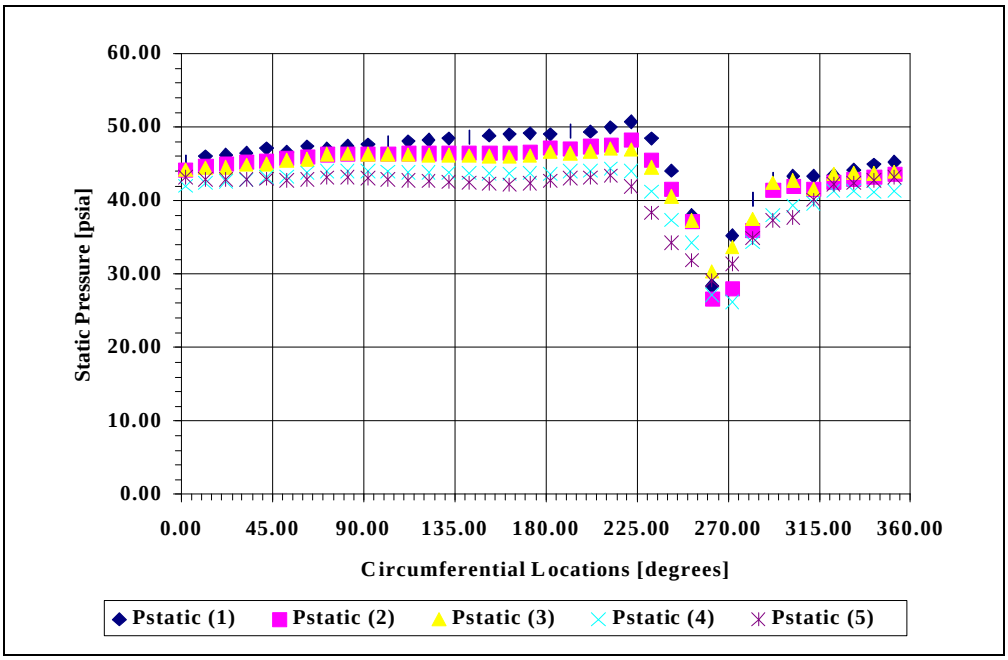

Figure 3.9 Turbine Exit Static Pressure Distribution (Square Volute with 180-Points Circumferential Coverage)

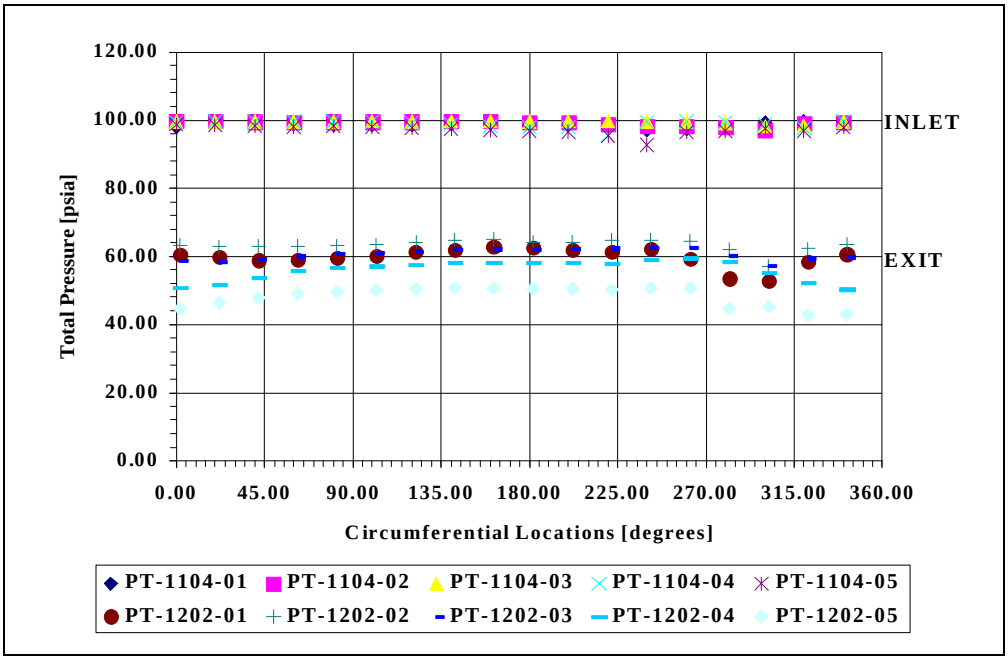

Figure 3.10 Turbine Inlet and Exit Total Pressure Distributions (Square Volute with 90-Points Circumferential Coverage)

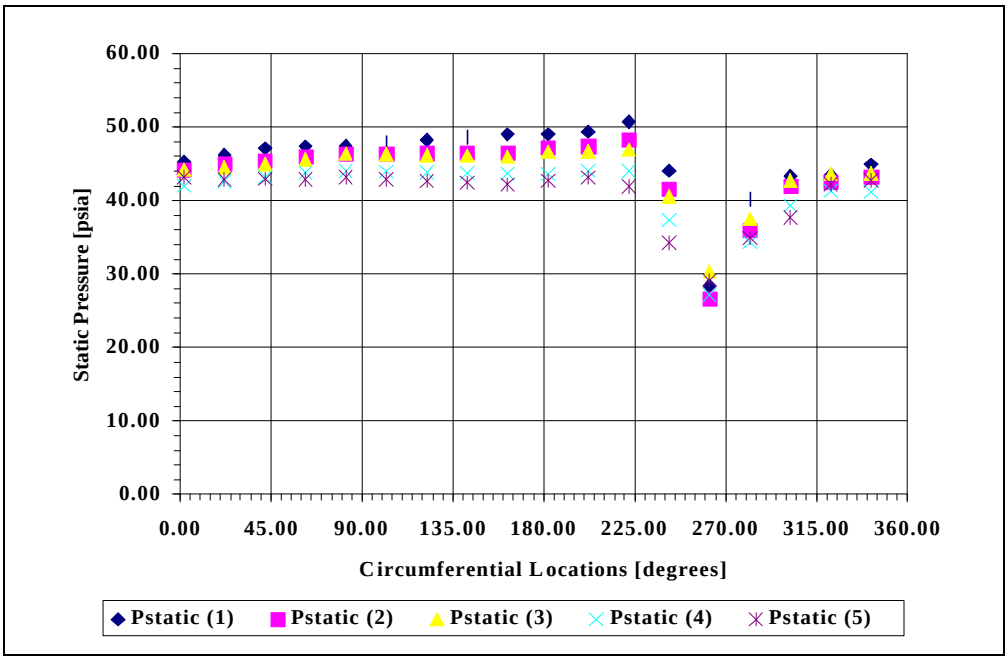

Figure 3.11 Turbine Exit Static Pressure Distribution (Square Volute with 90-Points Circumferential Coverage)

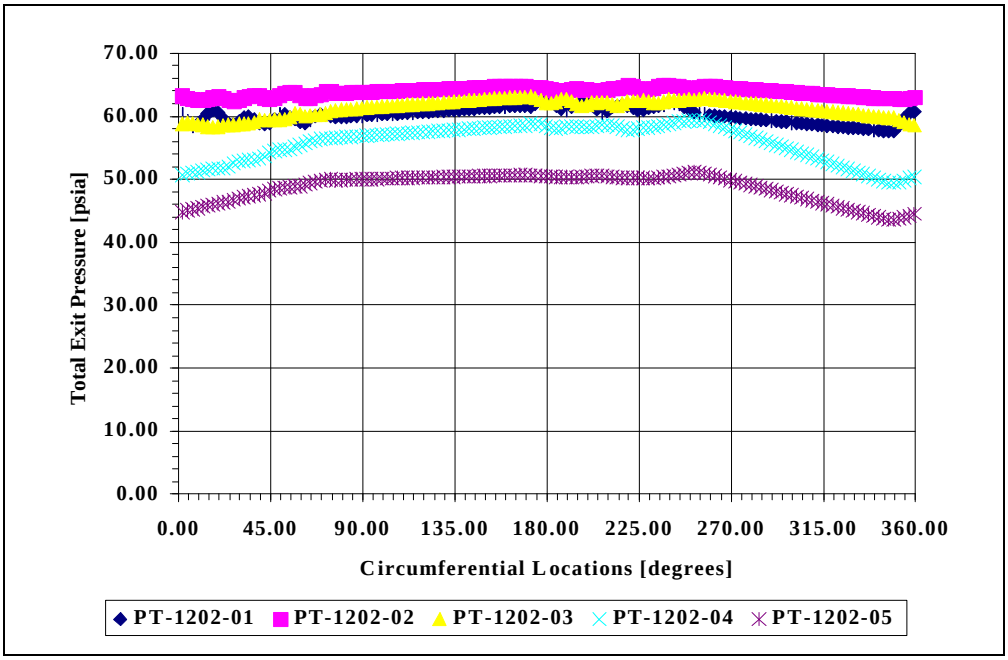

Figure 3.12 Turbine Exit Total Pressure Distribution (Square Volute with 720-Points Cobra Probe Quadrants Coverage)

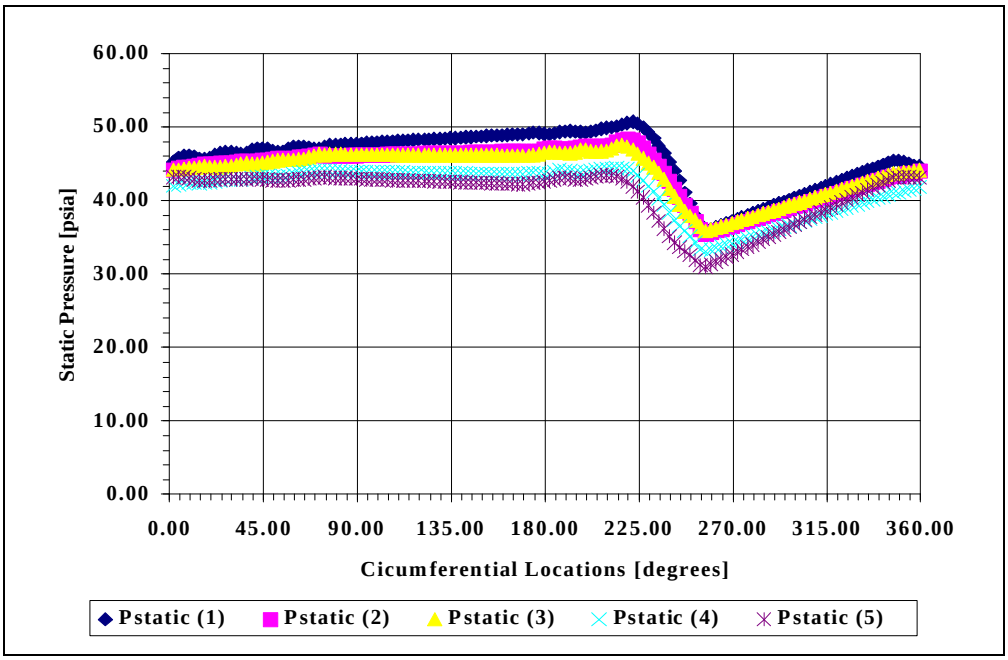

Figure 3.13 Turbine Exit Static Pressure Distribution (Square Volute with 720-Points Cobra Probe Quadrants Coverage)

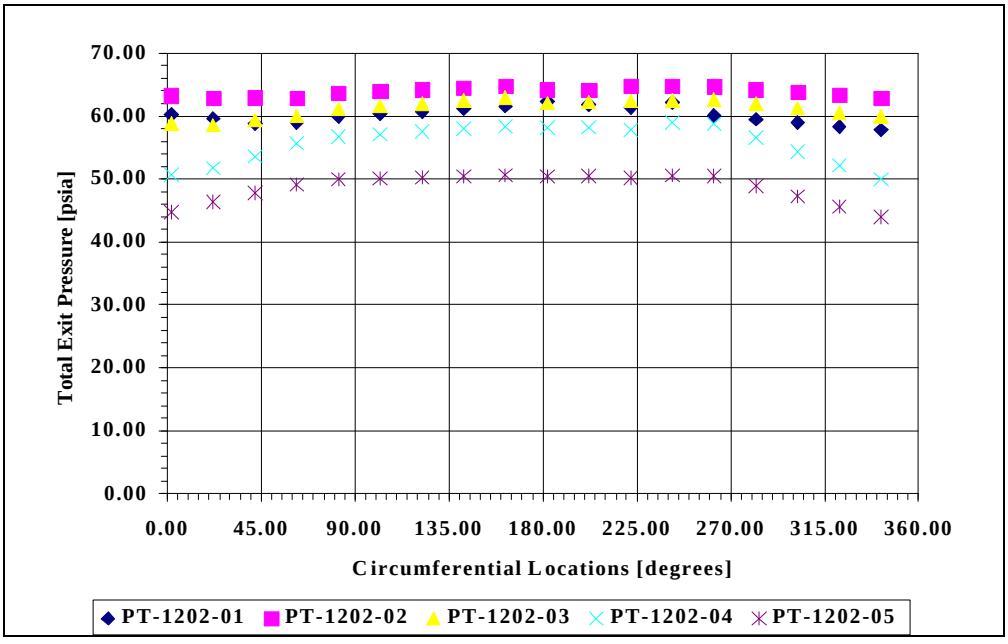

Figure 3.14 Turbine Exit Total Pressure Distribution (Square Volute with 90-Points Cobra Probe Quadrants Coverage)

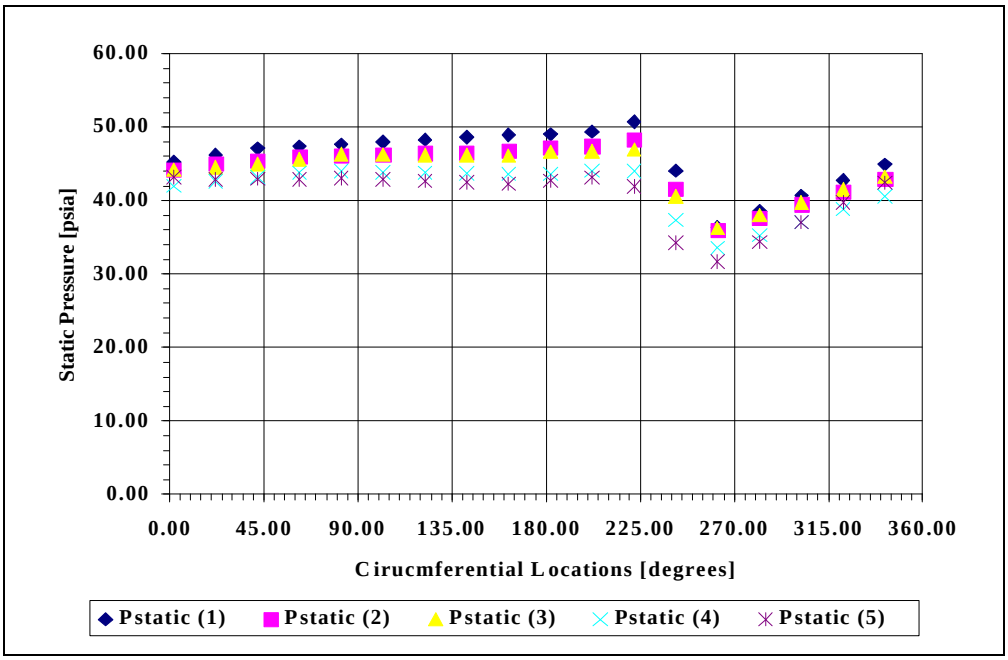

Figure 3.15 Turbine Exit Static Pressure Distribution (Square Volute with 90-Points Cobra Probe Quadrants Coverage)

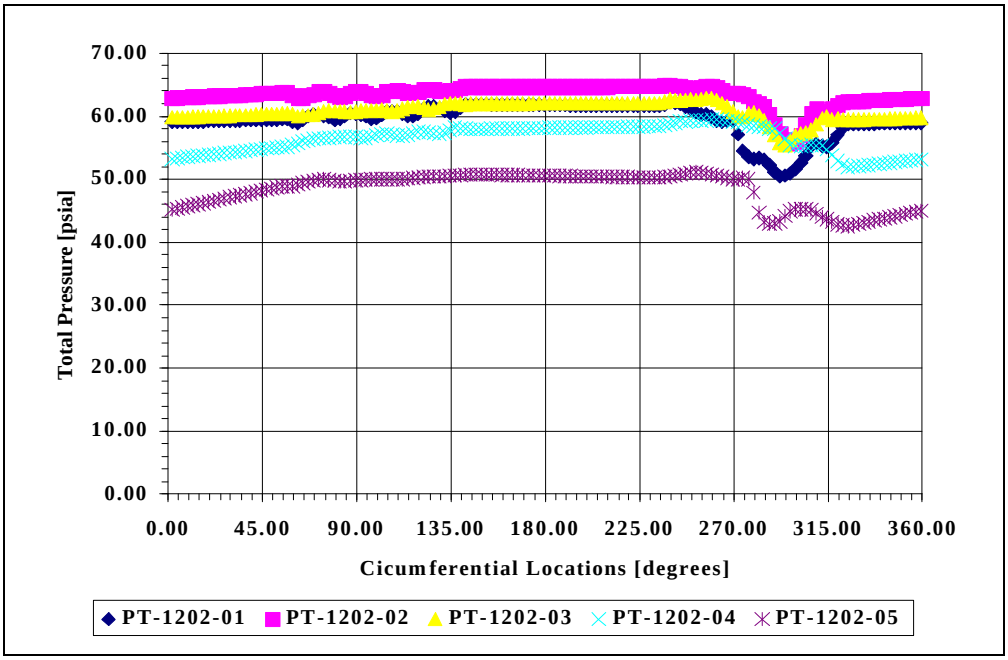

Figure 3.16 Turbine Exit Total Pressure Distribution (Square Volute with 720-Points YC Probe Quadrants Coverage)

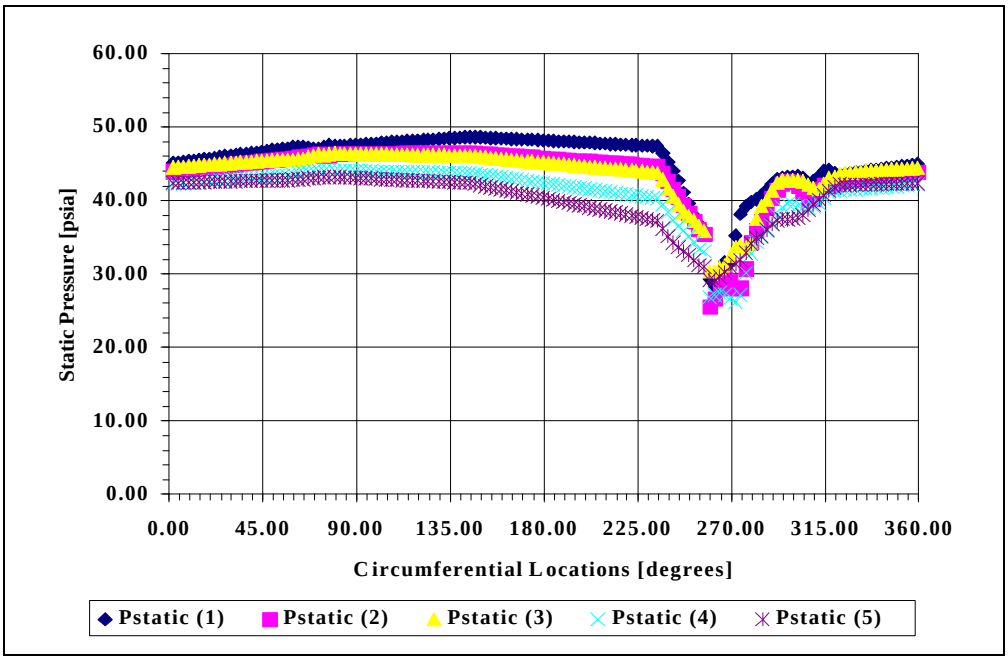

Figure 3.17 Turbine Exit Static Pressure Distribution (Square Volute with 720-Points YC Probe Quadrants Coverage)

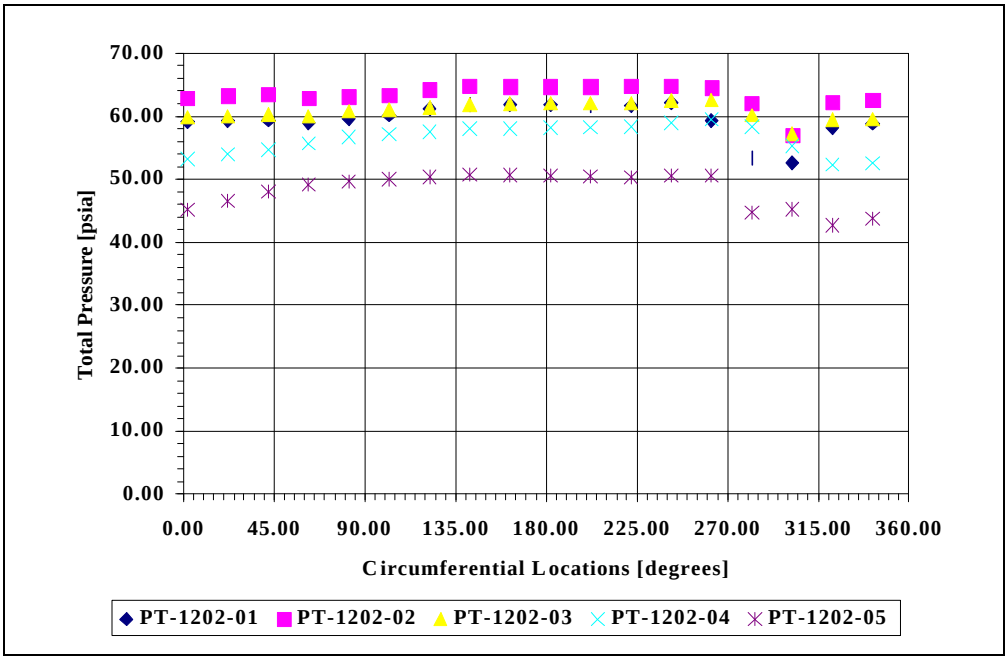

Figure 3.18 Turbine Exit Total Pressure Distribution (Square Volute with 90-Points YC Probe Quadrants Coverage)

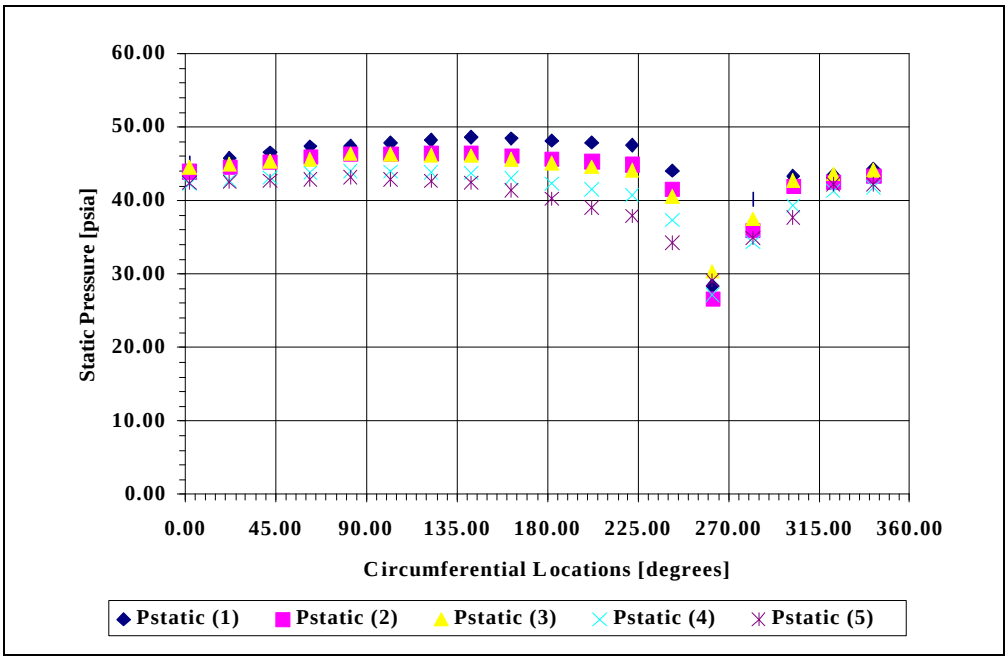

Figure 3.19 Turbine Exit Static Pressure Distribution (Square Volute with 90-Points YC Probe Quadrants Coverage)

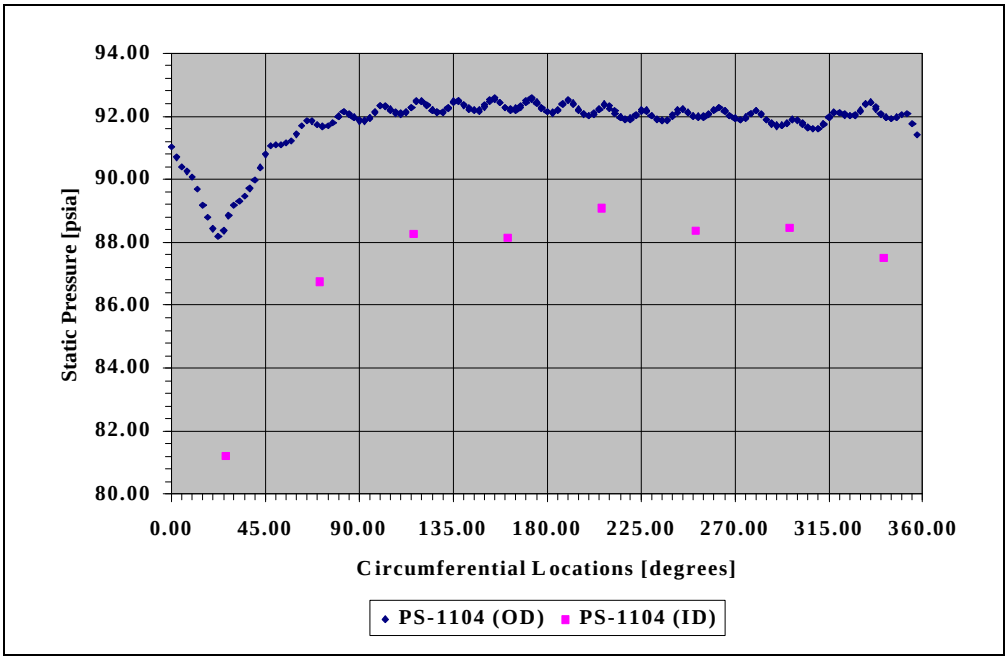

Figure 3.20 Turbine Inlet Wall-Static Pressure Distribution (Square Volute)

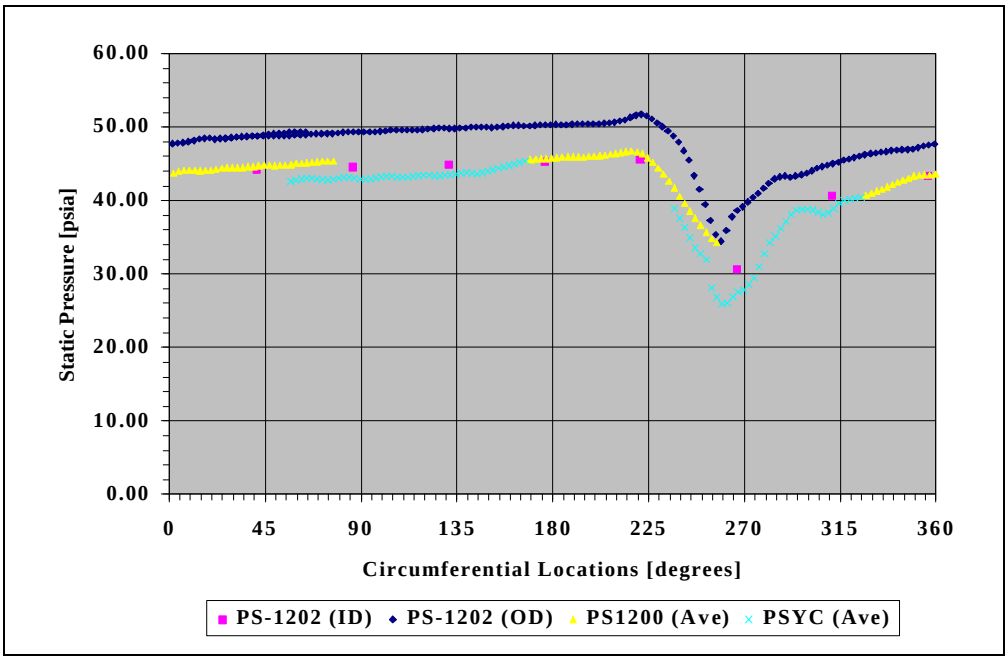

Figure 3.21 Turbine Exit Static Pressure Distribution (Square Volute)

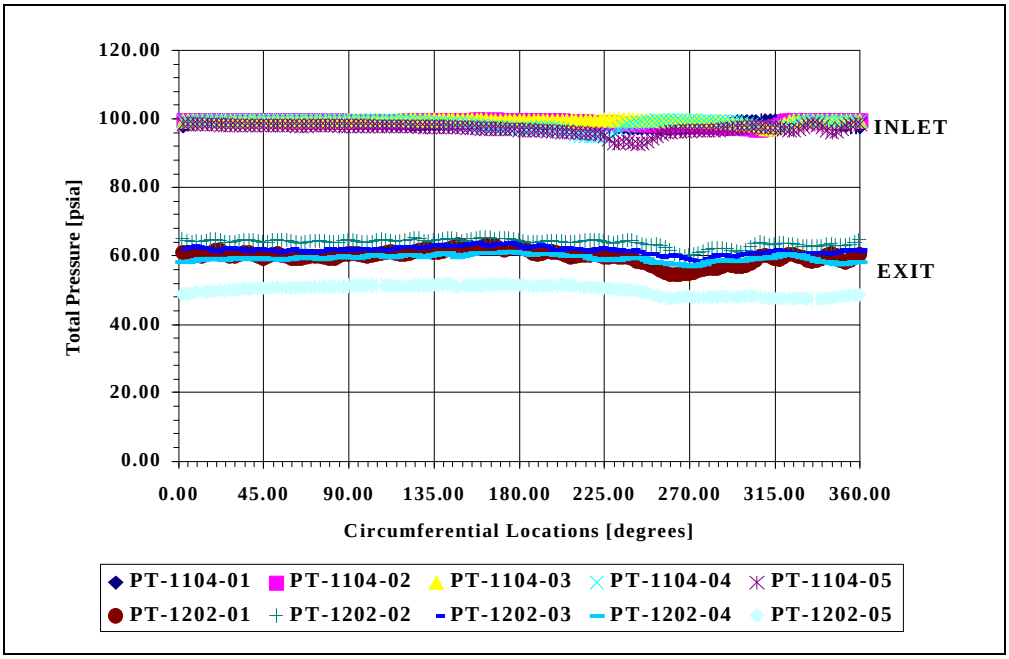

Figure 3.22 Turbine Inlet and Exit Total Pressure Distributions (Circular Volute with 720-Points Circumferential Coverage)

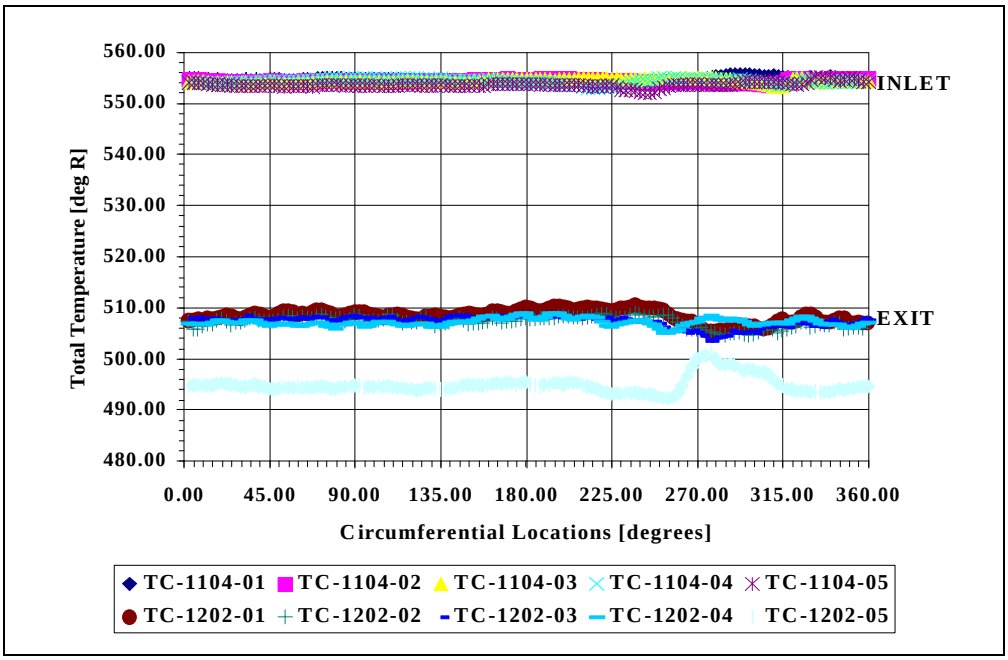

Figure 3.23 Turbine Inlet and Exit Total Temperature Distributions (Circular Volute with 720-Points Circumferential Coverage)

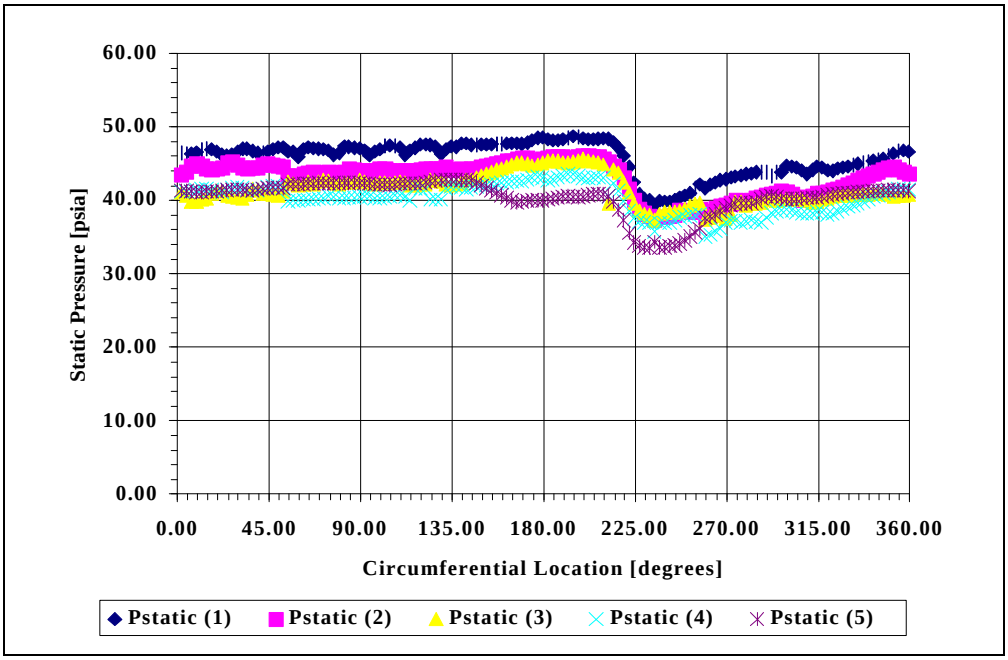

Figure 3.24 Turbine Exit Static Pressure Distribution (Circular Volute with 720-Points Circumferential Coverage)

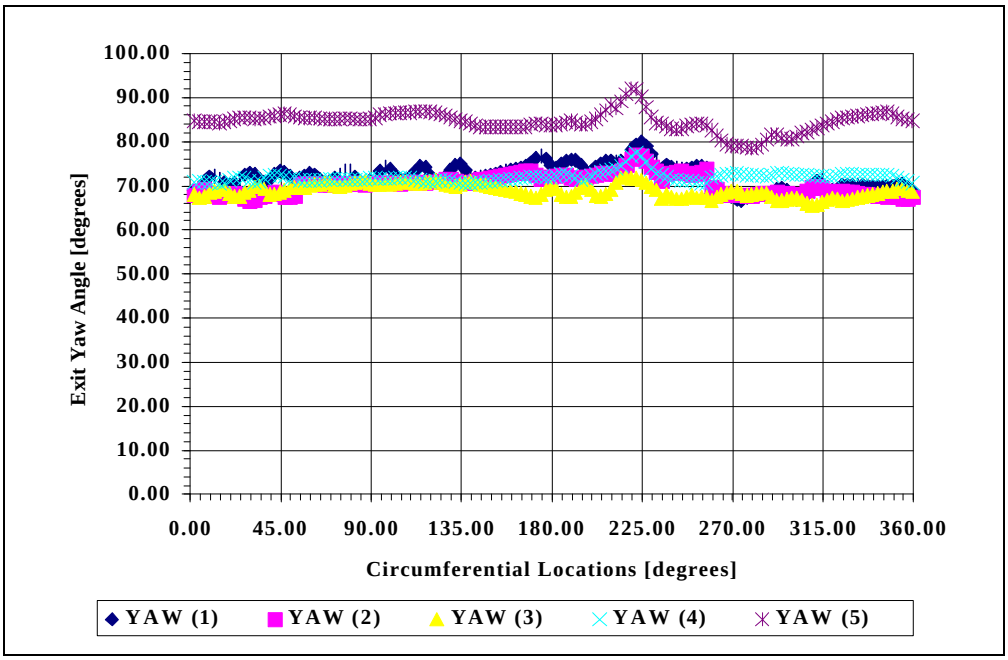

Figure 3.25 Turbine Exit Yaw Angle Distribution (Circular Volute with 720-Points Circumferential Coverage)

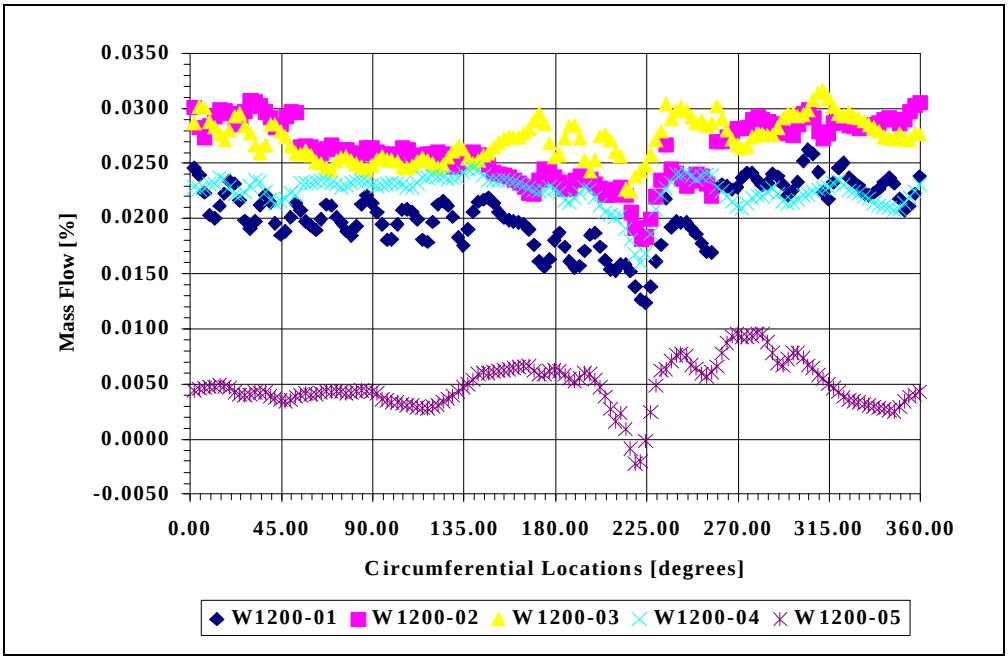

Figure 3.26 Turbine Exit Mass Flow Distribution (Circular Volute with 720-Points Circumferential Coverage)

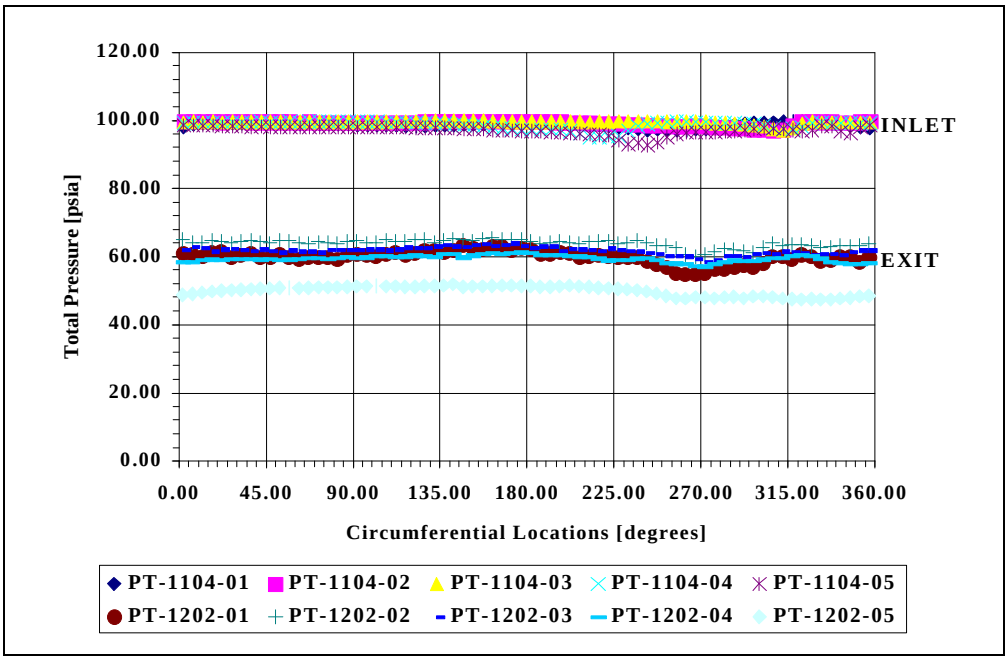

Figure 3.27 Turbine Inlet and Exit Total Pressure Distributions (Circular Volute with 360-Points Circumferential Coverage)

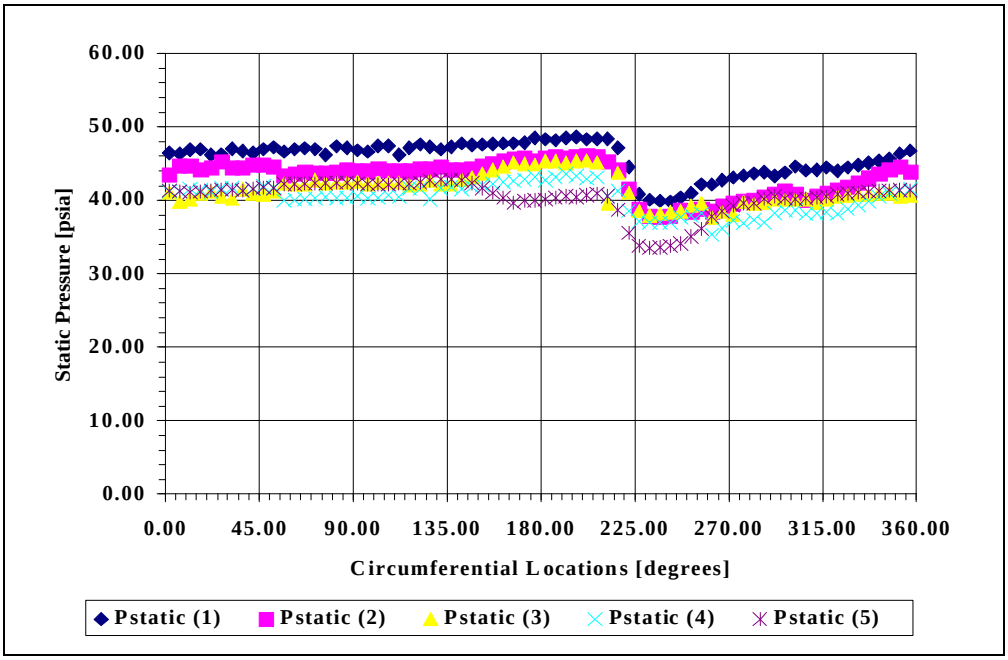

Figure 3.28 Turbine Exit Static Pressure Distribution (Circular Volute with 360-Points Circumferential Coverage)

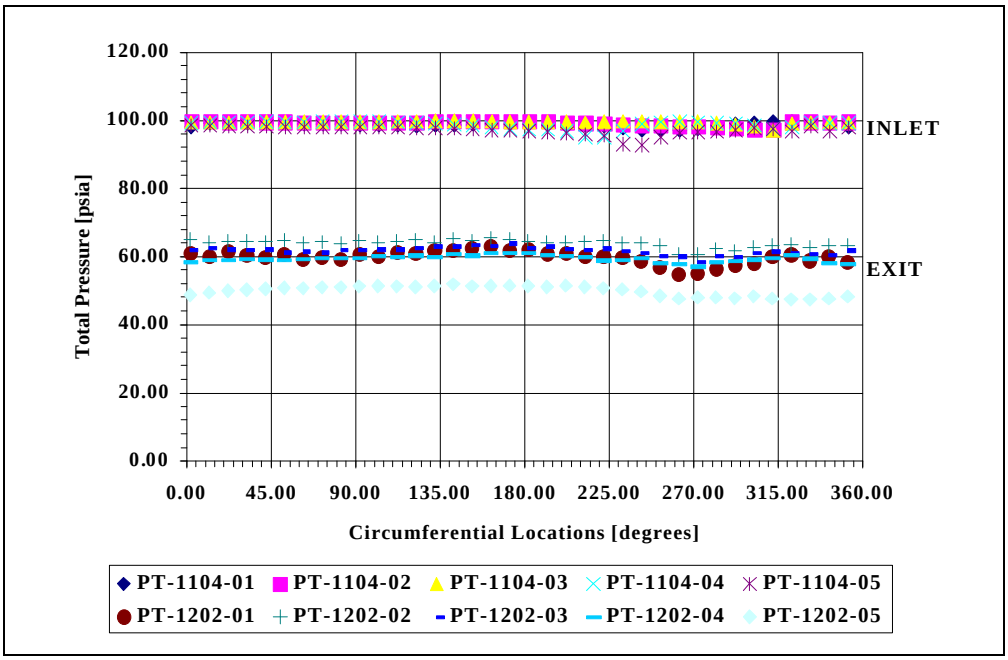

Figure 3.29 Turbine Inlet and Exit Total Pressure Distributions (Circular Volute with 180-Points Circumferential Coverage)

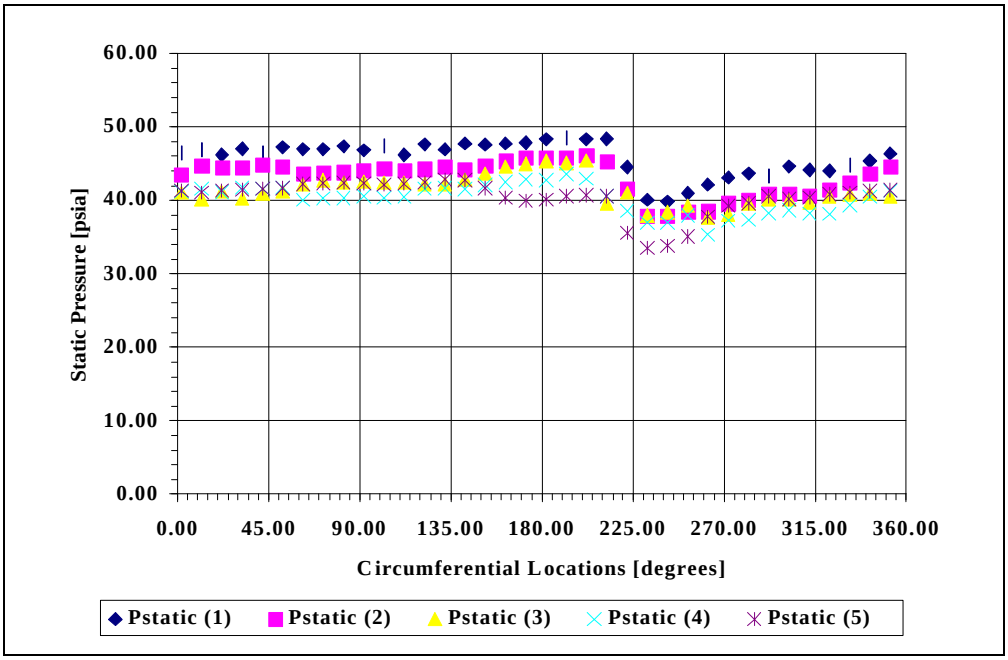

Figure 3.30 Turbine Exit Static Pressure Distribution (Circular Volute with 180-Points Circumferential Coverage)

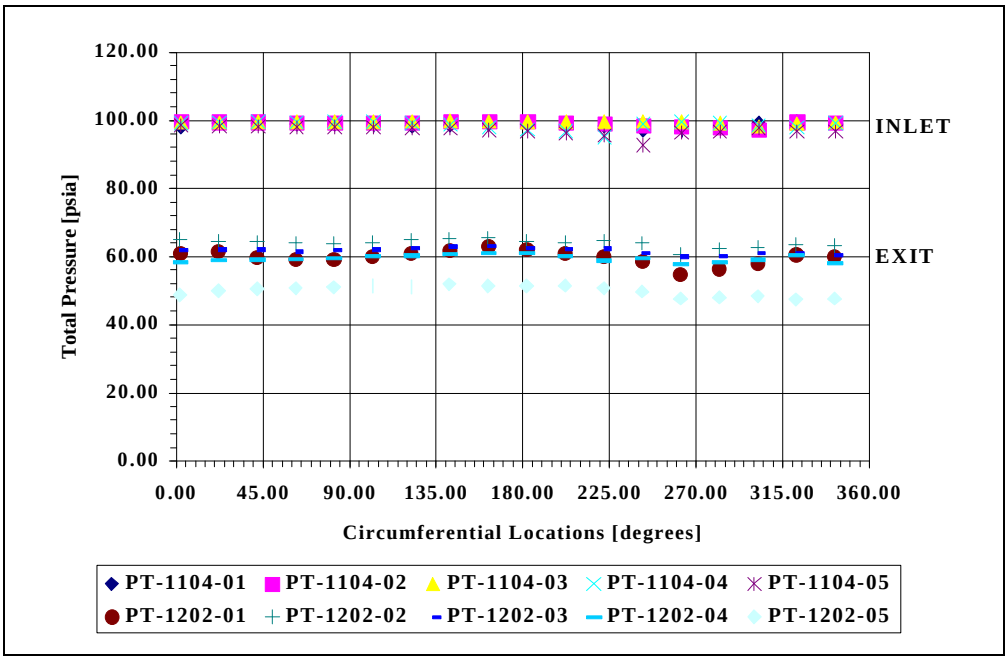

Figure 3.31 Turbine Inlet and Exit Total Pressure Distributions (Circular Volute with 90-Points Circumferential Coverage)

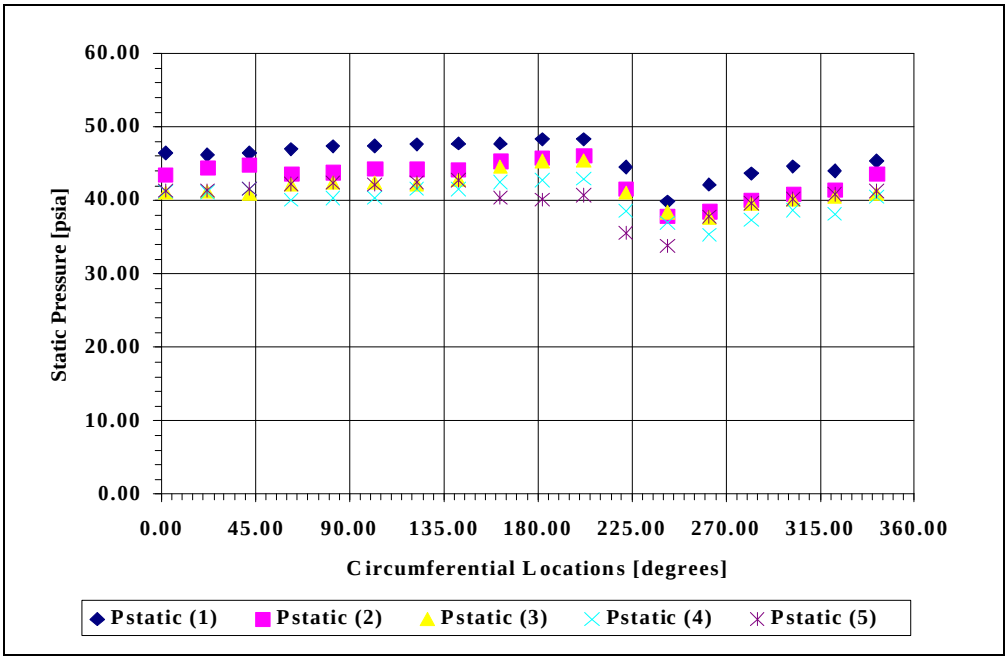

Figure 3.32 Turbine Exit Static Pressure Distribution (Circular Volute with 90-Points Circumferential Coverage)

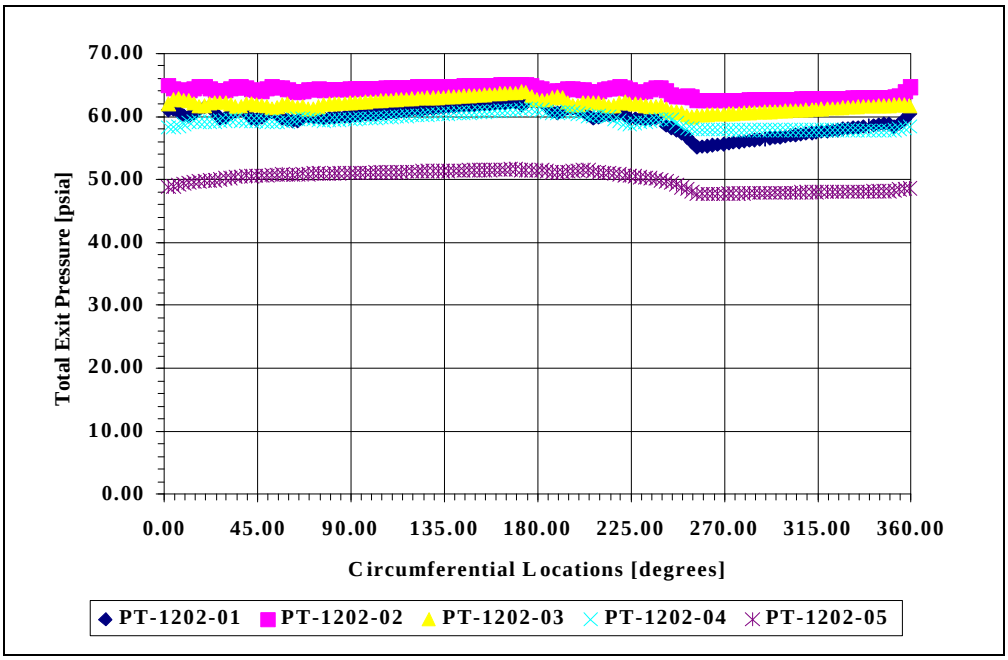

Figure 3.33 Turbine Exit Total Pressure Distribution (Circular Volute with 720-Points Cobra Probe Quadrants Coverage)

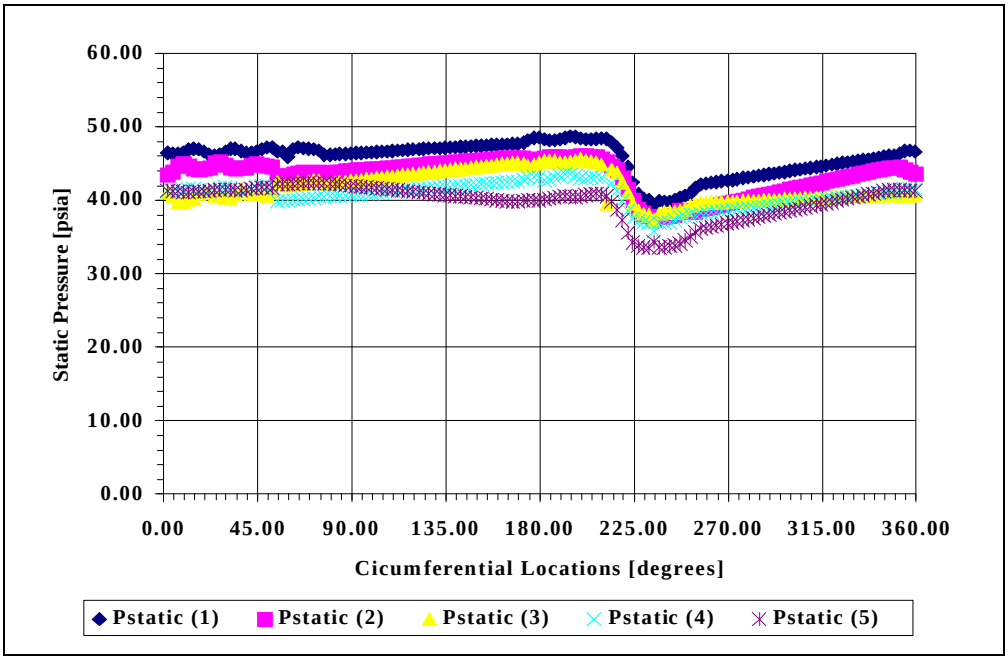

Figure 3.34 Turbine Exit Static Pressure Distribution (Circular Volute with 720-Points Cobra Probe Quadrants Coverage)

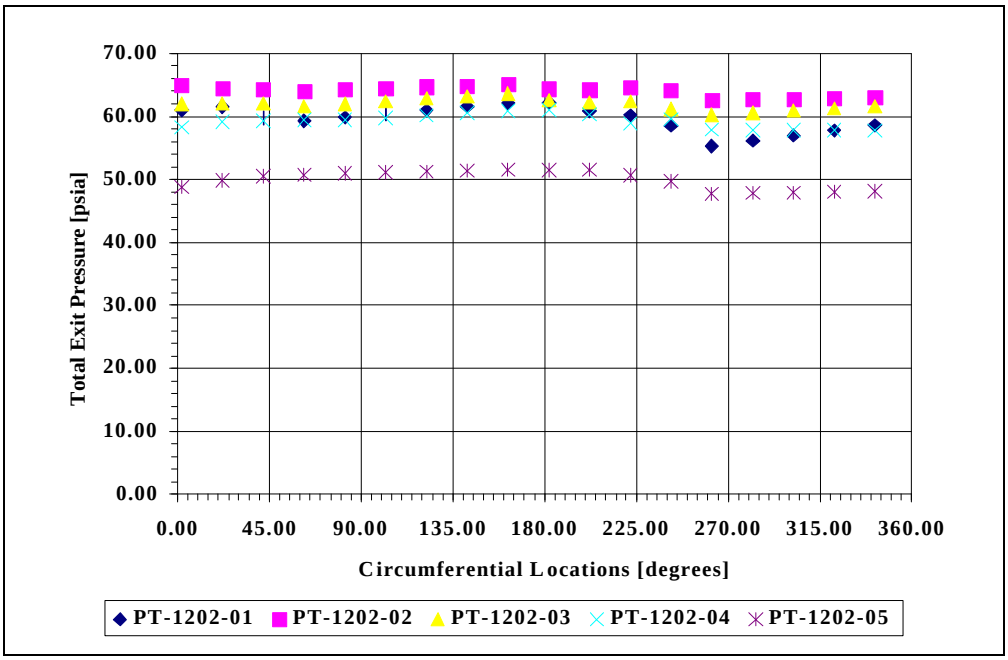

Figure 3.35 Turbine Exit Total Pressure Distribution (Circular Volute with 90-Points Cobra Probe Quadrants Coverage)

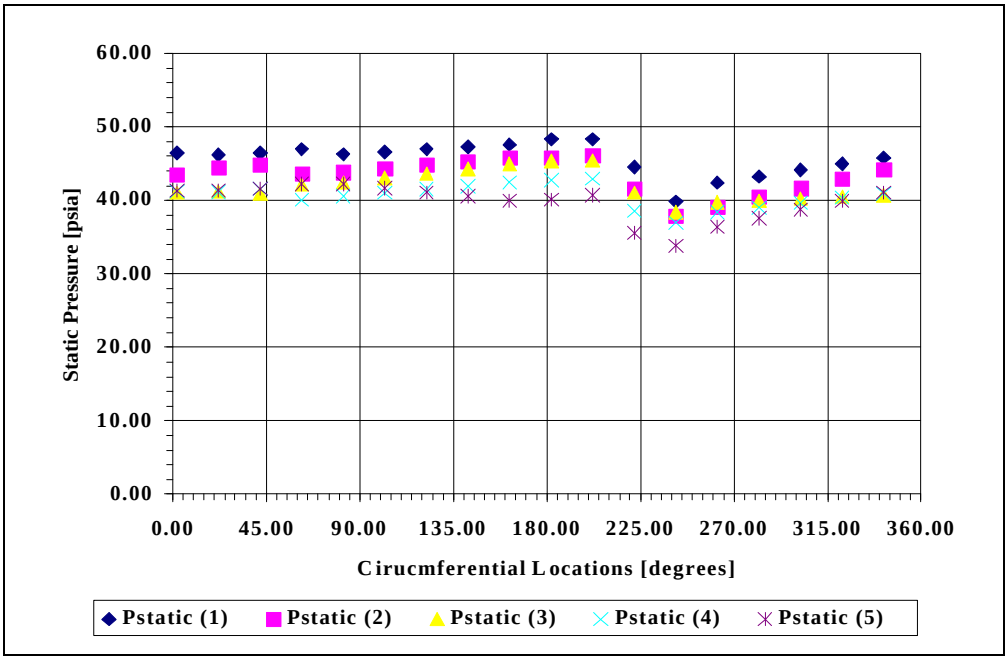

Figure 3.36 Turbine Exit Static Pressure Distribution (Circular Volute with 90-Points Cobra Probe Quadrants Coverage)

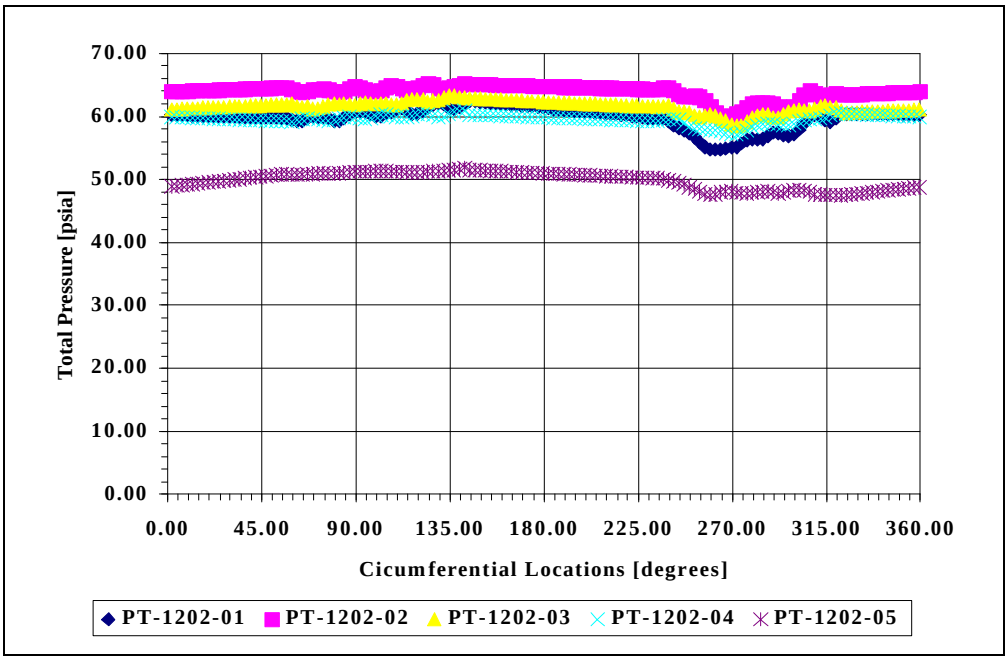

Figure 3.37 Turbine Exit Total Pressure Distribution (Circular Volute with 720-Points YC Probe Quadrants Coverage)

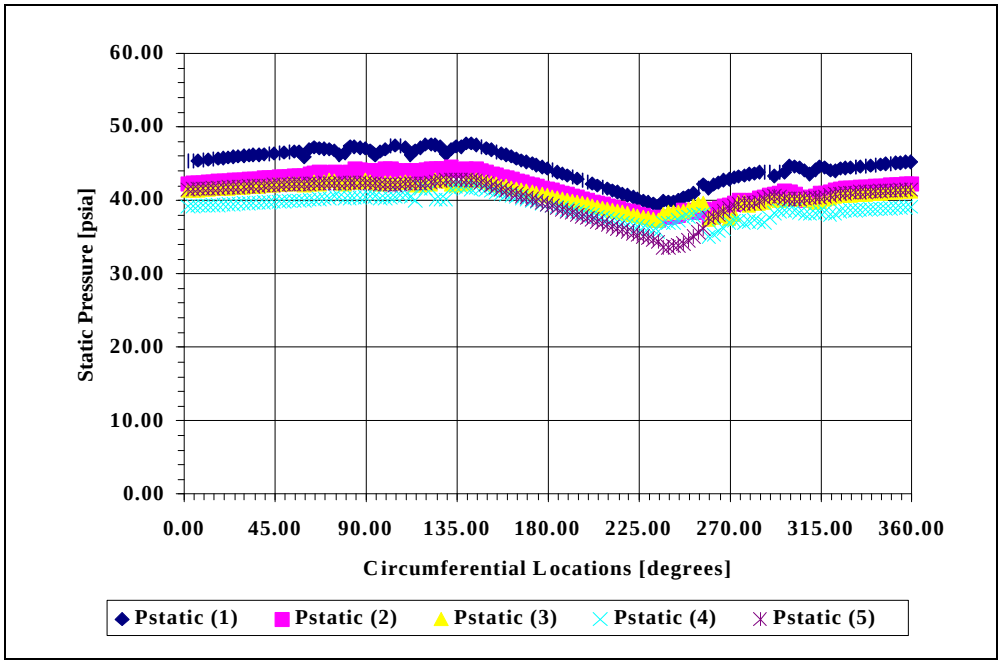

Figure 3.38 Turbine Exit Static Pressure Distribution (Circular Volute with 720-Points YC Probe Quadrants Coverage)

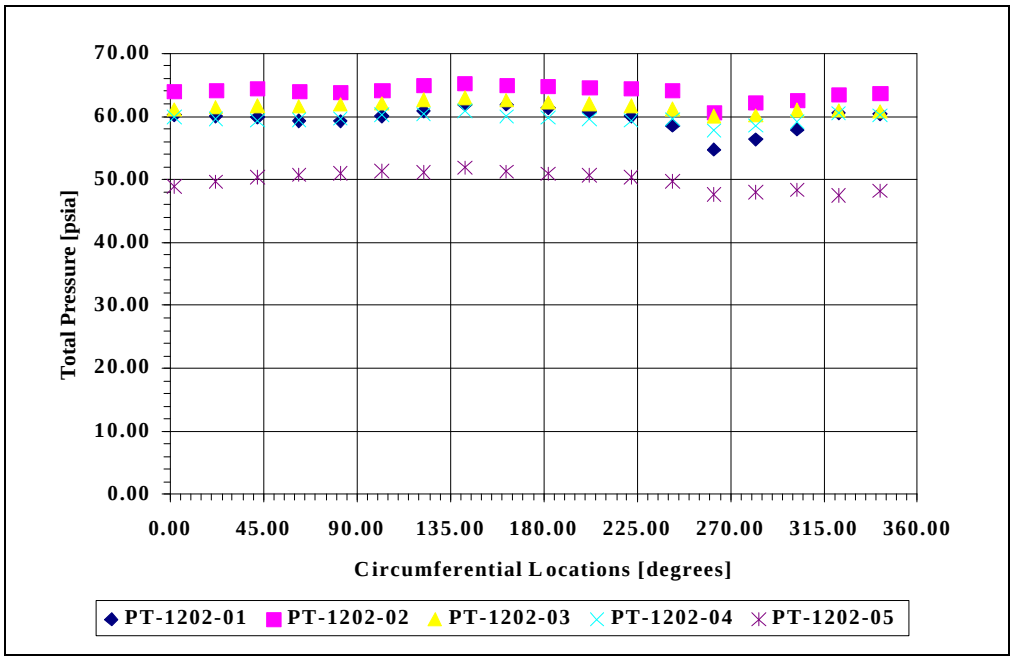

Figure 3.39 Turbine Exit Total Pressure Distribution (Circular Volute with 90-Points YC Probe Quadrants Coverage)

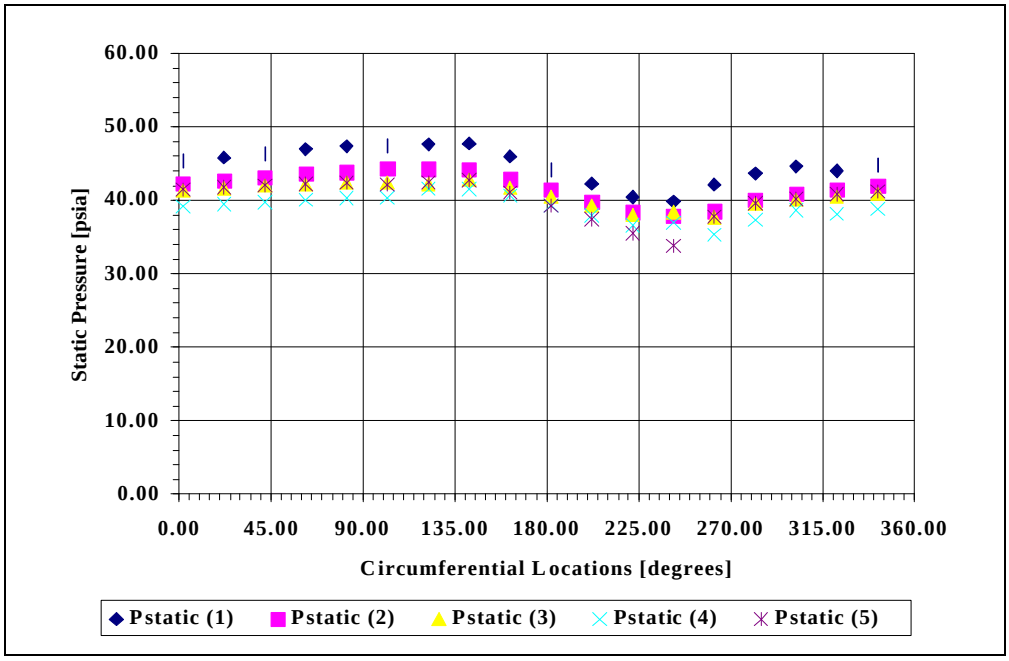

Figure 3.40 Turbine Exit Static Pressure Distribution (Circular Volute with 90-Points YC Probe Quadrants Coverage)

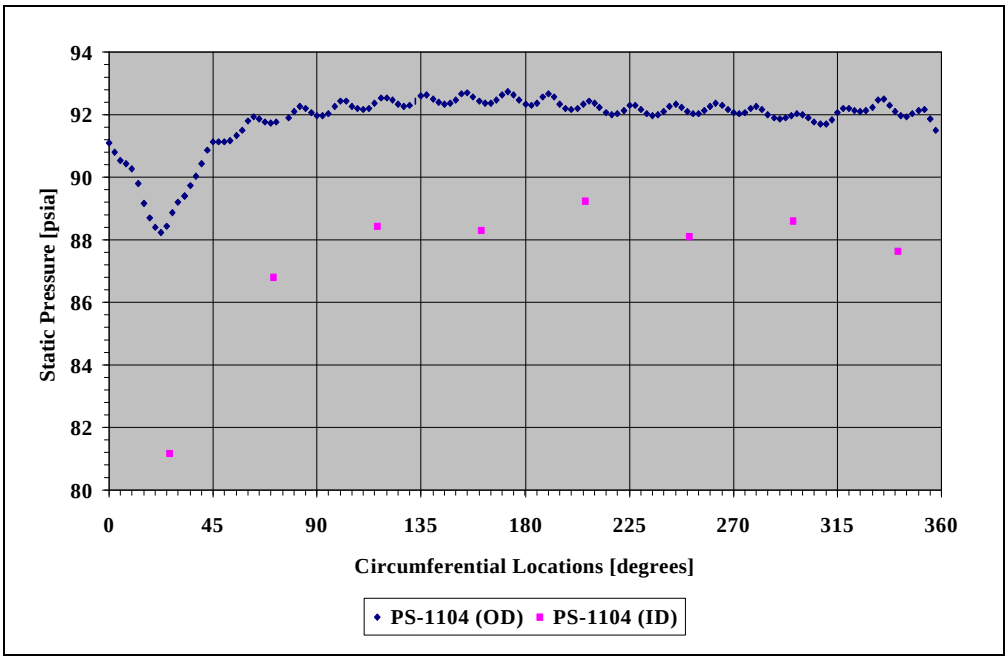

Figure 3.41 Turbine Inlet Wall-Static Pressure Distribution (Circular Volute)

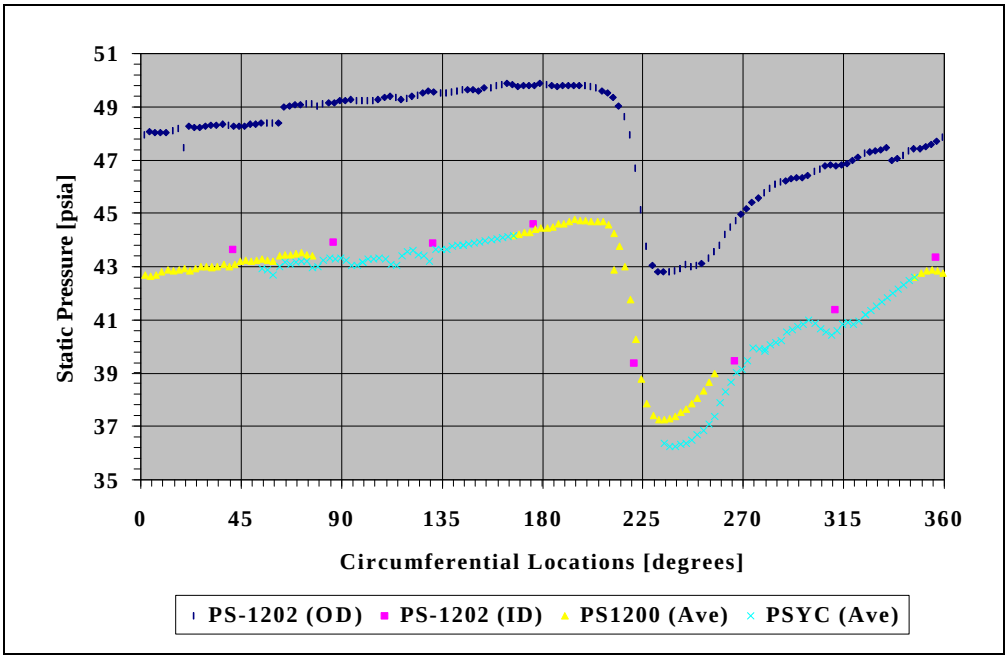

Figure 3.42 Turbine Exit Static Pressure Distribution (Circular Volute)

CHAPTER IV

UNCERTAINTY ANALYSIS METHODOLOGY

4.1 Basic Methodology

A brief overview of basic uncertainty analysis will be presented in this section. The details of uncertainty analysis techniques can be obtained from references 1, 4, 6, and 14.

The word accuracy is generally used to indicate the relative closeness of agreement between an experimentally-determined value of a quantity and its true value. Error is the difference between the experimentally-determined value and the truth; therefore, as error decreases, accuracy is said to increase. Only in rare instances is the true value of a quantity known. Thus, it is necessary to estimate error, and that estimate is called an uncertainty, U. Uncertainty estimates are made at some confidence level–a 95% confidence estimate, for example, means that the true value of the quantity is expected to be within the $\pm U$ interval about the experimentally-determined value 95 times out of 100.

Total error can be considered to be composed of two components: a precision (random) component, e, and a bias (systematic) component, b. An error is classified as random if it contributes to the scatter of the data; otherwise, it is a systematic error. As

an estimate of b, a systematic uncertainty or bias limit, B, is defined. A 95% confidence estimate is interpreted as the experimenter being 95% confident that the true value of the systematic error, if known, would fall within $\pm$B. A useful approach to estimating the magnitude of a systematic error is to assume that the systematic error for a given case is a single realization drawn from some statistical parent distribution of possible systematic errors. As an estimate of the magnitude of the random errors, a precision uncertainty or precision limit, *P*, for a single reading is defined. A 95% confidence estimate of *P* is interpreted to mean that the $\pm P$ interval about the single reading of X_i should cover the (biased) parent population mean, m, 95 times out of 100.

In nearly all experiments, the measured values of different variables are combined using a data reduction equation (DRE) to form some desired result. A general representation of a data reduction equation is

$$r = r(X_1, X_2, \cdots, X_J) \tag{4.1}$$

where *r* is the experimental result determined from *J* measured variables X_J. Each of the measured variables contains systematic errors and random errors. These errors in the measured values then propagate through the data reduction equation, thereby generating the systematic and random errors in the experimental result, *r*.

If the "large sample assumption" is made [6, 14], then the 95% confidence expression for U_r becomes

$$U_r^2 = B_r^2 + P_r^2 \tag{4.2}$$

where the systematic uncertainty (bias limit) of the result is defined as

$$B_r^2 = \sum_{i=1}^{J} q_i^2 B_i^2 + 2\sum_{i=1}^{J-1}\sum_{k=i+1}^{J} q_i q_k B_{ik} \tag{4.3}$$

The q_i are the partial derivatives of each measured variable defined as

$$q_i = \frac{\partial r}{\partial X_i} \tag{4.4}$$

The bias limit estimate for each X_i variable is the root sum square combination of its elemental systematic uncertainties.

$$B_i = \left[\sum_{j=1}^{M} (B_i)_j^2 \right]^{1/2} = \left[(B_i)_1^2 + (B_i)_2^2 + \cdots + (B_i)_M^2 \right]^{1/2} \tag{4.5}$$

B_{ik} is the 95% confidence estimates of the covariance appropriate for the systematic errors in X_i and X_k and is determined from

$$B_{ik} = \sum_{a=1}^{L} (B_i)_a (B_k)_a \tag{4.6}$$

where the variables X_i and X_k share *L* identical error sources.

The precision uncertainty (precision limit) of the result is

$$P_r^2 = \sum_{i=1}^{J} q_i^2 P_i^2 + 2 \sum_{i=1}^{J-1} \sum_{k=i+1}^{J} q_i q_k P_{ik} \tag{4.7}$$

where P_{ik} is the 95% confidence estimate of the covariance appropriate for the precision errors in X_i and X_k, and the 95% confidence large sample precision limit for a variable X_i is estimated as

$$P_{X_i} = 2 S_{X_i} \tag{4.8}$$

where the sample standard deviation for X_i is

$$S_{X_i} = \left[\frac{1}{N-1} \sum_{k=1}^{N} \left[(X_i)_k - \overline{X_i} \right]^2 \right]^{1/2} \tag{4.9}$$

and the mean value for variable X_i is defined as

$$\overline{X_i} = \frac{1}{N}\left[\sum_{k=1}^{N}(X_i)_k\right] \tag{4.10}$$

and $N \geq 10$. The sample standard deviation for the mean value of X_i is

$$S_{\overline{X_i}} = \frac{S_{X_i}}{\sqrt{N}} \tag{4.11}$$

and the 95% confidence large sample random uncertainty limit for the mean value is estimated as

$$P_{\overline{X_i}} = 2S_{\overline{X_i}} \tag{4.12}$$

Typically, correlated precision uncertainties have been neglected so that the P_{ik}'s in Equation 4.7 are taken as zero. These covariance terms account for correlation between errors in different measurements. The precision errors have been considered to be random; therefore, the correlation between them has been assumed to be zero. That assumption is true in the work here.

The methodology discussed above was used to obtain uncertainty estimates for all of the measured variables. Most of these estimates were made in previous work [1]. Additional uncertainty estimates needed for this work will be discussed later in this chapter.

An uncertainty analysis idea that will be crucial in this thesis work is the conceptual bias. The conceptual bias is the difference between a value required for a data reduction equation and the value actually measured [14]. This thesis work will expand the understanding of these conceptual bias errors related to obtaining spatially averaged

values from multiple point measurements by showing how to properly account for them in an uncertainty analysis and showing their significance [1].

Two approaches can be used to evaluate the influence of the uncertainty of each variable on the uncertainty of the result. The first is the uncertainty magnification factor (UMF), and the second is the uncertainty percentage contribution (UPC). The UMF indicates the influence of the uncertainty in each variable on the total uncertainty of the result (turbine efficiency in this case). A UMF greater than one indicates that the influence of the uncertainty of the variable magnifies the total uncertainty; a UMF less than one indicates that the influence of the uncertainty of the variable reduces the total uncertainty. (Note that the sign does not affect the overall uncertainty since all terms are squared in the uncertainty equation). The UMF is defined as

$$UMF_i = \frac{X_i}{r}\frac{\partial r}{\partial X_i} \tag{4.13}$$

This type of analysis is useful for a general case during the early planning phase of an experiment. A general uncertainty analysis was conducted and the results were used in the planning phase of the OTTR program. These results are documented in references 9 and 17. The second approach, the UPC, shows the percentage contribution of the uncertainty in each variable to the total uncertainty of the result (turbine efficiency) [1, 14]. The UPC are defined as

$$UPC_i = \frac{(q_i U_i)^2}{U_r^2} 100 \tag{4.14}$$

$$UPC_{ik} = \frac{2 q_i q_k B_{ik}}{U_r^2} 100$$

The UPC illustrates the influence of each variable and its uncertainty as a percent of the result uncertainty squared for each squared term. This approach shows the sensitivity of the squared uncertainty of the result to the squared uncertainty effect of each of the variables for a particular situation where values for the variables are known and the uncertainties for each variable have been estimated. Since this type of analysis incorporates the uncertainty estimates associated with a particular test situation, it is useful during the later planning and early design phases of an experiment. The UPC values are used extensively in Chapter 5 to study the influences of the uncertainties of the different variables on the efficiency uncertainty for the various cases studied.

4.2 Detailed Uncertainty Analyses

A general uncertainty analysis was done during the planning phase of the OTTR program. The analysis was performed to determine the uncertainty influence of each variable on the uncertainty of the efficiency. The equipment calibrations to improve critical measurements in Chapter 2 were done based on the results of the general uncertainty analysis [9]. A detailed uncertainty analysis was then done after each OTTR test. Detailed uncertainty estimates were refined based on the new calibration, measurement, and data acquisition techniques developed for high gradient regions [1]. The detailed uncertainty analysis method was developed to explicitly account for the averaging procedures used to calculate efficiency (mass and area averaging). The following sections of the thesis will concentrate on the detailed uncertainty analyses for ADP set points and for the thermodynamic and mechanical efficiency methods (Equation 1.1 and 1.2). The OTTR was tested in air; therefore, the detailed uncertainty analyses

will only address the uncertainty of the efficiency determined from the air test. To apply air test results to an engine, differences of gas thermodynamic properties, geometric dimensions, and higher temperature operation of different fluids must be considered [1].

The thermodynamic efficiency is a function of P_{01}, P_{02}, T_{01}, and T_{02}, and the mechanical efficiency is a function of P_{01}, P_{02}, T_{01}, $\dot{W}$, Tq, and N [1, 9]. Static pressure and flow angle measurements were needed for the mass averaging technique. Hence, the efficiency equations are functions of the following

$$h_{th} = h_{th}\left[\sum_{i=1}^{720}\left(P_{01}, P_{02}, T_{01}, T_{02}, P_2, a_2\right)_i\right] \tag{4.15}$$

and

$$h_{me} = h_{me}\left[\dot{W}, Tq, N\sum_{i=1}^{720}\left(P_{01}, P_{02}, T_{01}, P_2, a_2\right)_i\right] \tag{4.16}$$

Combining Equation 4.15 with Equations 4.2, 4.3, and 4.7, the equation for uncertainty in thermodynamic efficiency becomes

$$\begin{aligned} U_{h_{th}}{}^2 = &\sum_{i=1}^{720}\left(\frac{\partial h}{\partial P_{01i}}P_{P_{01i}}\right)^2 + \sum_{i=1}^{720}\left(\frac{\partial h}{\partial P_{02i}}P_{P_{02i}}\right)^2 + \sum_{i=1}^{720}\left(\frac{\partial h}{\partial T_{01i}}P_{T_{01i}}\right)^2 \\ &+ \sum_{i=1}^{720}\left(\frac{\partial h}{\partial T_{02i}}P_{T_{02i}}\right)^2 + \sum_{i=1}^{720}\left(\frac{\partial h}{\partial P_{2i}}P_{P_{2i}}\right)^2 + \sum_{i=1}^{720}\left(\frac{\partial h}{\partial a_{2i}}P_{a_{2i}}\right)^2 + \sum_{i=1}^{720}\left(\frac{\partial h}{\partial P_{01i}}B_{P_{01i}}\right)^2 \\ &+ \sum_{i=1}^{720}\left(\frac{\partial h}{\partial P_{02i}}B_{P_{02i}}\right)^2 + \sum_{i=1}^{720}\left(\frac{\partial h}{\partial T_{01i}}B_{T_{01i}}\right)^2 + \sum_{i=1}^{720}\left(\frac{\partial h}{\partial T_{02i}}B_{T_{02i}}\right)^2 + \sum_{i=1}^{720}\left(\frac{\partial h}{\partial P_{2i}}B_{P_{2i}}\right)^2 \\ &+ \sum_{i=1}^{720}\left(\frac{\partial h}{\partial a_{2i}}B_{a_{2i}}\right)^2 + 2\sum_{i=1}^{719}\sum_{j=i+1}^{720}\left(\frac{\partial h}{\partial P_{01}}\right)_i\left(\frac{\partial h}{\partial P_{01}}\right)_j B_{P_{01i}P_{01j}} \end{aligned} \tag{4.17}$$

$$+2\sum_{i=1}^{719}\sum_{j=i+1}^{720}\left(\frac{\partial h}{\partial P_{02}}\right)_i\left(\frac{\partial h}{\partial P_{02}}\right)_j B_{P_{02i}P_{02j}}+2\sum_{i=1}^{719}\sum_{j=i+1}^{720}\left(\frac{\partial h}{\partial T_{01}}\right)_i\left(\frac{\partial h}{\partial T_{01}}\right)_j B_{T_{01i}T_{01j}}$$

$$+2\sum_{i=1}^{719}\sum_{j=i+1}^{720}\left(\frac{\partial h}{\partial T_{02}}\right)_i\left(\frac{\partial h}{\partial T_{02}}\right)_j B_{T_{02i}T_{02j}}+2\sum_{i=1}^{719}\sum_{j=i+1}^{720}\left(\frac{\partial h}{\partial P_2}\right)_i\left(\frac{\partial h}{\partial P_2}\right)_j B_{P_{2i}P_{2j}}$$

$$+2\sum_{i=1}^{719}\sum_{j=i+1}^{720}\left(\frac{\partial h}{\partial a_2}\right)_i\left(\frac{\partial h}{\partial a_2}\right)_j B_{a_{2i}a_{2j}}+2\sum_{i=1}^{720}\sum_{j=1}^{720}\left(\frac{\partial h}{\partial P_{01}}\right)_i\left(\frac{\partial h}{\partial P_{02}}\right)_j B_{P_{01i}P_{02j}}$$

$$+2\sum_{i=1}^{720}\sum_{j=1}^{720}\left(\frac{\partial h}{\partial P_{01}}\right)_i\left(\frac{\partial h}{\partial P_2}\right)_j B_{P_{01i}P_{2j}}+2\sum_{i=1}^{720}\sum_{j=1}^{720}\left(\frac{\partial h}{\partial P_{01}}\right)_i\left(\frac{\partial h}{\partial a_2}\right)_j B_{P_{01i}a_{2j}}$$

$$+2\sum_{i=1}^{720}\sum_{j=1}^{720}\left(\frac{\partial h}{\partial P_{02}}\right)_i\left(\frac{\partial h}{\partial P_2}\right)_j B_{P_{02i}P_{2j}}+2\sum_{i=1}^{720}\sum_{j=1}^{720}\left(\frac{\partial h}{\partial P_{02}}\right)_i\left(\frac{\partial h}{\partial a_2}\right)_j B_{P_{02i}a_{2j}}$$

$$+2\sum_{i=1}^{720}\sum_{j=1}^{720}\left(\frac{\partial h}{\partial T_{01}}\right)_i\left(\frac{\partial h}{\partial T_{02}}\right)_j B_{T_{01i}T_{02j}}+2\sum_{i=1}^{720}\sum_{j=1}^{720}\left(\frac{\partial h}{\partial P_2}\right)_i\left(\frac{\partial h}{\partial a_2}\right)_j B_{P_{2i}a_{2j}}$$

Combining Equation 4.16 with Equations 4.2, 4.3, and 4.7, the equation for uncertainty in mechanical efficiency becomes

$$U_{h_{me}}{}^2=\sum_{i=1}^{720}\left(\frac{\partial h}{\partial P_{01i}}P_{P_{01i}}\right)^2+\sum_{i=1}^{720}\left(\frac{\partial h}{\partial P_{02i}}P_{P_{02i}}\right)^2+\sum_{i=1}^{720}\left(\frac{\partial h}{\partial T_{01i}}P_{T_{01i}}\right)^2 \tag{4.18}$$

$$+\sum_{i=1}^{720}\left(\frac{\partial h}{\partial P_{2i}}P_{P_{2i}}\right)^2+\sum_{i=1}^{720}\left(\frac{\partial h}{\partial a_{2i}}P_{a_{2i}}\right)^2+\left(\frac{\partial h}{\partial \dot{W}}P_{\dot{W}}\right)^2+\left(\frac{\partial h}{\partial Tq}P_{Tq}\right)^2+\left(\frac{\partial h}{\partial N}P_N\right)^2$$

$$+\sum_{i=1}^{720}\left(\frac{\partial h}{\partial P_{01i}}B_{P_{01i}}\right)^2+\sum_{i=1}^{720}\left(\frac{\partial h}{\partial P_{02i}}B_{P_{02i}}\right)^2+\sum_{i=1}^{720}\left(\frac{\partial h}{\partial T_{01i}}B_{T_{01i}}\right)^2+\sum_{i=1}^{720}\left(\frac{\partial h}{\partial P_{2i}}B_{P_{2i}}\right)^2$$

$$+\sum_{i=1}^{720}\left(\frac{\partial h}{\partial a_{2i}}B_{a_{2i}}\right)^2+\left(\frac{\partial h}{\partial \dot{W}}B_{\dot{W}}\right)^2+\left(\frac{\partial h}{\partial Tq}B_{Tq}\right)^2+\left(\frac{\partial h}{\partial N}B_N\right)^2$$

$$+2\sum_{i=1}^{719}\sum_{j=i+1}^{720}\left(\frac{\partial h}{\partial P_{01}}\right)_i\left(\frac{\partial h}{\partial P_{01}}\right)_j B_{P_{01i}P_{01j}}+2\sum_{i=1}^{719}\sum_{j=i+1}^{720}\left(\frac{\partial h}{\partial P_{02}}\right)_i\left(\frac{\partial h}{\partial P_{02}}\right)_j B_{P_{02i}P_{02j}}$$

$$+2\sum_{i=1}^{719}\sum_{j=i+1}^{720}\left(\frac{\partial h}{\partial T_{01}}\right)_i\left(\frac{\partial h}{\partial T_{01}}\right)_j B_{T_{01i}T_{01j}}+2\sum_{i=1}^{719}\sum_{j=i+1}^{720}\left(\frac{\partial h}{\partial P_2}\right)_i\left(\frac{\partial h}{\partial P_2}\right)_j B_{P_{2i}P_{2j}}$$

$$+2\sum_{i=1}^{719}\sum_{j=i+1}^{720}\left(\frac{\partial h}{\partial a_2}\right)_i\left(\frac{\partial h}{\partial a_2}\right)_j B_{a_{2i}a_{2j}}+2\sum_{i=1}^{720}\sum_{j=1}^{720}\left(\frac{\partial h}{\partial P_{01}}\right)_i\left(\frac{\partial h}{\partial P_{02}}\right)_j B_{P_{01i}P_{02j}}$$

$$+2\sum_{i=1}^{720}\sum_{j=1}^{720}\left(\frac{\partial h}{\partial P_{01}}\right)_i\left(\frac{\partial h}{\partial P_2}\right)_j B_{P_{01i}P_{2j}}+2\sum_{i=1}^{720}\sum_{j=1}^{720}\left(\frac{\partial h}{\partial P_{01}}\right)_i\left(\frac{\partial h}{\partial a_2}\right)_j B_{P_{01i}a_{2j}}$$

$$+2\sum_{i=1}^{720}\sum_{j=1}^{720}\left(\frac{\partial h}{\partial P_{02}}\right)_i\left(\frac{\partial h}{\partial P_2}\right)_j B_{P_{02i}P_{2j}}+2\sum_{i=1}^{720}\sum_{j=1}^{720}\left(\frac{\partial h}{\partial P_{02}}\right)_i\left(\frac{\partial h}{\partial a_2}\right)_j B_{P_{2i}a_{2j}}$$

$$+2\sum_{i=1}^{720}\sum_{j=1}^{720}\left(\frac{\partial h}{\partial P_2}\right)_i\left(\frac{\partial h}{\partial a_2}\right)_j B_{P_{2i}a_{2j}}$$

These efficiency uncertainty equations (Equations 4.17 and 4.18) were developed previously in references 1 and 9. Both efficiency uncertainty equations account for the number of point measurements, averaging procedure, conceptual bias, and correlation of the measured variables in the OTTR test. These two equations were assumed to be the best efficiency uncertainty calculation methods. The efficiency calculations using mass averaging of all 720-point measurements at the turbine exit were considered the “true” efficiencies of the OTTR, and the uncertainty results of mass averaging the 720-point measurements were considered the smallest uncertainties for the OTTR test. For the reduction in measurements study, the summation counter was changed according to the number of measurements made for the efficiency calculation. Hence, the counter was set for four cases (720-points, 360-points, 180-points, and 90-points) for the detailed uncertainty analyses. The uncertainty analyses for the cobra and YC test cases utilized the same uncertainty equations (Equations 4.17 and 4.18).

The efficiency uncertainty equation for thermodynamic efficiency calculation (Equation 4.17) was divided into four major portions. The uncertainty terms 1 through 6 on the right-hand side were the precision terms for each measured variable, terms 7 through 12 were the bias terms for each variable, terms 13 through 18 were the correlated bias terms between point measurements for the same variable, and terms 19 through 25 were the correlated bias terms for point measurements of different variables. The uncertainty terms for the mechanical efficiency method (Equation 4.18) were also broken down to four portions. The terms 1 through 8 on the right-hand side were the precision terms for each measured variable, terms 9 through 16 were the bias terms for each variable, terms 17 through 21 were the correlated bias terms between point measurements of the same variable, and terms 22 through 27 were correlated bias terms for point measurements of different variables. All correlated precision terms were set to zero [1, 9]. Further details on the uncertainty equations (Equations 4.17 and 4.18) can be obtained from reference 14 and 18.

4.2.1 Conceptual Bias Methodology

The original efficiency uncertainty equations (Equations 4.17 and 4.18) were modified to accommodate conceptual bias estimates from the measurement reduction study. Conceptual bias in this case is the bias that arises when a cross-sectional average value required in the data reduction equation is replaced by an average of multiple point measurements. The cross-sectional average is the integral, yet a summation of values must be made to approximate the integral. If enough measurements are made, then the summation is approximately equal to the integral, and the conceptual bias error is

negligible. However, how does one determine how many measurements are required to make the conceptual bias error negligible? The work in this thesis attempts to help answer that question. Since 720 measurements was the maximum number of truly independent spatial measurements possible given the annulus area and probe dimensions for the OTTR, it was assumed that conceptual bias error was negligible when 720 measurements were properly averaged to obtain the values ($\sum \approx \int$). Hence, these values were labeled the "true" values. Deviations from these "true" values were then studied for the various cases discussed previously, and the data were used to obtain conceptual bias estimates. These estimates were then incorporated into the uncertainty equations to study the influence of the conceptual bias terms on the efficiency uncertainty.

The thermodynamic efficiency method was a function of P_{01}, P_{02}, T_{01}, and T_{02}, and the mechanical efficiency method was a function of P_{01}, P_{02}, T_{01}, $\dot{W}$, Tq, and N for the OTTR. The pressure and temperature values were all cross-sectional averages of the turbine inlet and exit. The measurement reduction study described in Section 3.1.2 generated different average values for each property (Tables 3.7, 3.8, 3.9, 3.18, 3.19, 3.20). The OTTR $\dot{W}$, Tq, and N were numerical averages of repeated measurements taken over a period of time. Therefore, the conceptual bias estimates developed for the measurements reduction study do not apply to $\dot{W}$, Tq, and N. Conceptual bias terms were added for P_{01}, P_{02}, T_{01}, and T_{02}. These terms were the average values that were significant in the efficiency equations, and the measurement reduction study was done on those properties. The conceptual bias terms were needed to account for the differences in

the uncertainties of the average values for each measurement reduction case. The new uncertainty results will help to prove the generalized assumptions made in Chapter 3 and to determine the new turbine testing guidelines.

The conceptual bias must be added to the efficiency uncertainty equations without altering the original efficiency results. Hence, the data reduction equation must be modified to include the conceptual bias terms due to measurement reduction. The average value of each property needed for the efficiency calculations can be written as follows (assumed to be the "true" value)

$$X_{Ave} = \frac{\sum_{i=1}^{N} X_i}{N} \tag{4.19}$$

where X represents P_{01}, P_{02}, T_{01}, and T_{02}. Reducing the number of measurements would change the equation to the following

$$X_{Ave} = \frac{\sum_{i=1}^{N} X_i}{N} + X_C \tag{4.20}$$

where the term X_C is a dummy value used to implement the conceptual bias estimate into the averaging (N equals the number of measurements). The X_C term is set to zero for all the averaged properties. The derivative of X_C for Equation 4.20 would equal one. The square of the product of the derivative and the conceptual bias estimates would equal to the square of the conceptual bias. Hence, the conceptual bias estimate can be added to the DRE without altering the averaged value of each measurement reduction case (Table 3.4, 3.5, 3.6, 3.15, 3.16, 3.17).

The conceptual bias estimate for each value was determined from the test data for each measurement reduction case. Differences were present when comparing averaged values of the 720-point measurements (the "true" values) with the averaged values of the other cases. Therefore, the conceptual bias was estimated using the differences in averaged values between measurement reduction cases (averages of 720-point, 360-point, 180-point, and 90-point measurement cases). The new method added to the averaging of the four properties (P_{01}, P_{02}, T_{01}, and T_{02}) a means of accounting for the differences of the averaged values. The new method also offered the implementation of conceptual bias estimates without altering the original efficiency calculations.

The efficiency equations were redefined with the consideration of the conceptual bias for the measurement reduction study. The thermodynamic efficiency equation was modified to become

$$h_{th} = \frac{\left(\overline{T_{01}} + T_{01C}\right) - \left(\overline{T_{02}} + T_{02C}\right)}{\left(\overline{T_{01}} + T_{01C}\right)\left[1 - \left(\frac{\left(\overline{P_{02}} + P_{02C}\right)}{\left(\overline{P_{01}} + P_{01C}\right)}\right)^{\frac{g-1}{g}}\right]} \tag{4.21}$$

The mechanical efficiency equation was modified to become

$$h_{me} = \frac{K \cdot Tq \cdot N}{J \cdot C_p \cdot \dot{W} \cdot \left(\overline{T_{01}} + T_{01C}\right)\left[1 - \left(\frac{\left(\overline{P_{02}} + P_{02C}\right)}{\left(\overline{P_{01}} + P_{01C}\right)}\right)^{\frac{g-1}{g}}\right]} \tag{4.22}$$

The new thermodynamic efficiency uncertainty equation will have four new bias terms

$$U_{h_{thNew}}{}^2 = U_{h_{th}}{}^2 + \left(\frac{\partial h}{\partial P_{01C}} B_{P_{01C}}\right)^2 + \left(\frac{\partial h}{\partial P_{02C}} B_{P_{02C}}\right)^2 + \left(\frac{\partial h}{\partial T_{01C}} B_{T_{01C}}\right)^2 + \left(\frac{\partial h}{\partial T_{02C}} B_{T_{02C}}\right)^2 \quad (4.23)$$

The new mechanical efficiency uncertainty equation will have three new bias terms.

$$U_{h_{meNew}}{}^2 = U_{h_{me}}{}^2 + \left(\frac{\partial h}{\partial P_{01C}} B_{P_{01C}}\right)^2 + \left(\frac{\partial h}{\partial P_{02C}} B_{P_{02C}}\right)^2 + \left(\frac{\partial h}{\partial T_{01C}} B_{T_{01C}}\right)^2 \quad (4.24)$$

The new terms in the efficiency uncertainty equations (Equations 4.23 and 4.24) were added to the FORTRAN program provided by reference 1 (Appendix). The FORTRAN program was modified to accommodate mass and area averaging, and the uncertainty equations were changed to include the conceptual bias terms. The detailed uncertainty results are presented in Chapter 5.

4.2.2 Wall-Static Pressure Methodology

The averaging of the wall-static pressures for the turbine exit plane was described in Section 3.1.3. Two methods of averaging were analyzed. The first method was to numerically average all wall-static measurements (Numerical Wall Averaging, NWA). The second method was to average the turbine outer wall-static pressure with the inner wall static pressure at each circumferential location (Circumferential Wall Averaging, CWA). The new wall-static pressure averaging methods prompted the need to estimate the uncertainties for these static pressure calculations.

The “true” static pressure average value was defined as the value by mass averaging the 720-point measurements across the annulus obtained using the cobra and

YC probe. The difference of the wall-static averaging and the "true" static pressure average was taken as the conceptual bias estimate. This estimate was the same for both NWA and CWA. The conceptual bias estimate was treated as one of the uncertainty sources for the static pressure. The complete list of uncertainty sources is provided in Table 4.1.

The first wall-static pressure averaging case (NWA) involved numerical averaging of the turbine inner wall and outer wall measurements. The random uncertainty estimate for this case was obtained using Equation 4.12 and was negligible. The nature of the CWA wall-static pressure averaging suggested the use of the uncertainty methodology provided in reference 5. The turbine wall-static measurement region was divided into 8 sections (Refer to Section 3.1.3 for details of the averaging procedure of each section). The calculation of the additional uncertainty source began by assuming the turbine exit outer wall as the second traverse point and the inner wall as the first traverse point. The eight sections are assumed to be the radii described in reference 5. The average of each traverse point was calculated as

$$\overline{X}_{ij} = \sum_{k=1}^{18} X_{ijk} \tag{4.25}$$

where the subscript i was equal to the designated radius or section ranging from 1 to 8, j was the traverse position ranging from 1 to 2, and k was equal to the number of point measurements within each radius or section.

The average static pressure along each radius was defined as

$$\overline{\mathrm{P}}_i = \sum_{j=1}^{10} \frac{\overline{X}_{ij}}{2} \tag{4.26}$$

Next, the overall average static pressure of the turbine exit plane was defined as

$$\bar{\mathrm{P}} = \sum_{i=1}^{8} \frac{\bar{\mathrm{P}}_i}{8} \tag{4.27}$$

Once, the averages were determined, the standard deviation for each static pressure along a radius, $S_{\bar{\mathrm{P}}_i}$, was calculated

$$S_{\bar{\mathrm{P}}_i} = \left[\sum_{j=1}^{2} \left(\frac{\partial \bar{\mathrm{P}}_i}{\partial \bar{X}_{ij}} \frac{S_{Xij}}{\sqrt{18}} \right)^2 \right]^{1/2} \tag{4.28}$$

where

$$\frac{\partial \bar{\mathrm{P}}_i}{\partial \bar{X}_{ij}} = \frac{1}{2}$$

$$S_{Xij} = \sqrt{\sum_{k=1}^{18} \frac{\left(X_{ijk} - \bar{\mathrm{P}} \right)^2}{18-1}} \tag{4.29}$$

The overall standard deviation of the average wall-static pressure at the turbine exit plane was defined as

$$S_{\bar{\mathrm{P}}} = \left[\sum_{i=1}^{8} \left(\frac{\partial \mathrm{P}}{\partial \bar{\mathrm{P}}_i} S_{\bar{\mathrm{P}}_i} \right)^2 \right]^{1/2} \tag{4.30}$$

where

$$\frac{\partial \bar{\mathrm{P}}}{\partial \bar{\mathrm{P}}_i} = \frac{1}{8} \tag{4.31}$$

The overall standard deviation, $S_{\bar{\mathrm{P}}}$, was added to the uncertainty sources determined in reference 18 (Table 4.1).

4.3 Uncertainty Estimates

The uncertainty estimates provided by reference 1 are listed in Table 4.2. Information on how these estimates were obtained is in the reference.

The conceptual bias estimates for the measurement reduction cases were taken from the efficiency comparison results in Chapter 3. The differences between the measurement reduction averages and the "true" averages were taken as the values for conceptual bias estimates. Tables 3.7, 3.8, and 3.9 are the conceptual bias estimates for the square exit volute test, and Tables 3.18, 3.19, and 3.20 are the conceptual bias estimates for the circular exit volute test. The total temperature and total pressure measurements were critical for efficiency calculation (general uncertainty analysis results). The inlet total pressure and total temperature measurements were flat, and the averaged values for different data reduction cases were equal. Therefore, the conceptual bias estimates were insignificant at the turbine inlet because of the relatively flat flow field. The exit total temperature and exit total pressure were the only properties that had significant conceptual bias errors.

The conceptual bias estimates for wall-static pressure averaging and the overall uncertainty estimates for the static pressure measurements are included in Table 4.1. The results were used in the detailed uncertainty analyses for turbine efficiency.

The detailed uncertainty analyses of turbine efficiency were performed and the results will be presented in Chapter 5. A discussion of averaging technique comparisons, measurement reduction comparisons, and the evaluation of critical measurements will also be presented in Chapter 5.

Table 4.1 Elemental Sources for Static Pressure Measurements

Systematic Uncertainty	**Elemental Bias Error Estimates**	
Quartz X-ducers	0.025	
Barometer (Cal.)	0.098	
Barometer (Readings)	0.050	
Conceptual Bias (Square Volute)	3.220	
Conceptual Bias (Circular Volute)	2.952	
Random Uncertainty	**NWA**	**CWA**
Precision of Ave. (Square Volute)	0.09	0.211
Precision of Ave. (Circular Volute)	0.06	0.120
Overall Uncertainty for Wall-Static Pressure Averaging	**NWA**	**CWA**
Square Volute	3.257	3.257
Circular Volute	2.979	2.979

Table 4.2 Detailed Analysis Uncertainty Estimates

Variable, X	P_X	B_X	U_X	Comments
P_{01} (psia)	0.15	0.11		
T_{01} ($^\circ R$)	0.71	0.18		
P_{02} (psia)	0.15	0.11		
T_{02} ($^\circ R$)			0.74	
P_2 (psia)			0.30	Cobra
			0.36	Fit---Cobra
			0.54	Scaled YC, Fit---YC
a_2 ($^\circ$)			0.50	Cobra
			0.90	YC
			1.00	Fit
$\dot{W}$ (lb_m/s)			0.089	
Tq (ft-lb_f)	0.11	0.70		
N (RPM)	0.42	1.00		
Variables, $X_i X_j$		B_{XiXj}		**Comments**
$P_{01}P_{01}$ (psia)		0.013		
$T_{01}T_{01}$ ($^\circ R$)		0.023		
$P_{02}P_{02}$ (psia)		0.013		
$T_{02}T_{02}$ ($^\circ R$)		0.023		
P_2P_2 (psia)		0.013		
a_2a_2 ($^\circ$)		0.250		Cobra with same cobra
		0.810		YC with YC
$P_{01}P_{02}$ (psia)		0.013		
$P_{01}P_2$ (psia)		0.013		
$P_{01}a_2$ (psia)		0.000		
$P_{02}P_2$ (psia)		0.013		
$P_{02}a_2$ (psia)		0.000		
$T_{01}T_{02}$ ($^\circ R$)		0.023		
P_2a_2 (psia)		0.000		

CHAPTER V

UNCERTAINTY ANALYSIS RESULTS

5.1 Square Exit Volute Test

The detailed uncertainty results obtained from the new uncertainty analysis methodology stated in the previous chapter will now be given. The uncertainty results generated from mass averaging are presented in Tables 5.1, 5.2, 5.3, 5.4, and 5.5, while the results from area averaging are presented in Tables 5.6, 5.7, and 5.8. Tables 5.1 through 5.3 and Tables 5.6 through 5.8 are the uncertainty results for the measurement reduction analysis. Tables 5.4 and 5.5 are the uncertainty results for the wall-static averaging analysis. In addition, the summary plots of the mass averaging results with error bands are in Figures 5.1 and 5.2. Figure 5.1 represents the uncertainty of the thermodynamic efficiency, and Figure 5.2 represents the uncertainty of the mechanical efficiency. Figures 5.3 and 5.4 are plots of the area averaging uncertainty results with error bands. The UPC values of all of the measured variables and the correlation terms are presented in all of the tables. The summation of all UPC terms for each cases equals 100%. The general trend for the mass averaged results (Table 5.1) was that the correlation terms $P_{01}P_{01}$, $P_{02}P_{02}$, $T_{01}T_{01}$, and $T_{02}T_{02}$ were the major contributing factors to the overall uncertainty, and the correlation terms $P_{01}P_{02}$ and $T_{01}T_{02}$ served to reduce the overall uncertainty. In addition, the conceptual bias terms were very small for cases with

360° circumferential coverage. Reducing the number of measurements changed the UPC values of each term. The changes of $P_{01}P_{02}$, $T_{01}T_{02}$, $P_{02}P_{02}$, and $T_{02}T_{02}$ were the most dramatic as the total number of measurements decreased. Those correlation terms were dominated by the high gradient flow field of the turbine exit. Hence, reducing the number of measurements greatly altered the average values of exit total pressure and total temperature, which in turn affected the UPC values that included those terms. For most quadrants coverage test cases the conceptual bias terms had very large UPC values (Tables 5.2 and 5.3). The YC probe covered most of the highest gradient section, hence the UPC's of the conceptual bias terms were smaller (Table 5.3) compared to the cobra probe test (Table 5.2), and the $P_{01}P_{01}$, $P_{02}P_{02}$, $T_{01}T_{01}$, $P_{01}P_{02}$, $T_{01}T_{02}$, and $T_{02}T_{02}$ terms had moderate UPC values. As for area averaging the conceptual bias terms contributed approximately 90% of the uncertainty (Tables 5.6, 5.7, and 5.8). More details of these data comparing averaging technique, number of measurements required, and types of measurements are discussed in the following sections.

5.1.1 Averaging Techniques

The comparison between mass and area averaging showed that the area averaging generated large overall uncertainty, U_h, as expected (Tables 5.6 through 5.8, and Figures 5.1 and 5.3). The mass averaging results gave much lower uncertainty values. The mass flow near the turbine walls was minimum, and the measurements were very different compared to the rest of the flow field. Mass averaging correctly accounted for the gradients in the exit flow field by weighting each measurement properly to obtain the

average value. The uncertainty results for area averaging are given in Tables 5.6 through 5.8 (Figures 5.3 and 5.4). The area averages did not account for the influence of gradients in the turbine exit flow field; therefore, the area averaged values were very different from the "true" values. Area averaging ignored the impact of mass flow because the method was a numerical average (equal weights for all measurements). Area averaging produced overall uncertainties in efficiency of approximately $\pm 7\%$ for the thermodynamic method and $\pm 8\%$ for the mechanical method. These results were unreliable because the turbine exit flow field average values had large errors. The analysis proved that mass averaging is crucial for turbine systems that generate high gradients in the flow field. Area averaging was not suitable for the OTTR turbine exit flow field with its large gradients and low uncertainty requirements. Area averaging should only be applied when the flow field has small gradients or when the uncertainty requirements are much less strict.

5.1.2 Reducing Number of Measurements

The uncertainty results using 720-point measurements and mass averaging at the turbine exit were considered the "true" or "best" uncertainty estimates for the OTTR with the square exit volute. Results from reducing the number of measurements were compared with these "true" values. The overall uncertainty percentages for 720-point measurements were approximately $\pm 0.17\%$ of the thermodynamic efficiency and $\pm 0.85\%$ of the mechanical efficiency. The uncertainty band increased as the number of measurements decreased when mass averaging was used at the turbine exit (Tables 5.1 through 5.3 and Figures 5.1 and 5.2). This increase in uncertainty was due to the

uncertainty contribution of the conceptual bias terms (UPC). As the number of measurements decreased, the conceptual bias estimates increased. In addition, the uncertainty percentages of the thermodynamic method became higher than the mechanical method as the number of measurements were reduced. The conceptual bias contribution to the thermodynamic method caused the overall uncertainty to be slightly higher than the mechanical method (Note UPC of conceptual bias, Table 5.1). The thermodynamic method had two conceptual bias contributors, whereas the mechanical method only had one conceptual bias contributor. Hence, reducing the number of measurements affected the thermodynamic efficiency more because both the exit total pressure and temperature increased the conceptual bias error. The mechanical efficiency only had exit total pressure that increased the uncertainty (Table 5.1).

The results proved that the reduction of measurements to 360-points was still good enough to maintain an accuracy below the 1% goal set for the OTTR test. An important fact was that the entire circumferential area of the turbine exit flow field was mapped (This fact will become more clear when the quadrants coverage cases are discussed). The full coverage provided the possibility to maintain accuracy and kept the uncertainty low as the number of measurements was reduced to 360-points. The 180-points and 90-points test cases were quite accurate, but exceeded the OTTR test accuracy requirement.

The averaging of two 90° quadrants of the turbine exit plane gave unpredictable results. The uncertainty increased as the number of measurements decreased for both the cobra probes and YC probe cases, as expected. However, Figures 5.1 and 5.2 show that the cobra averaging uncertainty was much higher than the uncertainty generated by YC

averaging. Including the regression of the two missing sections, the uncertainty percentages for 720-point cobra probe measurements were $\pm 2.76\%$ for the thermodynamic efficiency and $\pm 2.51\%$ for the mechanical efficiency. Even with the largest number of measurements, the results were not suitable for the OTTR test. The YC probes measured a large portion of the highest gradient section at the turbine exit plane; hence, the average values calculated were closer to the "true" average values. The conceptual bias estimates and the overall uncertainties were than much smaller for the YC coverage. The overall uncertainty percentages at 720-point YC probe measurements were approximately $\pm 0.42\%$ of the thermodynamic efficiency and $\pm 0.89\%$ of the mechanical efficiency. The trends of the uncertainty percentages (UPC) in Table 5.3 were very similar to the ones in Table 5.1. The uncertainty results showed that the uncertainty with the point YC probe measurements still met the OTTR test goal. These results show that mapping only certain quadrants in highest gradient flow fields can be very dangerous–the results are not predictable. It is important to cover the full 360° to have confidence in the results. The uncertainty analysis for the circular exit volute test will strengthen the conclusions in this section.

The uncertainty results for area averaging are given in Tables 5.6 through 5.8 (Figures 5.3 and 5.4). The area averages did not use a weighting factor to account for the influence of gradients in the turbine exit flow field; therefore, the area averaged values were very different from the "true" values. The uncertainty results showed that weighting all measurements equally generated a relatively constant uncertainty band, and this band was always much greater than the test goal of 1%. Reducing the number of measurements should increase the uncertainty. However, with the area averaging

weighting all measurements equally, the average values were approximately equal regardless of the number of measurements taken. Therefore, the conceptual bias estimates were equal for all measurement reduction cases (Tables 3.7, 3.8, and 3.9). The observations proved that area averaging offered little account of the effects of measurement reduction or the effects of high gradients in the turbine flow field.

One obvious observation when comparing the uncertainty results of the thermodynamic efficiency and the mechanical efficiency has yet to be explained. The mechanical efficiency was lower than the thermodynamic efficiency for all case studies, and the uncertainty bands do not reconcile the large differences in efficiency. These differences are due to the torque value required in the mechanical efficiency calculation and are explained in reference 1. This is also believed to be the reason that the error bands in Figure 5.4 do not quite cover the "true" value for all of the mechanical efficiency cases. On the other hand, the efficiency results provided by the thermodynamic method had lower uncertainties than those with the mechanical method. This was due to the extreme care taken with the calibration of the temperature probes due to the general uncertainty analysis results obtained in the planning phase of the OTTR test program. The thermodynamic method was superior to the mechanical method for determining turbine efficiency for the OTTR [1]. However, in some cases, the mechanical method could be more suitable [1, 4, 9].

5.1.3 Evaluation of Measurement Types

The uncertainty results for wall-static averaging are summarized in Figures 5.1 and 5.2. The details of the uncertainty results are provided in Tables 5.4 and 5.5. The

wall-static pressures were averaged to replace the static pressure measurements across the annulus at the turbine exit provided by the cobra and YC probes. The uncertainty results of wall-static averaging were very promising. The measurement reduction cases for both wall-static averaging methods (NWA and CWA) were done. The Figures 5.1 and 5.2 best illustrate the impact of wall-static averaging for both CWA and NWA. The uncertainty results seen in Figures 5.1 and 5.2 show that the efficiency uncertainty increased and exceed the OTTR test goal of 1% for NWA. However, the CWA results were similar to the uncertainty bands of the original uncertainty methodology provided in the first four columns of the figures. The CWA captured the relative changes in static pressure circumferentially because the wall-static pressure taps were located on the rotating ring. These circumferential changes in static pressure were very similar at all radial positions although the absolute level of the static pressure varied with radial position. The relative changes in static pressure rather than the absolute level were important in obtaining accurate mass averaged values. The NWA approach did not capture the circumferential variations. Therefore, the CWA mass averaged quantities, efficiency calculations, and efficiency uncertainties were very close to the “true” values, whereas the NWA values differed significantly causing the uncertainties to increase. Future static pressure measurements needed for turbine efficiency calculations in high gradient flow fields could be obtained by measuring wall static pressures if enough circumferential measurements can be made. This could save both time and money by reducing the number of probe calibrations and the test time required to obtain the necessary measurements.

Recall from Chapter 3 that the cobra and YC probes used to measure static pressure across the annulus were also used to measure flow angle. Eliminating the need to use these probes for static pressure measurements greatly reduces the calibration requirements relative to their use for flow angle measurements only. However, reducing the need for 360° coverage with flow angle measurements would provide further benefits. Initial results from a simple sensitivity study for flow angle showed that the efficiency calculation was not extremely sensitive to flow angle. Therefore, obtaining flow angles in limited regions where access with cobra probes on radial actuators is possible making the flow angle measurements relatively quick and easy to obtain may be all that is needed. However, further study in required to draw a firm conclusion. Caution is advised when deciding if static pressure and flow angle measurements across the annulus are necessary for a particular test. Remember that this study looked at the effect on turbine efficiency only. Obtaining these measurements would most likely be necessary for complete flow field maps and code validation.

5.2 Circular Exit Volute Test

The uncertainty results for the OTTR circular exit volute test were similar to the results collected for the square exit volute. The uncertainty results for mass averaging are presented in Tables 5.9, 5.10, 5.11, 5.12, and 5.13, while the results from area averaging are presented in Tables 5.14, 5.15, and 5.16. Tables 5.9 through 5.11 and Tables 5.14 through 5.16 are the uncertainty results for the measurement reduction analysis. Tables 5.12 and 5.13 are the uncertainty results for the wall-static averaging analysis. In addition, the summary plots of the mass averaging results with error bands are in Figures

5.5 and 5.6. Figure 5.5 represents the uncertainty of the thermodynamic efficiency, and Figure 5.6 represents the uncertainty of the mechanical efficiency. Figures 5.7 and 5.8 are plots of the area averaging uncertainty results with error bands. The same analyses that were done for the square volute test were repeated for these sets of uncertainty results. The following sections discuss these uncertainty results. The comparisons of results for the square versus the circular exit volute tests will also be presented.

5.2.1 Averaging Techniques

The comparison between mass and area averaging for the circular exit volute test generated the same conclusions made for the square volute test (Figures 5.5 and 5.7). The major difference between the two tests was that the circular volute test efficiencies were higher. There were only minor differences in uncertainty results. The overall uncertainty for mass averaging was between $\pm 0.17\%$ and $\pm 2.94\%$ of the efficiency. The UPC trends for the circular volute test (Table 5.9) were similar to those for the square volute test. The area averaging ignored the impact of mass flow rate; hence, the area averaging generated higher uncertainties. The area averaging results were unreliable because the uncertainties observed for 720-point measurements were between $\pm 6.78\%$ and $\pm 7.12\%$ of the efficiency for both the thermodynamic and mechanical methods. The uncertainties were slightly lower than those obtained for area averaging with the square volute. This was expected since the gradients were lower for the circular volute; therefore, the area averaged values did not differ from the “true” values by as much as they did with the square volute. The results help proved again that weighting all measurements equally generates a constant uncertainty band, as illustrated in Figures 5.7

and 5.8. Again, the uncertainty results for area averaging were equal for all cases because the conceptual bias estimates were equal for all measurement reduction cases (Uncertainty results in Figures 5.7, and 5.8 and conceptual bias estimates in Table 5.14, 5.15, and 5.16). The circular volute uncertainty analysis reinforced the need to mass average when the turbine system generates a high gradient flow field. In conclusion, the use of area averaging was not suitable for the OTTR testing, as stated in Section 5.1.2.

5.2.2 Reducing Number of Measurements

The measurement reduction uncertainty results for the circular volute test were similar to those of the square volute test. The uncertainty results for area averaging were uniform (Figures 5.7 and 5.8). The uncertainty results using 720-point measurements and mass averaging at the turbine exit were again considered the "true" or "best" uncertainty estimates for the OTTR with the circular exit volute. Results from reducing the number of measurements were compared with these "true" values as with the square volute test data. The overall uncertainty percentages for 720-point measurements were approximately $\pm 0.17\%$ of the thermodynamic efficiency and $\pm 0.85\%$ of the mechanical efficiency. The uncertainty percentages for the circular volute test had trends similar to the square volute test with 720-points circumferential coverage (Tables 5.9, 5.10, and 5.11). The mass averaging results (Figures 5.5 and 5.6) again showed a gradual increase in overall uncertainty percentage as the total number of measurement decreased. The circular volute results proved that the reduction of measurements to 360-points still allowed the uncertainty goal of $\pm 1\%$ to be met for the OTTR test. The 180-points and

90-points test cases were quite accurate but exceeded the OTTR test accuracy requirement.

The averaging of two 90˚ quadrants of the turbine exit plane again gave an increase in uncertainty as the number of measurements decreased. Unlike the square volute test, however, Figures 5.5 and 5.6 show that the cobra averaging uncertainty was similar to the uncertainty trend generated by YC averaging. The uncertainty percentages for 720-point cobra probe measurements were $\pm 0.18\%$ for the thermodynamic efficiency and $\pm 0.85\%$ for the mechanical efficiency. The results with the largest number of cobra probe measurements generated uncertainties that were very close to the "true" uncertainties. The close match in efficiency and uncertainty results to the "true" was determined by the averaging of the highest gradients at the turbine exit. The cobra probes covered 85.5% of the highest gradient section at the turbine exit for the circular volute test, and the averages of those measurements were very close to the "true" averaged values. On the other hand, the YC probe measurements covered a much smaller portion (14.5%) of the highest gradient section. The overall uncertainty percentages for 720-point YC probe measurements were approximately $\pm 0.30\%$ for the thermodynamic efficiency and $\pm 0.88\%$ for the mechanical efficiency. The percentages of uncertainty were only slightly higher than the results from the cobra probe uncertainty analysis. Hence, the averaging of the lower gradient portion of the flow field also generated averaged properties which were very close to the "true" averaged properties for all cases.

Caution is advised in generalizing these results. The unpredictable results obtained from the quadrants averaging indicate that the accuracy of the averaged values are highly dependent on the locations of the measurements relative to large gradients, and

a means of defining where the measurements should be made was not clear. It seems that it would be extremely difficult to know where to make these measurements based on pretest predictions. Therefore, the recommendation is that it would be much better to cover the full 360° even with a smaller number of measurements than it would be to cover only certain quadrants with more dense measurements.

5.2.3 Evaluation of Measurement Types

The uncertainty results for wall-static averaging are similar to those from the square volute test. The results for the circular volute wall-static averaging are summarized in Figures 5.5 and 5.6. The details of the uncertainty results are provided in Tables 5.4 and 5.5. Again, the uncertainty bands of the CWA were very similar to the uncertainty bands of the original uncertainty methodology provided in the first four columns. The uncertainty increased with NWA; however, all of the uncertainty values were lower than they were for the square volute test. This is most likely due to the fact because the gradients were lower for the circular volute test. Therefore, NWA may be suitable for flow fields with lower gradients. These results reinforced the conclusions made by the square volute test wall-static averaging results. The wall-static pressure measurements could replace the cobra and YC probes annulus static pressure measurements without a loss in accuracy for turbine efficiency. However, the CWA method is recommended. This could provide considerable savings of both time and money, but the considerations and limitation given in Section 5.1.3 are still applicable.

Table 5.1 Mass Averaging Detailed Uncertainty Results (Square Volute with 360° Circumferential Coverage)

OTTR with Square Exit Volute		**Thermodynamic Method**				**Mechanical Method**				
Mass Avg.		**Points**	**Points**	**Points**	**Points**		**720 Points**	**360 Points**	**180 Points**	**90 Points**
	h_{th}	0.6480	0.6457	0.6479	0.6506	h_{me}	0.6034	0.6035	0.6034	0.6045
	$U_{h_{th}}$	0.0011	0.0042	0.0091	0.0188	$U_{h_{me}}$	0.0051	0.0056	0.0072	0.0118
	U_h / h *100	0.17	0.62	1.4	2.9	U_h / h *100	0.85	0.93	1.2	2.0
	Terms	UPC				Terms	UPC			
	P_{01}	0.59	0.08	0.03	0.02	P_{01}	0.02	0.04	0.05	0.04
	P_{02}	1.96	0.27	0.11	0.05	P_{02}	0.08	0.14	0.16	0.12
	T_{01}	9.34	1.28	0.55	0.26	T_{01}	0.00	0.01	0.01	0.01
	T_{02}	13.87	1.90	0.81	0.38	Tq	11.82	9.80	5.93	2.22
	P_2	0.16	0.02	0.01	0.00	N	0.12	0.10	0.06	0.02
	a_2	0.82	0.11	0.05	0.02	P_2	0.02	0.03	0.05	0.04
	$P_{01}P_{01}$	159.01	43.33	37.15	35.25	a_2	0.11	0.18	0.21	0.16
	$P_{02}P_{02}$	420.50	28.59	6.12	1.44	$\dot{W}$	86.19	71.50	43.23	16.16
	$T_{01}T_{01}$	287.18	78.88	67.13	63.13	$P_{01}P_{01}$	6.41	21.29	51.47	77.26
	$T_{02}T_{02}$	344.99	23.63	5.01	1.17	$P_{02}P_{02}$	16.68	13.80	8.35	3.12
	P_2P_2	0.11	0.01	0.00	0.00	$T_{01}T_{01}$	0.10	0.34	0.83	1.25
	a_2a_2	0.00	0.00	0.00	0.00	P_2P_2	0.01	0.01	0.00	0.00
	$P_{01}P_{02}$	-518.69	-35.33	-7.58	-1.80	a_2a_2	0.00	0.00	0.00	0.00
	$P_{01}P_2$	-8.46	-0.57	-0.11	-0.03	$P_{01}P_{02}$	-20.75	-17.21	-10.43	-3.92
	$P_{01}a_2$	0.00	0.00	0.00	0.00	$P_{01}P_2$	-0.49	-0.42	-0.23	-0.08
	$P_{02}P_2$	13.74	0.93	0.19	0.04	$P_{01}a_2$	0.00	0.00	0.00	0.00
	$P_{02}a_2$	0.00	0.00	0.00	0.00	$P_{02}P_2$	0.79	0.67	0.37	0.13
	$T_{01}T_{02}$	-631.38	-43.34	-9.22	-2.17	$P_{02}a_2$	0.00	0.00	0.00	0.00
	P_2a_2	0.00	0.00	0.00	0.00	P_2a_2	0.00	0.00	0.00	0.00
	P_{01C}		0.00	0.00	0.00	P_{01C}		0.00	0.00	0.00
	P_{02C}		0.09	0.21	1.20	P_{02C}		0.04	0.29	2.65
	T_{01C}		0.00	0.00	0.00	T_{01C}		0.00	0.00	0.00
	T_{02C}		1.57	0.23	0.91					

Table 5.2 Mass Averaging Detailed Uncertainty Results (Square Volute with Cobra Quadrants Coverage)

OTTR with Square Exit Volute		**Thermodynamic Method**				**Mechanical Method**				
Mass Avg.		**Cobra 720 Pt (Reg.)**	**Cobra 360 Pt (Reg.)**	**Cobra 180 Pt (Reg.)**	**Cobra 90 Pt (Reg.)**		**Cobra 720 Pt (Reg.)**	**Cobra 360 Pt (Reg.)**	**Cobra 180 Pt (Reg.)**	**Cobra 90 Pt (Reg.)**
	h_{th}	0.6513	0.6512	0.6509	0.6535	h_{me}	0.6175	0.6175	0.6175	0.6176
	$U_{h_{th}}$	0.0180	0.0189	0.0201	0.0255	$U_{h_{me}}$	0.0155	0.0159	0.0161	0.0188
	U_h / h *100	2.8	2.9	3.1	3.9	U_h / h *100	2.5	2.6	2.6	3.0
	Terms	UPC				Terms	UPC			
	P_{01}	0.00	0.00	0.01	0.01	P_{01}	0.00	0.01	0.01	0.02
	P_{02}	0.01	0.01	0.03	0.03	P_{02}	0.01	0.02	0.04	0.05
	T_{01}	0.04	0.07	0.12	0.15	T_{01}	0.00	0.00	0.00	0.00
	T_{02}	0.06	0.10	0.18	0.23	Tq	1.34	1.27	1.24	0.91
	P_2	0.00	0.00	0.00	0.00	N	0.01	0.01	0.01	0.01
	a_2	0.00	0.00	0.01	0.01	P_2	0.00	0.00	0.00	0.01
	$P_{01}P_{01}$	0.63	2.30	8.11	20.31	a_2	0.01	0.03	0.05	0.08
	$P_{02}P_{02}$	1.66	1.50	1.32	0.82	$\dot{W}$	9.77	9.29	9.06	6.64
	$T_{01}T_{01}$	1.13	4.09	14.46	35.93	$P_{01}P_{01}$	0.77	2.92	11.37	33.38
	$T_{02}T_{02}$	1.35	1.22	1.08	0.66	$P_{02}P_{02}$	1.99	1.89	1.84	1.33
	P_2P_2	0.00	0.00	0.00	0.00	$T_{01}T_{01}$	0.01	0.04	0.17	0.51
	a_2a_2	0.00	0.00	0.00	0.00	P_2P_2	0.00	0.00	0.00	0.00
	$P_{01}P_{02}$	-2.06	-1.87	-1.65	-1.03	a_2a_2	0.00	0.00	0.00	0.00
	$P_{01}P_2$	-0.01	-0.01	-0.01	-0.01	$P_{01}P_{02}$	-2.48	-2.36	-2.30	-1.68
	$P_{01}a_2$	0.00	0.00	0.00	0.00	$P_{01}P_2$	-0.03	-0.03	-0.03	-0.02
	$P_{02}P_2$	0.02	0.02	0.02	0.01	$P_{01}a_2$	0.00	0.00	0.00	0.00
	$P_{02}a_2$	0.00	0.00	0.00	0.00	$P_{02}P_2$	0.05	0.04	0.05	0.04
	$T_{01}T_{02}$	-2.47	-2.24	-1.98	-1.23	$P_{02}a_2$	0.00	0.00	0.00	0.00
	P_2a_2	0.00	0.00	0.00	0.00	P_2a_2	0.00	0.00	0.00	0.00
	P_{01C}	0.00	0.00	0.00	0.00	P_{01C}	0.00	0.00	0.00	0.00
	P_{02C}	72.37	67.88	56.07	35.96	P_{02C}	87.96	86.29	78.63	58.88
	T_{01C}	0.00	0.00	0.00	0.00	T_{01C}	0.00	0.00	0.00	0.00
	T_{02C}	27.69	26.45	22.65	8.19					

Table 5.3 Mass Averaging Detailed Uncertainty Results (Square Volute with YC Quadrants Coverage)

OTTR with Square Exit Volute		**Thermodynamic Method**				**Mechanical Method**				
Mass Avg.		**YC 720 Pt (Reg.)**	**YC 360 Pt (Reg.)**	**YC 180 Pt (Reg.)**	**YC 90 Pt (Reg.)**		**YC 720 Pt (Reg.)**	**YC 360 Pt (Reg.)**	**YC 180 Pt (Reg.)**	**YC 90 Pt (Reg.)**
	h_{th}	0.6455	0.6545	0.6452	0.6456	h_{me}	0.6049	0.6050	0.6049	0.6045
	$U_{h_{th}}$	0.0027	0.0050	0.0094	0.0186	$U_{h_{me}}$	0.0054	0.0059	0.0074	0.0116
	U_h / h *100	0.42	0.76	1.5	2.9	U_h / h *100	0.89	0.98	1.2	1.9
	Terms	UPC				Terms	UPC			
	P_{01}	0.10	0.06	0.03	0.02	P_{01}	0.02	0.04	0.05	0.04
	P_{02}	0.32	0.19	0.11	0.05	P_{02}	0.07	0.12	0.15	0.12
	T_{01}	1.56	0.91	0.51	0.26	T_{01}	0.00	0.01	0.01	0.01
	T_{02}	2.32	1.35	0.76	0.39	Tq	10.59	8.88	5.64	2.29
	P_2	0.02	0.01	0.01	0.00	N	0.10	0.09	0.06	0.02
	a_2	0.14	0.08	0.05	0.02	P_2	0.01	0.02	0.02	0.01
	$P_{01}P_{01}$	26.33	30.72	34.73	35.47	a_2	0.11	0.18	0.23	0.18
	$P_{02}P_{02}$	68.58	19.97	5.62	1.43	$\dot{W}$	77.26	64.74	41.14	16.72
	$T_{01}T_{01}$	47.96	55.96	63.31	64.59	$P_{01}P_{01}$	5.78	19.39	49.25	79.96
	$T_{02}T_{02}$	57.55	16.76	4.72	1.20	$P_{02}P_{02}$	14.56	12.18	7.70	3.11
	P_2P_2	0.03	0.01	0.00	0.00	$T_{01}T_{01}$	0.09	0.31	0.79	1.29
	a_2a_2	0.00	0.00	0.00	0.00	P_2P_2	0.02	0.02	0.01	0.00
	$P_{01}P_{02}$	-85.24	-24.86	-7.03	-1.80	a_2a_2	0.00	0.00	0.00	0.00
	$P_{01}P_2$	-1.94	-0.57	-0.16	-0.04	$P_{01}P_{02}$	-18.40	-15.43	-9.80	-3.98
	$P_{01}a_2$	0.00	0.00	0.00	0.00	$P_{01}P_2$	-0.72	-0.61	-0.39	-0.16
	$P_{02}P_2$	3.13	0.91	0.26	0.06	$P_{01}a_2$	0.00	0.00	0.00	0.00
	$P_{02}a_2$	0.00	0.00	0.00	0.00	$P_{02}P_2$	1.15	0.96	0.62	0.25
	$T_{01}T_{02}$	-105.38	-30.74	-8.69	-2.22	$P_{02}a_2$	0.00	0.00	0.00	0.00
	P_2a_2	0.00	0.00	0.00	0.00	P_2a_2	0.00	0.00	0.00	0.00
	P_{01C}	0.00	0.00	0.00	0.00	P_{01C}	0.00	0.00	0.00	0.00
	P_{02C}	35.21	13.50	2.51	0.41	P_{02C}	7.77	8.46	3.54	0.93
	T_{01C}	0.00	0.00	0.00	0.00	T_{01C}	0.00	0.00	0.00	0.00
	T_{02C}	49.16	16.55	3.80	0.44					

Table 5.4 Mass Averaging Detailed Uncertainty Results (Square Volute with CWA)

OTTR with Square Exit Volute		**Thermodynamic Method**					**Mechanical Method**			
Mass Avg.		**CWA 720 Pt**	**CWA 360 Pt**	**CWA 180 Pt**	**CWA 90 Pt**		**CWA 720 Pt**	**CWA 360 Pt**	**CWA 180 Pt**	**CWA 90 Pt**
	h_{th}	0.6491	0.6454	0.6491	0.6517	h_{me}	0.6058	0.6050	0.6058	0.6069
	$U_{h_{th}}$	0.0011	0.0043	0.0092	0.0189	$U_{h_{me}}$	0.0052	0.0057	0.0073	0.0119
	U_h / h *100	0.17	0.67	1.4	2.9	U_h / h *100	0.86	0.94	1.2	2.0
	Terms	UPC				Terms	UPC			
	P_{01}	0.60	0.08	0.03	0.02	P_{01}	0.02	0.04	0.05	0.04
	P_{02}	1.98	0.26	0.11	0.05	P_{02}	0.08	0.13	0.16	0.12
	T_{01}	9.42	1.23	0.54	0.26	T_{01}	0.00	0.01	0.01	0.01
	T_{02}	14.04	1.84	0.81	0.38	Tq	11.46	9.54	5.81	2.20
	P_2	7.46	0.92	0.44	0.22	N	0.11	0.09	0.06	0.02
	a_2	0.80	0.10	0.04	0.02	P_2	1.02	1.62	2.15	1.75
	$P_{01}P_{01}$	161.01	41.85	36.82	35.33	a_2	0.11	0.18	0.20	0.16
	$P_{02}P_{02}$	418.02	27.11	5.95	1.42	$\dot{W}$	83.56	69.56	42.40	16.01
	$T_{01}T_{01}$	289.59	75.88	66.24	62.97	$P_{01}P_{01}$	6.27	20.90	50.95	77.26
	$T_{02}T_{02}$	347.73	22.72	4.95	1.17	$P_{02}P_{02}$	15.72	13.05	7.96	3.01
	P_2P_2	0.22	0.01	0.00	0.00	$T_{01}T_{01}$	0.10	0.34	0.82	1.23
	a_2a_2	0.00	0.00	0.00	0.00	P_2P_2	0.03	0.02	0.01	0.00
	$P_{01}P_{02}$	-520.41	-33.82	-7.44	-1.79	a_2a_2	0.00	0.00	0.00	0.00
	$P_{01}P_2$	-12.18	-0.79	-0.17	-0.04	$P_{01}P_{02}$	-19.93	-16.58	-10.13	-3.85
	$P_{01}a_2$	0.00	0.00	0.00	0.00	$P_{01}P_2$	-0.82	-0.69	-0.40	-0.14
	$P_{02}P_2$	19.60	1.28	0.27	0.06	$P_{01}a_2$	0.00	0.00	0.00	0.00
	$P_{02}a_2$	0.00	0.00	0.00	0.00	$P_{02}P_2$	1.30	1.09	0.63	0.22
	$T_{01}T_{02}$	-636.53	-41.68	-9.10	-2.16	$P_{02}a_2$	0.00	0.00	0.00	0.00
	P_2a_2	0.00	0.00	0.00	0.00	P_2a_2	0.00	0.00	0.00	0.00
	P_{01C}	0.00	0.00	0.00	0.00	P_{01C}	0.00	0.00	0.00	0.00
	P_{02C}	0.00	0.09	0.20	1.21	P_{02C}	0.00	0.04	0.27	2.66
	T_{01C}	0.00	0.00	0.00	0.00	T_{01C}	0.00	0.00	0.00	0.00
	T_{02C}	0.00	1.51	0.23	0.90					

Table 5.5 Mass Averaging Detailed Uncertainty Results (Square Volute with NWA)

OTTR with Square Exit Volute		**Thermodynamic Method**				**Mechanical Method**				
Mass Avg.		**NWA 720 Pt**	**NWA 360 Pt**	**NWA 180 Pt**	**NWA 90 Pt**		**NWA 720 Pt**	**NWA 360 Pt**	**NWA 180 Pt**	**NWA 90 Pt**
	h_{th}	0.6440	0.6468	0.6491	0.6517	h_{me}	0.5855	0.6059	0.6058	0.6059
	$U_{h_{th}}$	0.0077	0.0092	0.0124	0.0215	$U_{h_{me}}$	0.0082	0.0089	0.0102	0.0147
	U_h / h *100	1.2	1.4	2.0	3.3	U_h / h *100	1.4	1.5	1.7	2.4
	Terms	UPC				Terms	UPC			
	P_{01}	0.01	0.02	0.02	0.01	P_{01}	0.01	0.02	0.02	0.02
	P_{02}	0.03	0.06	0.06	0.04	P_{02}	0.03	0.05	0.08	0.08
	T_{01}	0.18	0.27	0.30	0.20	T_{01}	0.00	0.00	0.00	0.00
	T_{02}	0.23	0.40	0.44	0.29	Tq	4.30	3.91	2.98	1.44
	P_2	0.96	0.20	0.24	0.17	N	0.04	0.04	0.03	0.01
	a_2	0.01	0.02	0.02	0.02	P_2	3.24	0.66	1.10	1.14
	$P_{01}P_{01}$	2.99	9.14	20.27	27.30	a_2	0.03	0.07	0.10	0.10
	$P_{02}P_{02}$	7.25	5.92	3.28	1.10	$\dot{W}$	31.39	28.53	21.72	10.49
	$T_{01}T_{01}$	5.49	16.58	36.47	48.66	$P_{01}P_{01}$	2.18	8.57	26.10	50.63
	$T_{02}T_{02}$	6.63	4.96	2.72	0.90	$P_{02}P_{02}$	4.24	5.35	4.08	1.97
	P_2P_2	0.04	0.00	0.00	0.00	$T_{01}T_{01}$	0.04	0.14	0.42	0.81
	a_2a_2	0.00	0.00	0.00	0.00	P_2P_2	0.17	0.01	0.01	0.00
	$P_{01}P_{02}$	-9.34	-7.39	-4.10	-1.38	a_2a_2	0.00	0.00	0.00	0.00
	$P_{01}P_2$	-0.74	-0.17	-0.09	-0.03	$P_{01}P_{02}$	-6.10	-6.80	-5.19	-2.52
	$P_{01}a_2$	0.00	0.00	0.00	0.00	$P_{01}P_2$	-1.23	-0.28	-0.21	-0.09
	$P_{02}P_2$	1.15	0.28	0.15	0.05	$P_{01}a_2$	0.00	0.00	0.00	0.00
	$P_{02}a_2$	0.00	0.00	0.00	0.00	$P_{02}P_2$	1.71	0.45	0.33	0.15
	$T_{01}T_{02}$	-12.11	-9.11	-5.01	-1.67	$P_{02}a_2$	0.00	0.00	0.00	0.00
	P_2a_2	0.00	0.00	0.00	0.00	P_2a_2	0.00	0.00	0.00	0.00
	P_{01C}	0.00	0.00	0.00	0.00	P_{01C}	0.00	0.00	0.00	0.00
	P_{02C}	81.88	62.48	37.53	19.13	P_{02C}	60.01	58.51	48.07	35.57
	T_{01C}	0.00	0.00	0.00	0.00	T_{01C}	0.00	0.00	0.00	0.00
	T_{02C}	15.70	16.15	8.48	5.33					

Table 5.6 Area Averaging Detailed Uncertainty Results (Square Volute with 360° Circumferential Coverage)

OTTR with Square Exit Volute		**Thermodynamic Method**				**Mechanical Method**				
Area Avg.		**720 Points**	**360 Points**	**180 Points**	**90 Points**		**720 Points**	**360 Points**	**180 Points**	**90 Points**
	h_{th}	0.6341	0.6321	0.6337	0.6364	h_{me}	0.5644	0.5645	0.5644	0.5653
	$U_{h_{th}}$	0.0501	0.0504	0.0511	0.0541	$U_{h_{me}}$	0.0374	0.0375	0.0376	0.0378
	U_h / h *100	7.9	8.0	8.1	8.5	U_h / h *100	6.6	6.6	6.7	6.7
	Terms	UPC				Terms	UPC			
	P_{01}	0.00	0.00	0.00	0.00	P_{01}	0.00	0.00	0.00	0.00
	P_{02}	0.00	0.00	0.00	0.00	P_{02}	0.00	0.00	0.00	0.01
	T_{01}	0.00	0.01	0.02	0.03	T_{01}	0.00	0.00	0.00	0.00
	T_{02}	0.00	0.01	0.02	0.03	Tq	0.19	0.19	0.19	0.19
	P_2	0.00	0.00	0.00	0.00	N	0.00	0.00	0.00	0.00
	a_2	0.00	0.00	0.00	0.00	P_2	0.00	0.00	0.00	0.00
	$P_{01}P_{01}$	0.06	0.25	0.97	3.49	a_2	0.00	0.00	0.00	0.00
	$P_{02}P_{02}$	0.19	0.18	0.18	0.16	$\dot{W}$	1.40	1.40	1.39	1.38
	$T_{01}T_{01}$	0.12	0.48	1.85	6.61	$P_{01}P_{01}$	0.09	0.36	1.41	5.63
	$T_{02}T_{02}$	0.15	0.14	0.14	0.12	$P_{02}P_{02}$	0.26	0.26	0.26	0.26
	P_2P_2	0.00	0.00	0.00	0.00	$T_{01}T_{01}$	0.00	0.01	0.03	0.11
	a_2a_2	0.00	0.00	0.00	0.00	P_2P_2	0.00	0.00	0.00	0.00
	$P_{01}P_{02}$	-0.22	-0.21	-0.21	-0.19	a_2a_2	0.00	0.00	0.00	0.00
	$P_{01}P_2$	0.00	0.00	0.00	0.00	$P_{01}P_{02}$	-0.31	-0.31	-0.30	-0.30
	$P_{01}a_2$	0.00	0.00	0.00	0.00	$P_{01}P_2$	0.00	0.00	0.00	0.00
	$P_{02}P_2$	0.00	0.00	0.00	0.00	$P_{01}a_2$	0.00	0.00	0.00	0.00
	$P_{02}a_2$	0.00	0.00	0.00	0.00	$P_{02}P_2$	0.00	0.00	0.00	0.00
	$T_{01}T_{02}$	-0.27	-0.26	-0.25	-0.23	$P_{02}a_2$	0.00	0.00	0.00	0.00
	P_2a_2	0.00	0.00	0.00	0.00	P_2a_2	0.00	0.00	0.00	0.00
	P_{01C}	0.00	0.00	0.00	0.00	P_{01C}	0.00	0.00	0.00	0.00
	P_{02C}	68.87	135.94	66.11	57.47	P_{02C}	98.29	196.44	96.84	92.80
	T_{01C}	0.00	0.00	0.00	0.00	T_{01C}	0.00	0.00	0.00	0.00
	T_{02C}	31.14	61.26	31.31	32.33					

Table 5.7 Area Averaging Detailed Uncertainty Results (Square Volute with Cobra Quadrants Coverage)

OTTR with Square Exit Volute		**Thermodynamic Method**					**Mechanical Method**			
Area Avg.		**Cobra 720 Pt (Reg.)**	**Cobra 360 Pt (Reg.)**	**Cobra 180 Pt (Reg.)**	**Cobra 90 Pt (Reg.)**		**Cobra 720 Pt (Reg.)**	**Cobra 360 Pt (Reg.)**	**Cobra 180 Pt (Reg.)**	**Cobra 90 Pt (Reg.)**
	h_{th}	0.6384	0.6383	0.6380	0.6402	h_{me}	0.5722	0.5723	0.5723	0.5720
	$U_{h_{th}}$	0.0423	0.0426	0.0431	0.0470	$U_{h_{me}}$	0.0306	0.0306	0.0308	0.0317
	U_h / h *100	6.6	6.7	6.8	7.3	U_h / h *100	5.3	5.3	5.4	5.5
	Terms	UPC				Terms	UPC			
	P_{01}	0.00	0.00	0.00	0.00	P_{01}	0.00	0.00	0.00	0.00
	P_{02}	0.00	0.00	0.00	0.01	P_{02}	0.00	0.00	0.01	0.01
	T_{01}	0.01	0.01	0.02	0.04	T_{01}	0.00	0.00	0.00	0.00
	T_{02}	0.01	0.01	0.03	0.05	Tq	0.30	0.30	0.29	0.27
	P_2	0.00	0.00	0.00	0.00	N	0.00	0.00	0.00	0.00
	a_2	0.00	0.00	0.00	0.00	P_2	0.00	0.00	0.00	0.00
	$P_{01}P_{01}$	0.09	0.36	1.42	4.81	a_2	0.00	0.00	0.00	0.00
	$P_{02}P_{02}$	0.27	0.26	0.26	0.22	$\dot{W}$	2.15	2.15	2.13	2.00
	$T_{01}T_{01}$	0.17	0.68	2.67	8.98	$P_{01}P_{01}$	0.14	0.57	2.24	8.44
	$T_{02}T_{02}$	0.21	0.21	0.20	0.17	$P_{02}P_{02}$	0.41	0.41	0.40	0.38
	P_2P_2	0.00	0.00	0.00	0.00	$T_{01}T_{01}$	0.00	0.01	0.04	0.15
	a_2a_2	0.00	0.00	0.00	0.00	P_2P_2	0.00	0.00	0.00	0.00
	$P_{01}P_{02}$	-0.32	-0.31	-0.30	-0.26	a_2a_2	0.00	0.00	0.00	0.00
	$P_{01}P_2$	0.00	0.00	0.00	0.00	$P_{01}P_{02}$	-0.48	-0.48	-0.48	-0.45
	$P_{01}a_2$	0.00	0.00	0.00	0.00	$P_{01}P_2$	0.00	0.00	0.00	0.00
	$P_{02}P_2$	0.00	0.00	0.00	0.00	$P_{01}a_2$	0.00	0.00	0.00	0.00
	$P_{02}a_2$	0.00	0.00	0.00	0.00	$P_{02}P_2$	0.00	0.00	0.00	0.00
	$T_{01}T_{02}$	-0.38	-0.38	-0.37	-0.31	$P_{02}a_2$	0.00	0.00	0.00	0.00
	P_2a_2	0.00	0.00	0.00	0.00	P_2a_2	0.00	0.00	0.00	0.00
	P_{01C}	0.00	0.00	0.00	0.00	P_{01C}	0.00	0.00	0.00	0.00
	P_{02C}	62.97	62.44	60.75	50.69	P_{02C}	97.41	96.79	95.68	88.87
	T_{01C}	0.00	0.00	0.00	0.00	T_{01C}	0.00	0.00	0.00	0.00
	T_{02C}	37.13	36.71	35.46	35.41					

Table 5.8 Area Averaging Detailed Uncertainty Results (Square Volute with YC Quadrants Coverage)

OTTR with Square Exit Volute		**Thermodynamic Method**					**Mechanical Method**			
Area Avg.		**YC 720 Pt (Reg.)**	**YC 360 Pt (Reg.)**	**YC 180 Pt (Reg.)**	**YC 90 Pt (Reg.)**		**YC 720 Pt (Reg.)**	**YC 360 Pt (Reg.)**	**YC 180 Pt (Reg.)**	**YC 90 Pt (Reg.)**
	h_{th}	0.6316	0.6316	0.6314	0.6321	h_{me}	0.5671	0.5672	0.5670	0.5670
	$U_{h_{th}}$	0.0458	0.0459	0.0463	0.0489	$U_{h_{me}}$	0.0349	0.0351	0.0349	0.0358
	U_h / h *100	7.3	7.3	7.3	7.7	U_h / h *100	6.2	6.2	6.2	6.3
	Terms	UPC				Terms	UPC			
	P_{01}	0.00	0.00	0.00	0.00	P_{01}	0.00	0.00	0.00	0.00
	P_{02}	0.00	0.00	0.00	0.01	P_{02}	0.00	0.00	0.00	0.01
	T_{01}	0.00	0.01	0.02	0.03	T_{01}	0.00	0.00	0.00	0.00
	T_{02}	0.01	0.01	0.02	0.04	Tq	0.22	0.22	0.22	0.21
	P_2	0.00	0.00	0.00	0.00	N	0.00	0.00	0.00	0.00
	a_2	0.00	0.00	0.00	0.00	P_2	0.00	0.00	0.00	0.00
	$P_{01}P_{01}$	0.08	0.30	1.18	4.24	a_2	0.00	0.00	0.00	0.00
	$P_{02}P_{02}$	0.22	0.22	0.22	0.19	$\dot{W}$	1.63	1.61	1.63	1.54
	$T_{01}T_{01}$	0.15	0.58	2.27	8.15	$P_{01}P_{01}$	0.10	0.41	1.68	6.37
	$T_{02}T_{02}$	0.18	0.17	0.17	0.15	$P_{02}P_{02}$	0.31	0.30	0.31	0.29
	P_2P_2	0.00	0.00	0.00	0.00	$T_{01}T_{01}$	0.00	0.01	0.03	0.12
	a_2a_2	0.00	0.00	0.00	0.00	P_2P_2	0.00	0.00	0.00	0.00
	$P_{01}P_{02}$	-0.26	-0.26	-0.25	-0.23	a_2a_2	0.00	0.00	0.00	0.00
	$P_{01}P_2$	0.00	0.00	0.00	0.00	$P_{01}P_{02}$	-0.36	-0.36	-0.36	-0.34
	$P_{01}a_2$	0.00	0.00	0.00	0.00	$P_{01}P_2$	0.00	0.00	0.00	0.00
	$P_{02}P_2$	0.00	0.00	0.00	0.00	$P_{01}a_2$	0.00	0.00	0.00	0.00
	$P_{02}a_2$	0.00	0.00	0.00	0.00	$P_{02}P_2$	0.00	0.00	0.00	0.00
	$T_{01}T_{02}$	-0.32	-0.32	-0.31	-0.28	$P_{02}a_2$	0.00	0.00	0.00	0.00
	P_2a_2	0.00	0.00	0.00	0.00	P_2a_2	0.00	0.00	0.00	0.00
	P_{01C}	0.00	0.00	0.00	0.00	P_{01C}	0.00	0.00	0.00	0.00
	P_{02C}	71.28	70.60	68.30	60.99	P_{02C}	98.34	97.93	96.60	92.05
	T_{01C}	0.00	0.00	0.00	0.00	T_{01C}	0.00	0.00	0.00	0.00
	T_{02C}	28.68	28.63	28.27	26.49					

Table 5.9 Mass Averaging Detailed Uncertainty Results (Circular Volute with 360° Circumferential Coverage)

OTTR with Circular Exit Volute		**Thermodynamic Method**					**Mechanical Method**			
Mass Avg.		**720 Points**	**360 Points**	**180 Points**	**90 Points**		**720 Points**	**360 Points**	**180 Points**	**90 Points**
	h_{th}	0.6624	0.6621	0.6621	0.6633	h_{me}	0.6262	0.6261	0.6261	0.6273
	$U_{h_{th}}$	0.0011	0.0044	0.0095	0.0195	$U_{h_{me}}$	0.0053	0.0059	0.0076	0.0125
	U_h / h *100	0.17	0.66	1.4	2.9	U_h / h *100	0.85	0.94	1.2	2.0
	Terms	UPC				Terms	UPC			
	P_{01}	0.67	0.08	0.04	0.02	P_{01}	0.03	0.04	0.05	0.04
	P_{02}	2.07	0.26	0.11	0.05	P_{02}	0.08	0.13	0.16	0.12
	T_{01}	10.09	1.26	0.54	0.26	T_{01}	0.00	0.01	0.01	0.00
	T_{02}	14.43	1.80	0.77	0.37	Tq	11.78	9.51	5.73	2.13
	P_2	0.03	0.00	0.00	0.00	N	0.12	0.09	0.06	0.02
	a_2	0.91	0.11	0.05	0.02	P_2	0.00	0.00	0.01	0.00
	$P_{01}P_{01}$	180.05	44.96	38.59	36.92	a_2	0.12	0.19	0.23	0.17
	$P_{02}P_{02}$	464.17	28.93	6.19	1.47	$\dot{W}$	85.94	69.34	41.79	15.51
	$T_{01}T_{01}$	310.01	77.49	66.50	63.37	$P_{01}P_{01}$	6.93	22.36	53.92	80.38
	$T_{02}T_{02}$	371.55	23.18	4.96	1.17	$P_{02}P_{02}$	17.55	14.13	8.49	3.14
	P_2P_2	0.05	0.00	0.00	0.00	$T_{01}T_{01}$	0.10	0.34	0.81	1.20
	a_2a_2	0.00	0.00	0.00	0.00	P_2P_2	0.01	0.00	0.00	0.00
	$P_{01}P_{02}$	-579.88	-36.20	-7.77	-1.86	a_2a_2	0.00	0.00	0.00	0.00
	$P_{01}P_2$	-6.15	-0.38	-0.08	-0.02	$P_{01}P_{02}$	-22.12	-17.85	-10.76	-4.01
	$P_{01}a_2$	0.00	0.00	0.00	0.00	$P_{01}P_2$	-0.42	-0.34	-0.21	-0.08
	$P_{02}P_2$	9.86	0.61	0.13	0.03	$P_{01}a_2$	0.00	0.00	0.00	0.00
	$P_{02}a_2$	0.00	0.00	0.00	0.00	$P_{02}P_2$	0.67	0.54	0.33	0.12
	$T_{01}T_{02}$	-680.74	-42.54	-9.13	-2.17	$P_{02}a_2$	0.00	0.00	0.00	0.00
	P_2a_2	0.00	0.00	0.00	0.00	P_2a_2	0.00	0.00	0.00	0.00
	P_{01C}	0.00	0.00	0.00	0.00	P_{01C}	0.00	0.00	0.00	0.00
	P_{02C}	0.00	0.00	0.00	0.40	P_{02C}	0.00	0.00	0.00	0.88
	T_{01C}	0.00	0.00	0.00	0.00	T_{01C}	0.00	0.00	0.00	0.00
	T_{02C}	0.00	0.53	0.12	0.06					

Table 5.10 Mass Averaging Detailed Uncertainty Results (Circular Volute with Cobra Quadrants Coverage)

OTTR with Circular Exit Volute		**Thermodynamic Method**					**Mechanical Method**			
Mass Avg.		**Cobra 720 Pt (Reg.)**	**Cobra 360 Pt (Reg.)**	**Cobra 180 Pt (Reg.)**	**Cobra 90 Pt (Reg.)**		**Cobra 720 Pt (Reg.)**	**Cobra 360 Pt (Reg.)**	**Cobra 180 Pt (Reg.)**	**Cobra 90 Pt (Reg.)**
	h_{th}	0.6624	0.6622	0.6624	0.6632	h_{me}	0.6266	0.6265	0.6268	0.6274
	$U_{h_{th}}$	0.0012	0.0046	0.0096	0.0195	$U_{h_{me}}$	0.0053	0.0059	0.0077	0.0125
	U_h / h *100	0.18	0.69	1.5	2.9	U_h / h *100	0.85	0.94	1.2	2.0
	Terms	UPC				Terms	UPC			
	P_{01}	0.56	0.08	0.04	0.02	P_{01}	0.03	0.04	0.05	0.04
	P_{02}	1.75	0.24	0.11	0.05	P_{02}	0.08	0.13	0.15	0.12
	T_{01}	8.49	1.15	0.53	0.26	T_{01}	0.00	0.01	0.01	0.00
	T_{02}	12.20	1.66	0.76	0.37	Tq	11.80	9.52	5.59	2.13
	P_2	0.02	0.00	0.00	0.00	N	0.12	0.09	0.06	0.02
	a_2	0.75	0.10	0.05	0.02	P_2	0.00	0.00	0.00	0.00
	$P_{01}P_{01}$	151.51	41.21	37.90	36.92	a_2	0.13	0.22	0.25	0.20
	$P_{02}P_{02}$	391.51	26.58	6.09	1.47	$\dot{W}$	86.05	69.43	40.79	15.51
	$T_{01}T_{01}$	260.85	71.00	65.25	63.39	$P_{01}P_{01}$	6.95	22.42	52.75	80.40
	$T_{02}T_{02}$	312.60	21.23	4.86	1.17	$P_{02}P_{02}$	17.68	14.24	8.34	3.15
	P_2P_2	0.03	0.00	0.00	0.00	$T_{01}T_{01}$	0.10	0.34	0.79	1.20
	a_2a_2	0.00	0.00	0.00	0.00	P_2P_2	0.00	0.00	0.00	0.00
	$P_{01}P_{02}$	-488.53	-33.22	-7.64	-1.86	a_2a_2	0.00	0.00	0.00	0.00
	$P_{01}P_2$	-4.47	-0.30	-0.07	-0.02	$P_{01}P_{02}$	-22.24	-17.94	-10.55	-4.02
	$P_{01}a_2$	0.00	0.00	0.00	0.00	$P_{01}P_2$	-0.36	-0.29	-0.17	-0.07
	$P_{02}P_2$	7.17	0.49	0.11	0.03	$P_{01}a_2$	0.00	0.00	0.00	0.00
	$P_{02}a_2$	0.00	0.00	0.00	0.00	$P_{02}P_2$	0.58	0.47	0.27	0.10
	$T_{01}T_{02}$	-572.76	-38.97	-8.96	-2.17	$P_{02}a_2$	0.00	0.00	0.00	0.00
	P_2a_2	0.00	0.00	0.00	0.00	P_2a_2	0.00	0.00	0.00	0.00
	P_{01C}	0.00	0.00	0.00	0.00	P_{01C}	0.00	0.00	0.00	0.00
	P_{02C}	11.92	1.55	0.42	0.43	P_{02C}	0.55	0.84	0.59	0.94
	T_{01C}	0.00	0.00	0.00	0.00	T_{01C}	0.00	0.00	0.00	0.00
	T_{02C}	12.23	6.91	0.49	0.10					

Table 5.11 Mass Averaging Detailed Uncertainty Results (Circular Volute with YC Quadrants Coverage)

OTTR with Circular Exit Volute		**Thermodynamic Method**					**Mechanical Method**			
Mass Avg.		**YC 720 Pt (Reg.)**	**YC 360 Pt (Reg.)**	**YC 180 Pt (Reg.)**	**YC 90 Pt (Reg.)**		**YC 720 Pt (Reg.)**	**YC 360 Pt (Reg.)**	**YC 180 Pt (Reg.)**	**YC 90 Pt (Reg.)**
	h_{th}	0.6601	0.6600	0.6599	0.6606	h_{me}	0.6247	0.6247	0.6245	0.6246
	$U_{h_{th}}$	0.0020	0.0047	0.0097	0.0194	$U_{h_{me}}$	0.0055	0.0060	0.0078	0.0124
	U_h / h *100	0.30	0.71	1.5	2.9	U_h / h *100	0.88	0.96	1.2	2.0
	Terms	UPC				Terms	UPC			
	P_{01}	0.20	0.07	0.03	0.02	P_{01}	0.02	0.04	0.05	0.04
	P_{02}	0.61	0.22	0.10	0.05	P_{02}	0.07	0.12	0.15	0.12
	T_{01}	3.04	1.10	0.52	0.26	T_{01}	0.00	0.01	0.01	0.00
	T_{02}	4.28	1.55	0.73	0.36	Tq	10.89	9.15	5.41	2.14
	P_2	0.01	0.00	0.00	0.00	N	0.11	0.09	0.05	0.02
	a_2	0.24	0.09	0.04	0.02	P_2	0.00	0.00	0.00	0.00
	$P_{01}P_{01}$	53.79	38.94	36.54	36.63	a_2	0.10	0.17	0.20	0.16
	$P_{02}P_{02}$	139.15	25.14	5.88	1.46	$\dot{W}$	79.42	66.74	39.47	15.62
	$T_{01}T_{01}$	93.35	67.62	63.46	63.47	$P_{01}P_{01}$	6.37	21.41	50.61	80.16
	$T_{02}T_{02}$	111.86	20.22	4.73	1.18	$P_{02}P_{02}$	16.14	13.54	7.98	3.13
	P_2P_2	0.01	0.00	0.00	0.00	$T_{01}T_{01}$	0.10	0.32	0.76	1.21
	a_2a_2	0.00	0.00	0.00	0.00	P_2P_2	0.01	0.01	0.00	0.00
	$P_{01}P_{02}$	-173.54	-31.41	-7.37	-1.85	a_2a_2	0.00	0.00	0.00	0.00
	$P_{01}P_2$	-1.81	-0.33	-0.08	-0.02	$P_{01}P_{02}$	-20.34	-17.09	-10.10	-4.00
	$P_{01}a_2$	0.00	0.00	0.00	0.00	$P_{01}P_2$	-0.42	-0.35	-0.21	-0.08
	$P_{02}P_2$	2.90	0.52	0.12	0.03	$P_{01}a_2$	0.00	0.00	0.00	0.00
	$P_{02}a_2$	0.00	0.00	0.00	0.00	$P_{02}P_2$	0.66	0.56	0.33	0.13
	$T_{01}T_{02}$	-204.96	-37.12	-8.71	-2.18	$P_{02}a_2$	0.00	0.00	0.00	0.00
	P_2a_2	0.00	0.00	0.00	0.00	P_2a_2	0.00	0.00	0.00	0.00
	P_{01C}	0.00	0.00	0.00	0.00	P_{01C}	0.00	0.00	0.00	0.00
	P_{02C}	62.59	11.51	3.25	0.74	P_{02C}	7.38	6.30	4.48	1.62
	T_{01C}	0.00	0.00	0.00	0.00	T_{01C}	0.00	0.00	0.00	0.00
	T_{02C}	11.84	3.06	0.65	0.02					

Table 5.12 Mass Averaging Detailed Uncertainty Results (Circular Volute with CWA)

OTTR with Circular Exit Volute		**Thermodynamic Method**					**Mechanical Method**			
Mass Avg.		**CWA 720 Pt**	**CWA 360 Pt**	**CWA 180 Pt**	**CWA 90 Pt**		**CWA 720 Pt**	**CWA 360 Pt**	**CWA 180 Pt**	**CWA 90 Pt**
	h_{th}	0.6639	0.6636	0.6636	0.6648	h_{me}	0.6297	0.6297	0.6297	0.6308
	$U_{h_{th}}$	0.0011	0.0044	0.0096	0.0197	$U_{h_{me}}$	0.0054	0.0059	0.0077	0.0126
	U_h / h *100	0.16	0.66	1.4	3.0	U_h / h *100	0.86	0.94	1.2	2.0
	Terms	UPC				Terms	UPC			
	P_{01}	0.68	0.08	0.04	0.02	P_{01}	0.03	0.04	0.05	0.04
	P_{02}	2.13	0.27	0.11	0.05	P_{02}	0.08	0.13	0.16	0.12
	T_{01}	10.21	1.28	0.54	0.26	T_{01}	0.00	0.01	0.01	0.00
	T_{02}	14.83	1.85	0.78	0.37	Tq	11.48	9.62	5.65	2.12
	P_2	2.71	0.34	0.14	0.07	N	0.11	0.10	0.06	0.02
	a_2	0.83	0.10	0.04	0.02	P_2	0.31	0.52	0.61	0.47
	$P_{01}P_{01}$	183.21	45.75	38.45	36.81	a_2	0.08	0.14	0.16	0.12
	$P_{02}P_{02}$	458.79	28.59	5.99	1.42	$\dot{W}$	83.72	70.12	41.17	15.43
	$T_{01}T_{01}$	313.69	78.42	65.90	62.83	$P_{01}P_{01}$	6.84	22.91	53.82	81.03
	$T_{02}T_{02}$	375.73	23.44	4.91	1.16	$P_{02}P_{02}$	16.26	13.59	7.95	2.97
	P_2P_2	0.24	0.01	0.00	0.00	$T_{01}T_{01}$	0.10	0.34	0.80	1.20
	a_2a_2	0.00	0.00	0.00	0.00	P_2P_2	0.04	0.03	0.02	0.01
	$P_{01}P_{02}$	-581.57	-36.30	-7.63	-1.82	a_2a_2	0.00	0.00	0.00	0.00
	$P_{01}P_2$	-13.30	-0.83	-0.17	-0.04	$P_{01}P_{02}$	-21.16	-17.72	-10.40	-3.91
	$P_{01}a_2$	0.00	0.00	0.00	0.00	$P_{01}P_2$	-1.05	-0.88	-0.52	-0.19
	$P_{02}P_2$	21.03	1.31	0.28	0.06	$P_{01}a_2$	0.00	0.00	0.00	0.00
	$P_{02}a_2$	0.00	0.00	0.00	0.00	$P_{02}P_2$	1.62	1.36	0.80	0.30
	$T_{01}T_{02}$	-688.63	-43.04	-9.04	-2.16	$P_{02}a_2$	0.00	0.00	0.00	0.00
	P_2a_2	0.00	0.00	0.00	0.00	P_2a_2	0.00	0.00	0.00	0.00
	P_{01C}	0.00	0.00	0.00	0.00	P_{01C}	0.00	0.00	0.00	0.00
	P_{02C}	0.00	0.00	0.00	0.39	P_{02C}	0.00	0.00	0.00	0.86
	T_{01C}	0.00	0.00	0.00	0.00	T_{01C}	0.00	0.00	0.00	0.00
	T_{02C}	0.00	0.54	0.11	0.06					

Table 5.13 Mass Averaging Detailed Uncertainty Results (Circular Volute with NWA)

OTTR with Circular Exit Volute		**Thermodynamic Method**					**Mechanical Method**			
Mass Avg.		**NWA 720 Pt**	**NWA 360 Pt**	**NWA 180 Pt**	**NWA 90 Pt**		**NWA 720 Pt**	**NWA 360 Pt**	**NWA 180 Pt**	**NWA 90 Pt**
	h_{th}	0.6639	0.6636	0.6636	0.6648	h_{me}	0.6297	0.6297	0.6297	0.6308
	$U_{h_{th}}$	0.0043	0.0062	0.0106	0.0204	$U_{h_{me}}$	0.0064	0.0069	0.0085	0.0134
	U_h / h *100	0.64	0.93	1.6	3.1	U_h / h *100	1.0	1.1	1.3	2.1
	Terms	UPC				Terms	UPC			
	P_{01}	0.04	0.04	0.03	0.02	P_{01}	0.02	0.03	0.04	0.03
	P_{02}	0.14	0.13	0.09	0.05	P_{02}	0.06	0.10	0.13	0.11
	T_{01}	0.67	0.64	0.44	0.24	T_{01}	0.00	0.00	0.01	0.00
	T_{02}	0.97	0.93	0.64	0.35	Tq	8.17	7.03	4.63	1.87
	P_2	0.18	0.17	0.12	0.06	N	0.08	0.07	0.05	0.02
	a_2	0.05	0.05	0.04	0.02	P_2	0.22	0.38	0.50	0.42
	$P_{01}P_{01}$	11.99	23.04	31.54	34.33	a_2	0.06	0.10	0.13	0.11
	$P_{02}P_{02}$	30.02	14.40	4.91	1.33	$\dot{W}$	59.60	51.27	33.79	13.65
	$T_{01}T_{01}$	20.53	39.50	54.05	58.59	$P_{01}P_{01}$	4.87	16.75	44.16	71.64
	$T_{02}T_{02}$	24.59	11.81	4.03	1.08	$P_{02}P_{02}$	11.58	9.94	6.52	2.62
	P_2P_2	0.02	0.01	0.00	0.00	$T_{01}T_{01}$	0.07	0.25	0.65	1.06
	a_2a_2	0.00	0.00	0.00	0.00	P_2P_2	0.03	0.02	0.02	0.01
	$P_{01}P_{02}$	-38.06	-18.28	-6.26	-1.70	a_2a_2	0.00	0.00	0.00	0.00
	$P_{01}P_2$	-0.87	-0.42	-0.14	-0.04	$P_{01}P_{02}$	-15.06	-12.95	-8.54	-3.46
	$P_{01}a_2$	0.00	0.00	0.00	0.00	$P_{01}P_2$	-0.75	-0.64	-0.43	-0.17
	$P_{02}P_2$	1.38	0.66	0.23	0.06	$P_{01}a_2$	0.00	0.00	0.00	0.00
	$P_{02}a_2$	0.00	0.00	0.00	0.00	$P_{02}P_2$	1.15	0.99	0.66	0.26
	$T_{01}T_{02}$	-45.06	-21.67	-7.42	-2.01	$P_{02}a_2$	0.00	0.00	0.00	0.00
	P_2a_2	0.00	0.00	0.00	0.00	P_2a_2	0.00	0.00	0.00	0.00
	P_{01C}	0.00	0.00	0.00	0.00	P_{01C}	0.00	0.00	0.00	0.00
	P_{02C}	75.62	36.48	12.46	5.90	P_{02C}	30.66	26.60	17.50	12.21
	T_{01C}	0.00	0.00	0.00	0.00	T_{01C}	0.00	0.00	0.00	0.00
	T_{02C}	19.15	12.64	4.33	1.34					

Table 5.14 Area Averaging Detailed Uncertainty Results (Circular Volute with 360° Circumferential Coverage)

OTTR with Circular Exit Volute		**Thermodynamic Method**					**Mechanical Method**			
Area Avg.		**720 Points**	**360 Points**	**180 Points**	**90 Points**		**720 Points**	**360 Points**	**180 Points**	**90 Points**
	h_{th}	0.6501	0.6497	0.6499	0.6514	h_{me}	0.5913	0.5913	0.5914	0.5925
	$U_{h_{th}}$	0.0441	0.0442	0.0445	0.0464	$U_{h_{me}}$	0.0338	0.0339	0.0338	0.0339
	U_h / h *100	6.8	6.8	4.8	7.1	U_h / h *100	5.7	5.7	5.7	5.7
	Terms	UPC				Terms	UPC			
	P_{01}	0.00	0.00	0.00	0.00	P_{01}	0.00	0.00	0.00	0.00
	P_{02}	0.00	0.00	0.00	0.01	P_{02}	0.00	0.00	0.01	0.01
	T_{01}	0.01	0.01	0.02	0.04	T_{01}	0.00	0.00	0.00	0.00
	T_{02}	0.01	0.01	0.03	0.05	Tq	0.26	0.26	0.26	0.26
	P_2	0.00	0.00	0.00	0.00	N	0.00	0.00	0.00	0.00
	a_2	0.00	0.00	0.00	0.00	P_2	0.00	0.00	0.00	0.00
	$P_{01}P_{01}$	0.09	0.38	1.49	5.51	a_2	0.00	0.00	0.00	0.00
	$P_{02}P_{02}$	0.26	0.26	0.26	0.24	$\dot{W}$	1.88	1.87	1.88	1.88
	$T_{01}T_{01}$	0.17	0.68	2.68	9.91	$P_{01}P_{01}$	0.13	0.53	2.13	8.55
	$T_{02}T_{02}$	0.21	0.20	0.20	0.19	$P_{02}P_{02}$	0.37	0.37	0.37	0.37
	P_2P_2	0.00	0.00	0.00	0.00	$T_{01}T_{01}$	0.00	0.01	0.04	0.15
	a_2a_2	0.00	0.00	0.00	0.00	P_2P_2	0.00	0.00	0.00	0.00
	$P_{01}P_{02}$	-0.32	-0.32	-0.31	-0.29	a_2a_2	0.00	0.00	0.00	0.00
	$P_{01}P_2$	0.00	0.00	0.00	0.00	$P_{01}P_{02}$	-0.45	-0.44	-0.45	-0.45
	$P_{01}a_2$	0.00	0.00	0.00	0.00	$P_{01}P_2$	0.00	0.00	0.00	0.00
	$P_{02}P_2$	0.00	0.00	0.00	0.00	$P_{01}a_2$	0.00	0.00	0.00	0.00
	$P_{02}a_2$	0.00	0.00	0.00	0.00	$P_{02}P_2$	0.00	0.00	0.00	0.00
	$T_{01}T_{02}$	-0.38	-0.37	-0.37	-0.34	$P_{02}a_2$	0.00	0.00	0.00	0.00
	P_2a_2	0.00	0.00	0.00	0.00	P_2a_2	0.00	0.00	0.00	0.00
	P_{01C}	0.00	0.00	0.00	0.00	P_{01C}	0.00	0.00	0.00	0.00
	P_{02C}	69.65	69.32	66.39	57.31	P_{02C}	97.93	97.34	95.95	89.03
	T_{01C}	0.00	0.00	0.00	0.00	T_{01C}	0.00	0.00	0.00	0.00
	T_{02C}	30.52	29.64	29.40	27.58					

Table 5.15 Area Averaging Detailed Uncertainty Results (Circular Volute with Cobra Quadrants Coverage)

OTTR with Circular Exit Volute		**Thermodynamic Method**					**Mechanical Method**			
Area Avg.		**Cobra 720 Pt (Reg.)**	**Cobra 360 Pt (Reg.)**	**Cobra 180 Pt (Reg.)**	**Cobra 90 Pt (Reg.)**		**Cobra 720 Pt (Reg.)**	**Cobra 360 Pt (Reg.)**	**Cobra 180 Pt (Reg.)**	**Cobra 90 Pt (Reg.)**
	h_{th}	0.6504	0.6503	0.6504	0.6512	h_{me}	0.5906	0.5905	0.5907	0.5912
	$U_{h_{th}}$	0.0455	0.0451	0.0457	0.0485	$U_{h_{me}}$	0.0346	0.0342	0.0343	0.0353
	U_h / h *100	7.0	6.9	7.0	7.4	U_h / h *100	5.8	5.8	5.8	6.0
	Terms	UPC				Terms	UPC			
	P_{01}	0.00	0.00	0.00	0.00	P_{01}	0.00	0.00	0.00	0.00
	P_{02}	0.00	0.00	0.00	0.01	P_{02}	0.00	0.00	0.01	0.01
	T_{01}	0.01	0.01	0.02	0.04	T_{01}	0.00	0.00	0.00	0.00
	T_{02}	0.01	0.01	0.03	0.05	Tq	0.25	0.25	0.25	0.24
	P_2	0.00	0.00	0.00	0.00	N	0.00	0.00	0.00	0.00
	a_2	0.00	0.00	0.00	0.00	P_2	0.00	0.00	0.00	0.00
	$P_{01}P_{01}$	0.09	0.36	1.41	5.02	a_2	0.00	0.00	0.00	0.00
	$P_{02}P_{02}$	0.25	0.25	0.25	0.22	$\dot{W}$	1.79	1.84	1.83	1.73
	$T_{01}T_{01}$	0.16	0.65	2.54	9.03	$P_{01}P_{01}$	0.13	0.52	2.06	7.80
	$T_{02}T_{02}$	0.19	0.20	0.19	0.17	$P_{02}P_{02}$	0.35	0.36	0.36	0.34
	P_2P_2	0.00	0.00	0.00	0.00	$T_{01}T_{01}$	0.00	0.01	0.04	0.13
	a_2a_2	0.00	0.00	0.00	0.00	P_2P_2	0.00	0.00	0.00	0.00
	$P_{01}P_{02}$	-0.30	-0.30	-0.30	-0.26	a_2a_2	0.00	0.00	0.00	0.00
	$P_{01}P_2$	0.00	0.00	0.00	0.00	$P_{01}P_{02}$	-0.42	-0.43	-0.43	-0.41
	$P_{01}a_2$	0.00	0.00	0.00	0.00	$P_{01}P_2$	0.00	0.00	0.00	0.00
	$P_{02}P_2$	0.00	0.00	0.00	0.00	$P_{01}a_2$	0.00	0.00	0.00	0.00
	$P_{02}a_2$	0.00	0.00	0.00	0.00	$P_{02}P_2$	0.00	0.00	0.00	0.00
	$T_{01}T_{02}$	-0.35	-0.36	-0.35	-0.31	$P_{02}a_2$	0.00	0.00	0.00	0.00
	P_2a_2	0.00	0.00	0.00	0.00	P_2a_2	0.00	0.00	0.00	0.00
	P_{01C}	0.00	0.00	0.00	0.00	P_{01C}	0.00	0.00	0.00	0.00
	P_{02C}	68.58	67.50	65.58	58.23	P_{02C}	97.97	97.23	95.89	90.24
	T_{01C}	0.00	0.00	0.00	0.00	T_{01C}	0.00	0.00	0.00	0.00
	T_{02C}	31.37	31.57	30.59	27.78					

Table 5.16 Area Averaging Detailed Uncertainty Results (Circular Volute with YC Quadrants Coverage)

OTTR with Circular Exit Volute		**Thermodynamic Method**					**Mechanical Method**			
Area Avg.		**YC 720 Pt (Reg.)**	**YC 360 Pt (Reg.)**	**YC 180 Pt (Reg.)**	**YC 90 Pt (Reg.)**		**YC 720 Pt (Reg.)**	**YC 360 Pt (Reg.)**	**YC 180 Pt (Reg.)**	**YC 90 Pt (Reg.)**
	h_{th}	0.6492	0.6490	0.6491	0.6499	h_{me}	0.5906	0.5906	0.5905	0.5908
	$U_{h_{th}}$	0.0446	0.0444	0.0451	0.0479	$U_{h_{me}}$	0.0346	0.034	0.0346	0.0352
	U_h / h *100	6.9	6.8	6.9	7.4	U_h / h *100	5.9	5.8	5.9	6.0
	Terms	UPC				Terms	UPC			
	P_{01}	0.00	0.00	0.00	0.00	P_{01}	0.00	0.00	0.00	0.00
	P_{02}	0.00	0.00	0.00	0.01	P_{02}	0.00	0.00	0.01	0.01
	T_{01}	0.01	0.01	0.02	0.04	T_{01}	0.00	0.00	0.00	0.00
	T_{02}	0.01	0.01	0.03	0.05	Tq	0.25	0.25	0.25	0.24
	P_2	0.00	0.00	0.00	0.00	N	0.00	0.00	0.00	0.00
	a_2	0.00	0.00	0.00	0.00	P_2	0.00	0.00	0.00	0.00
	$P_{01}P_{01}$	0.09	0.37	1.44	5.12	a_2	0.00	0.00	0.00	0.00
	$P_{02}P_{02}$	0.26	0.26	0.25	0.22	$\dot{W}$	1.79	1.86	1.79	1.73
	$T_{01}T_{01}$	0.17	0.67	2.61	9.25	$P_{01}P_{01}$	0.13	0.52	2.02	7.83
	$T_{02}T_{02}$	0.20	0.20	0.20	0.17	$P_{02}P_{02}$	0.35	0.37	0.35	0.34
	P_2P_2	0.00	0.00	0.00	0.00	$T_{01}T_{01}$	0.00	0.01	0.03	0.13
	a_2a_2	0.00	0.00	0.00	0.00	P_2P_2	0.00	0.00	0.00	0.00
	$P_{01}P_{02}$	-0.31	-0.31	-0.30	-0.27	a_2a_2	0.00	0.00	0.00	0.00
	$P_{01}P_2$	0.00	0.00	0.00	0.00	$P_{01}P_{02}$	-0.42	-0.44	-0.42	-0.41
	$P_{01}a_2$	0.00	0.00	0.00	0.00	$P_{01}P_2$	0.00	0.00	0.00	0.00
	$P_{02}P_2$	0.00	0.00	0.00	0.00	$P_{01}a_2$	0.00	0.00	0.00	0.00
	$P_{02}a_2$	0.00	0.00	0.00	0.00	$P_{02}P_2$	0.00	0.00	0.00	0.00
	$T_{01}T_{02}$	-0.37	-0.37	-0.36	-0.32	$P_{02}a_2$	0.00	0.00	0.00	0.00
	P_2a_2	0.00	0.00	0.00	0.00	P_2a_2	0.00	0.00	0.00	0.00
	P_{01C}	0.00	0.00	0.00	0.00	P_{01C}	0.00	0.00	0.00	0.00
	P_{02C}	70.80	69.64	67.23	59.27	P_{02C}	97.71	97.21	95.73	90.40
	T_{01C}	0.00	0.00	0.00	0.00	T_{01C}	0.00	0.00	0.00	0.00
	T_{02C}	29.35	29.44	28.87	26.54					

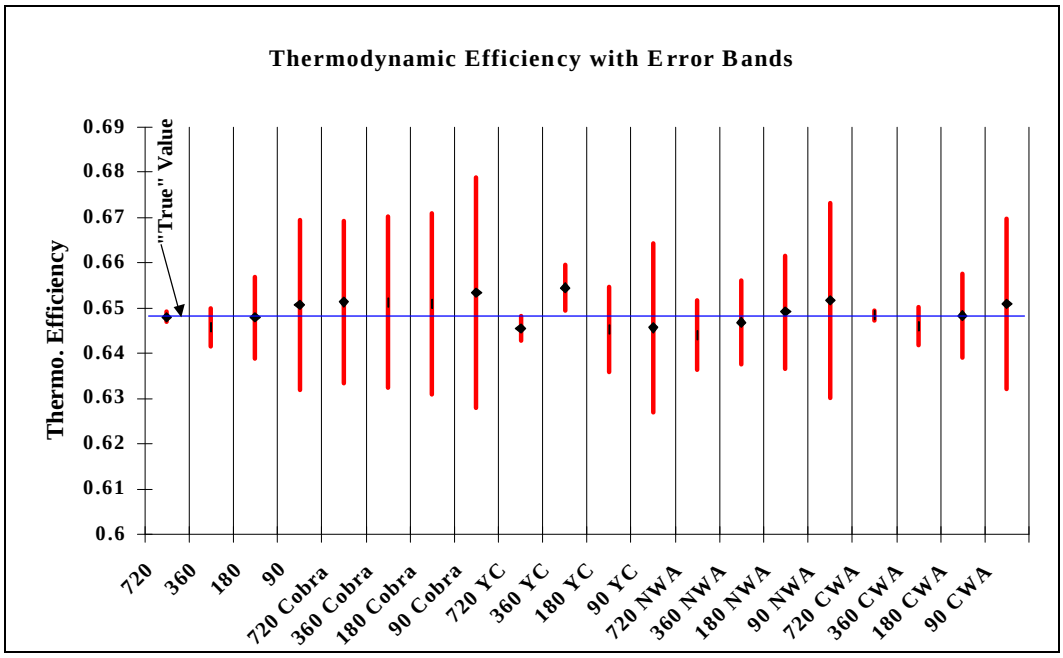

Figure 5.1 Uncertainty Results for OTTR with Square Volute (Mass Averaging with Thermodynamic Efficiency)

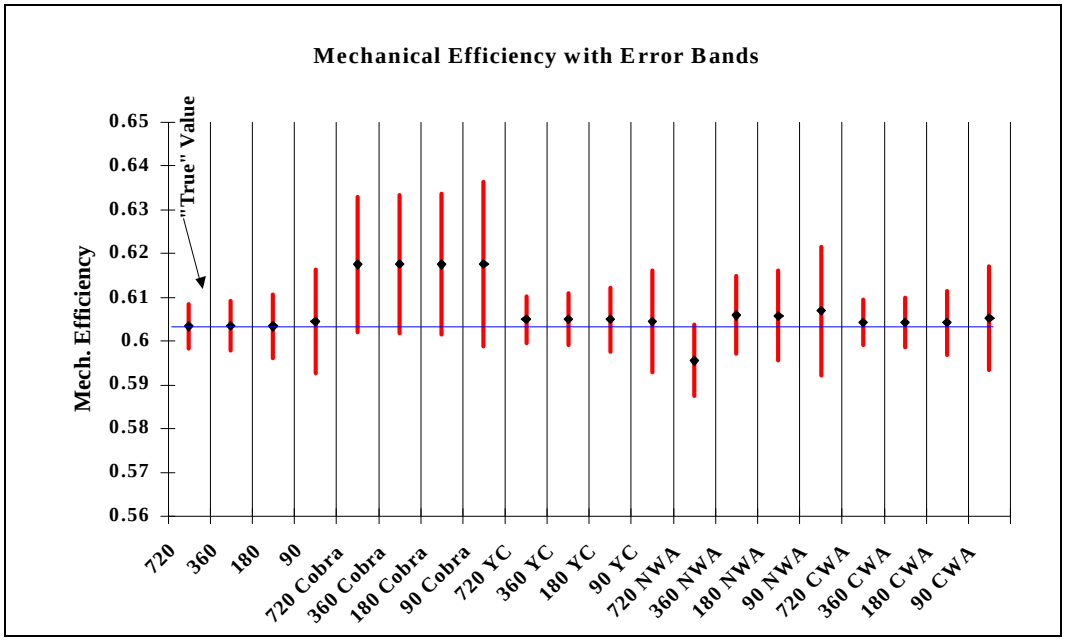

Figure 5.2 Uncertainty Results for OTTR with Square Volute (Mass Averaging with Mechanical Efficiency)

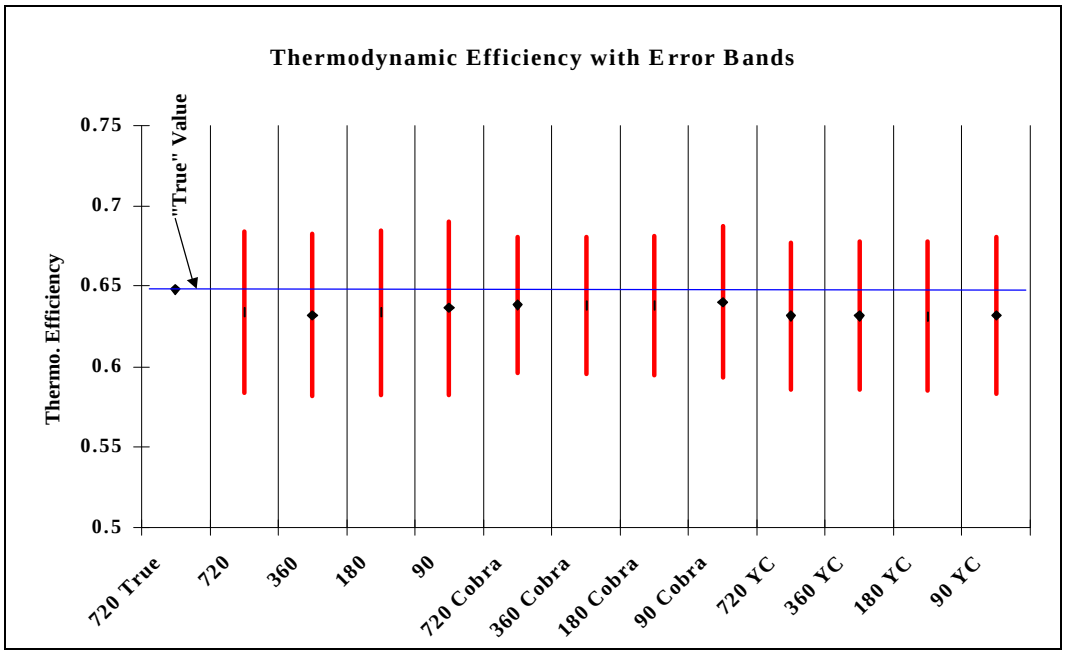

Figure 5.3 Uncertainty Results for OTTR with Square Volute (Area Averaging with Thermodynamic Efficiency)

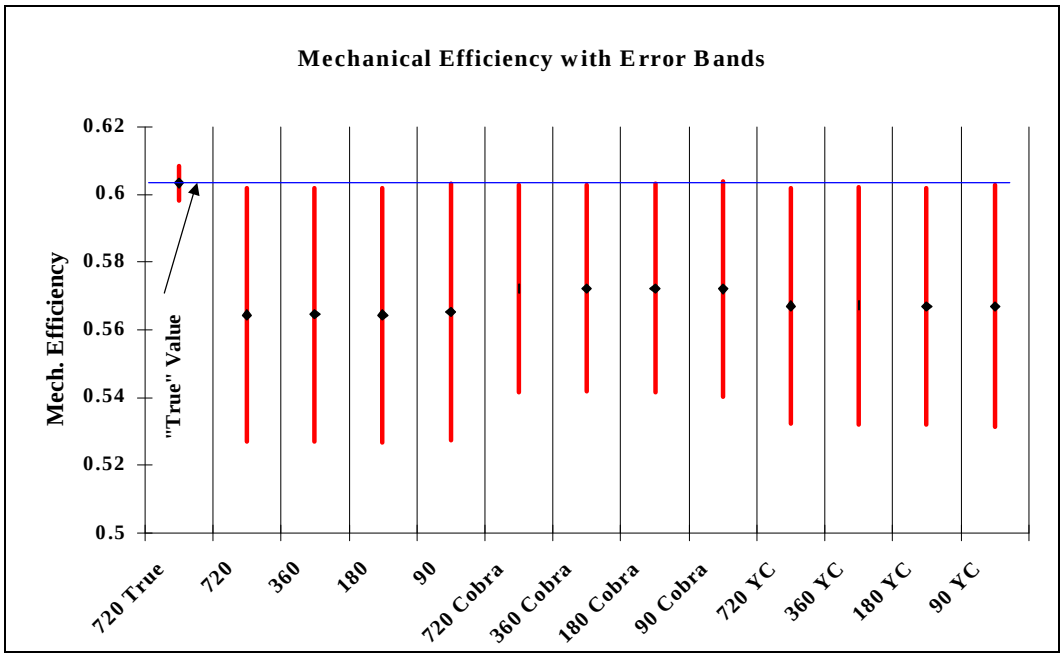

Figure 5.4 Uncertainty Results for OTTR with Square Volute (Area Averaging with Mechanical Efficiency)

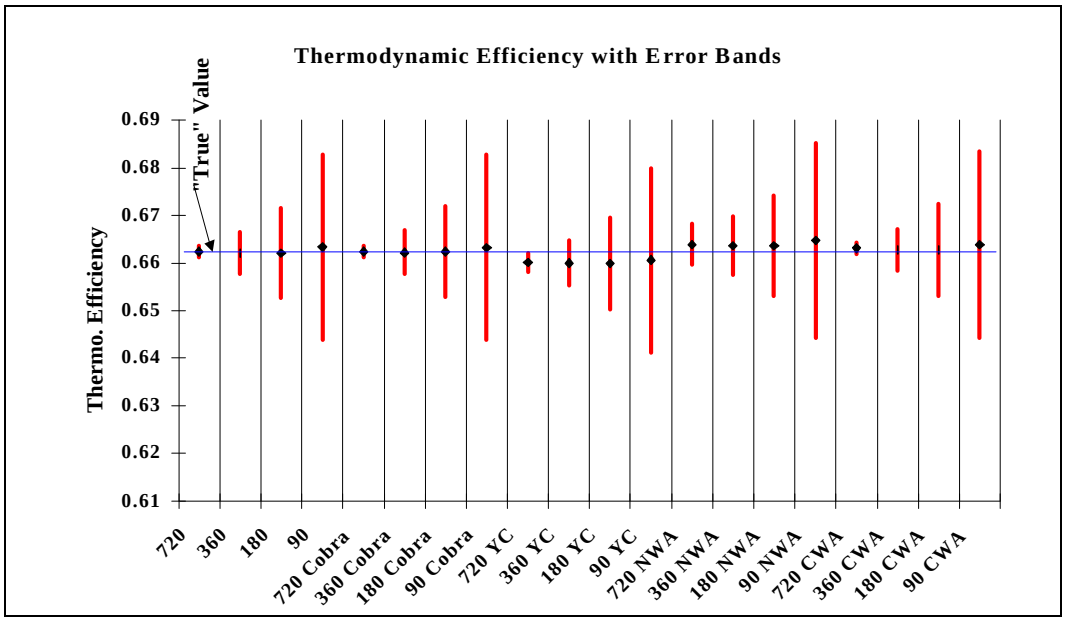

Figure 5.5 Uncertainty Results for OTTR with Circular Volute (Mass Averaging with Thermodynamic Efficiency)

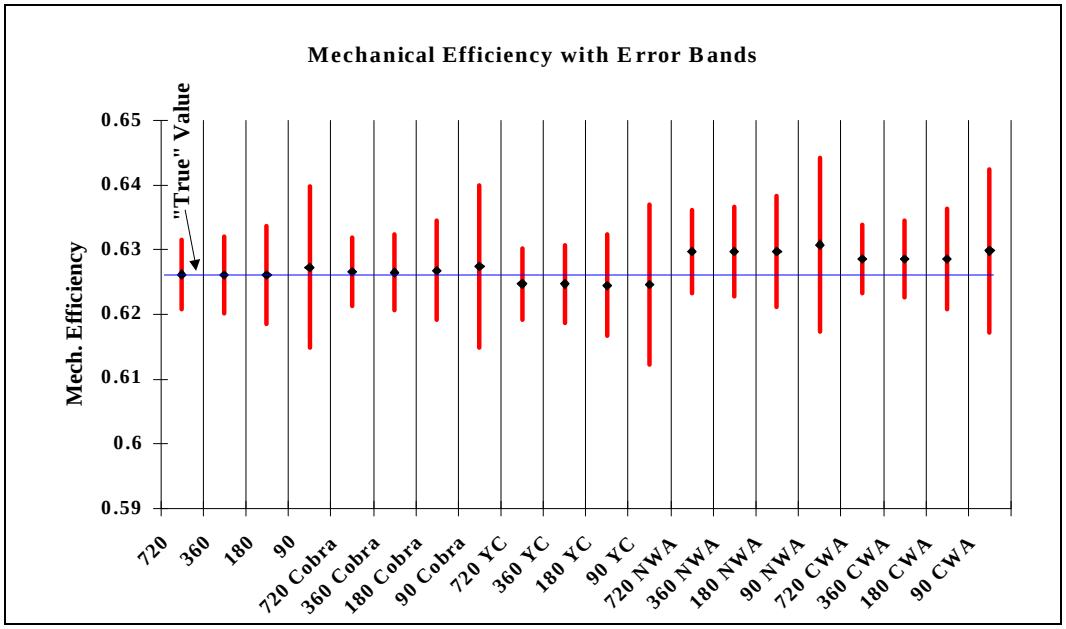

Figure 5.6 Uncertainty Results for OTTR with Circular Volute (Mass Averaging with Mechanical Efficiency)

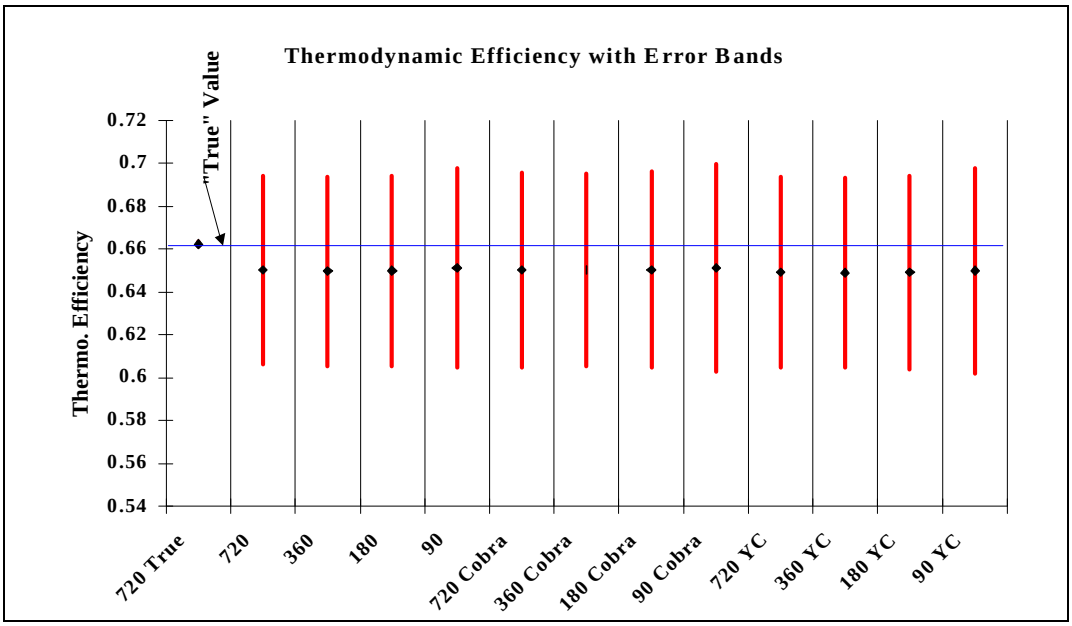

Figure 5.7 Uncertainty Results for OTTR with Circular Volute (Area Averaging with Thermodynamic Efficiency)

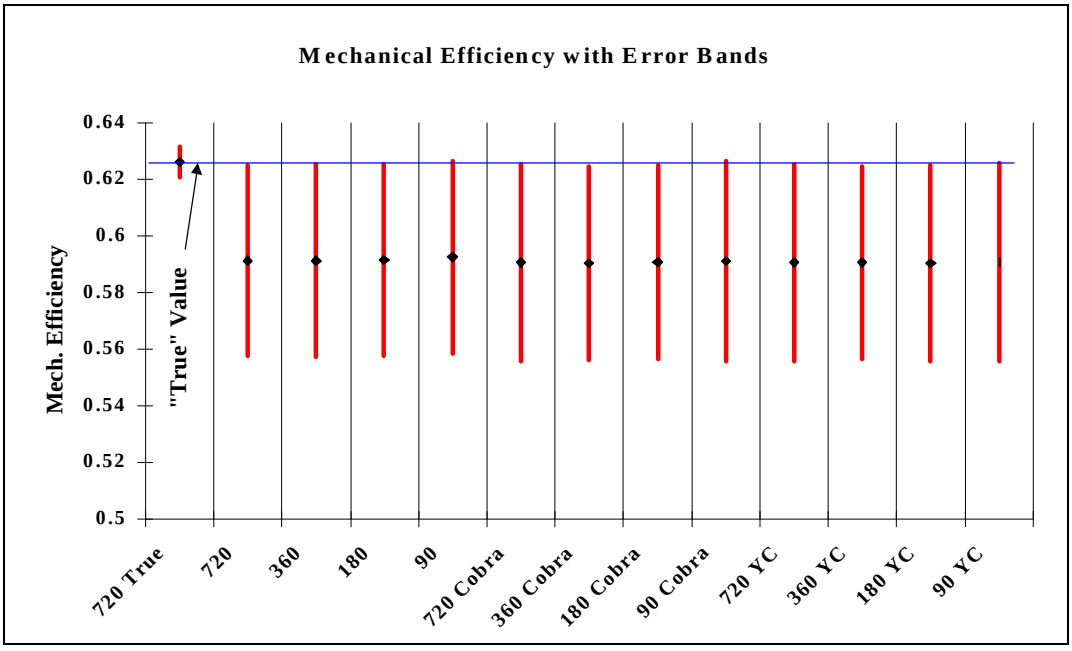

Figure 5.8 Uncertainty Results for OTTR with Circular Volute (Area Averaging with Mechanical Efficiency)

CHAPTER VI

SUMMARY AND CONCLUSIONS

6.1 General Overview of Analyses

The objective of the research was to establish guidelines for future turbine test requirements. The possible benefits included reduced testing time, reduced calibration requirements, and improvement of experimental techniques. The effort could help reduce the cost of experimentation while maintaining the accuracy of the results. In order to develop the guidelines, experimental data from the OTTR cold airflow test with a square and a circular exit volute were analyzed. An evaluation of data requirements, including the averaging technique, the number of measurements, and the types of measurements needed for high gradient flow fields was conducted. Two efficiency calculation methods were employed to evaluate the impact of averaging on each the efficiency results. The thermodynamic efficiency method and mechanical efficiency method were used for this research (Equations 1.1 and 1.2).

The accuracy requirements for the performance evaluation was strict for the OTTR test, and the uncertainty goal for the turbine efficiency was 1% ($U_h / h * 100 = \pm 1\%$). Therefore, detailed uncertainty analyses were done for both efficiency calculation methods. Test data were manipulated in different ways (averaging technique,

measurements reduction, and wall-static averaging) to verify minimum turbine test requirements while maintaining the 1% accuracy. A new uncertainty analysis technique was developed to include conceptual bias estimates. Conceptual bias is the bias that arises when the cross-sectional average value required in the data reduction equation is replaced by a spatial average of multiple point measurements. Conceptual bias estimates were developed based on the results form the different test cases.

The results of the two airflow tests and the related uncertainty analyses were presented in Chapter 3 and Chapter 5. These results were summarized to help develop guidelines for future turbine testing. Table 6.1 shows the summarized total-to-total efficiency uncertainties for square exit volute test, and Table 6.2 depicts similar results for the circular exit volute test. Tables 6.1 and 6.2 are presented with the conceptual bias estimates that are suitable for each test case. The relative % gradients for the two different tests were defined in Table 3.2.

The averaging technique comparisons proved that mass averaging was necessary to obtain accurate results in high gradient flow fields such as those at the turbine exit for both tests analyzed here. Mass averaging utilized mass flow rate to account for the gradients of the turbine exit for both volute tests. The uncertainty results of mass averaging were much better compared to the uncertainty of area averaging. The mass averaging technique had smaller conceptual bias estimates (Tables 6.1 and 6.2). Hence, the percent of uncertainty of efficiency was much lower compared to area averaging. The range of uncertainty was from 0.15% to 3% of the efficiency for all mass averaged cases studied. The area averaging, on the other hand, had poor uncertainty results ranging from 7% to 8% of the efficiency for all cases studied.

The measurement reduction analysis provided much insight for future tests. Mass averaging with reduced measurements offered the best uncertainty results. The measurement reduction for the square volute and circular volute tests generated similar uncertainty results (Tables 6.1 and 6.2). The reduction of measurements to 360-points was suitable for the OTTR with both the square and circular volutes because the uncertainty was kept below 1% of the efficiency. The results of the quadrants averaging cases were unpredictable. The YC probe results for the square volute test (Table 6.1) were very accurate; whereas the cobra probe results had high uncertainties. The circular volute test results were different in that both the YC and cobra probes generated low uncertainties. The best measurements of the turbine flow field were known for both the square and the circular volute tests, and the locations of the gradients were known for both test cases; therefore, an evaluation of the % of measurement coverage of the highest gradient section of the flow field was possible. Different percentages of the highest gradient sections were covered in each of the four cases (square cobra—64.4%, square YC—35.6%, circular cobra—85.5%, and circular YC-14.5%), yet there was no apparent correlation with the amount of coverage and the quality of the results. This fact along with the idea that the flow field of future turbine designs will not be truly understood prior to testing leads to the conclusion that the quadrants averaging should not be applied to new turbine designs. More data must be analyzed to understand this area better. In conclusion, the entire circumferential coverage of the turbine inlet and exit was needed to understand the gradients of the flow field. The minimum number of measurements needed to maintain the efficiency uncertainty goal within 1% was 360-point

measurements with circumferential coverage. However, reducing the number of measurements even further produced good results provided the full 360° was covered.

The CWA wall-static averaging offered promise. The CWA method generated little uncertainty because the circumferential gradients were captured. There were differences between the efficiency of the CWA and the "true" efficiency, but the low uncertainty contribution of CWA proved the usefulness of the method. Instead of using the cobra and YC probes to obtain static pressure measurements across the annulus, wall-static pressure measurements could be used provided that they can capture the circumferential gradients. This would remove the need to calibrate the cobra and YC probes for static pressure measurements; which is time consuming and difficult. The use of CWA would reduce the test time and calibration requirements.

6.2 Summary of Turbine Testing Guidelines

The guidelines for future turbine test requirements were compiled through the understanding of the analyses. For the OTTR, mass averaging of all turbine exit data was needed to maintain accuracy. In addition, only 360-point measurements were needed to maintain the uncertainty below 1% of the efficiency. Lastly, circumferential averaging of wall-static pressure measurements were sufficiently accurate for the OTTR system. The recommendations for future turbine systems are as follows:

1. Mass averaging for all measurements, when the expected flow field gradient is larger than that at the inlet of the OTTR (Table 3.2).
2. Determine the maximum number of independent measurements possible based on the size of the flow field and probes to be used. This number

divided by two ([maximum number of independent measurements]/2) should be sufficient to obtain highly accurate flow field maps and efficiency calculations provided other precautions (proper calibration) have been taken to minimize the uncertainty of the test data. Lower numbers of measurements may also be possible depending on the accuracy requirements. However, it is important to cover the full 360° of the flow field. Quadrants averaging is not recommended.

3. Wall-static pressure measurements may be used rather than static pressure measurements across the annulus provided that these measurements are sufficient to capture the circumferential gradients and the shape of these circumferential gradients is not expected to vary greatly radially.

The conceptual bias estimates are listed in Table 6.1 and 6.2. These can be used to help one estimate conceptual bias terms for future tests. These estimates along with the gradients in the flow field, for which the estimates were obtained, should provide enough information for one to obtain reasonable estimates for a new flow field with predictions for the expected gradients.

Table 6.1 Turbine Test Guidelines with Conceptual Bias Estimates (For High Gradient Flow Field Applications)

OTTR with Square Exit Volute Data Reduction			**Percent Uncertainty ($U_ç$ /ç * 100)**		**Conceptual Bias Estimate**	
			Thermo. Efficiency	**Mech. Efficiency**	P_{02}	T_{02}
Mass Avg.	720 pt Mea.		0.17%	0.85%	0.00	0.00
	360 pt Mea.		0.65%	0.93%	0.01	0.04
	180 pt Mea.		1.40%	1.19%	0.02	0.03
	90 pt Mea.		2.89%	1.95%	0.10	0.13
	2 Quadrants (YC Probe)	720 pt	0.41%	0.89%	0.08	0.14
		360 pt	0.76%	0.98%	0.09	0.15
		180 pt	1.46%	1.22%	0.07	0.14
		90 pt	2.88%	1.92%	0.06	0.09
	2 Quadrants (Cobra Probe)	720 pt	2.76%	2.51%	0.74	0.69
		360 pt	2.90%	2.57%	0.76	0.71
		180 pt	3.08%	2.61%	0.74	0.70
		90 pt	3.90%	3.04%	0.74	0.53
Area Avg.	720 pt Mea.		8%	8%	2.50	2.50
	360 pt Mea.		8%	8%	2.50	2.50
	180 pt Mea.		8%	8%	2.50	2.50
	90 pt Mea.		8%	8%	2.50	2.50
	2 Quadrants (YC Probe)	720 pt	8%	8%	1.75	2.20
		360 pt	8%	8%	1.75	2.20
		180 pt	8%	8%	1.75	2.20
		90 pt	8%	8%	1.75	2.20
	2 Quadrants (Cobra Probe)	720 pt	8%	8%	2.04	2.00
		360 pt	8%	8%	2.04	2.00
		180 pt	8%	8%	2.04	2.00
		90 pt	8%	8%	2.04	2.00

Table 6.2 Turbine Test Guidelines with Conceptual Bias Estimates (For Medium Gradient Flow Field Applications)

OTTR with Circular Exit Volute Data Reduction			Percent Uncertainty ($U_ç / ç$ * 100)		Conceptual Bias Estimate	
			Thermo. Efficiency	**Mech. Efficiency**	P_{02}	T_{02}
Mass Avg.	720 pt Mea.		0.17%	0.85%	0.00	0.00
	360 pt Mea.		0.66%	0.94%	0.00	0.02
	180 pt Mea.		1.43%	1.21%	0.00	0.02
	90 pt Mea.		2.94%	1.99%	0.06	0.03
	2 Quadrants (Cobra Probe)	720 pt	0.18%	0.85%	0.02	0.03
		360 pt	0.69%	0.94%	0.02	0.05
		180 pt	1.45%	1.23%	0.03	0.05
		90 pt	2.94%	1.99%	0.06	0.04
	2 Quadrants (YC Probe)	720 pt	0.30%	0.88%	0.08	0.05
		360 pt	0.71%	0.96%	0.08	0.06
		180 pt	1.47%	1.25%	0.08	0.06
		90 pt	2.94%	1.99%	0.08	0.02
Area Avg.	720 pt Mea.		7.5%	7.5%	1.88	1.85
	360 pt Mea.		7.5%	7.5%	1.88	1.85
	180 pt Mea.		7.5%	7.5%	1.88	1.85
	90 pt Mea.		7.5%	7.5%	1.88	1.85
	2 Quadrants (Cobra Probe)	720 pt	7.5%	7.5%	1.88	1.95
		360 pt	7.5%	7.5%	1.88	1.95
		180 pt	7.5%	7.5%	1.88	1.95
		90 pt	7.5%	7.5%	1.88	1.95
	2 Quadrants (YC Probe)	720 pt	7.5%	7.5%	1.88	1.95
		360 pt	7.5%	7.5%	1.88	1.95
		180 pt	7.5%	7.5%	1.88	1.95
		90 pt	7.5%	7.5%	1.88	1.95

LIST OF REFERENCES

[1] Hudson, S.T., "Improved Turbine Efficiency Test Techniques Based on Uncertainty Analysis Application," Ph.D. Dissertation, Dept. of Mechanical and Aerospace Engineering, University of Alabama, Huntsville, AL, April, 1998.

[2] Hudson, S.T., Johnson, P. D., and Wooler, A., "Baseline Design of the Oxidizer Technology Turbine Rig," Advance Earth-to-Orbit Propulsion Technology Conference, Huntville, AL, May 1994.

[3] Glassman, A.J., *Turbine Design and Application*, NASA SP-290, 1972.

[4] Hudson, S.T., and Coleman, H.W., "Analytical and Experimental Assessment of Two Methods of Determining Turbine Efficiency," AIAA, *Journal of Propulsion and Power*, Volume 16, No. 5, Sept-Oct, 2000, pp. 760-767.

[5] American National Standards Institute/American Society of Mechanical Engineering, *Test Uncertainty: Instruments and Apparatus*, PTC 19.1-1998, Section 10, ASME, 1998.

[6] Coleman, H.W. and Steele, W.G., "Engineering Application of Experimental Uncertainty Analysis," *AIAA Journal*, Vol. 33, No. 10, 1995, pp. 1888-1886.

[7] Hudson, S.T., and Coleman, H.W., "A Detailed Uncertainty Assessment of Measurements used in Determining Turbine Efficiency," AIAA 97-0776, 1997.

[8] Hudson, S.T., and Montesdeoca, X.A., "Aerodynamic Performance Test Results of Single Stage Oxidizer Turbine with Volute Manifolds," AIAA 97-3099, 1997.

[9] Hudson, S.T., and Coleman, H.W, "A Preliminary Assessment of Methods for Determining Turbine Efficiency," AIAA 96-0101, 1996.

[10] Hudson, S.T., Zoladz, T.F., and Griffin, L.W., "Blade Surface Pressure Distributions in a Rocket Engine Turbine: Experimental Work with On-Blade Pressure Transducers," AIAA 2000-3239, 2000.

[11] Hudson, S.T., Johnson, P.D., and Boynton, J.L., "Cold Flow Testing of the Space Shuttle Main Engine High Pressure Fuel Turbine Model," AIAA 91-2503, 1991.

[12] Hudson, S.T., Johnson, P.D., and Branick, R.E., "Performance Testing of a Highly Loaded Single Stage Oxidizer Turbine with Inlet and Exit Volute Manifolds," AIAA 95-2405, 1995.

[13] Kammeyer, M.E., and Rueger, M.L., "On the Classification of Errors: Systematic, Random, and Replication Level (Invited)," AIAA 2000-2203, 2000.

[14] Coleman, H.W. and Steele, W.G., *Experimentation and Uncertainty Analysis for Engineers*, 2nd Edition, Wiley, New York 1999.

[15] Griffin, L.W. and Huber, F.W., "Turbine Technology Team: An Overview of Current and Planned Activities relevant to the National Launch System," AIAA 92-3220, 1992.

[16] Huber, F.W., Johnson, P.D., Montesdeoca, X.A., Rowey, R.J., and Griffin, L.W., "Design of Advanced Turbopump Drive Turbines for National Launch Systems Application," AIAA 92-3221, 1992.

[17] Hudson, S.T., "Oxidizer Technology Turbine Rig Baseline Test Pretest Report," NASA/MSFC memo ED34-20-94, April 4, 1994.

[18] Huber, F.W., Johnson, P.D., and Montesdeoca, X.A., "Baseline Design of the Gas Generator Oxidizer Turbine (GGOT) and Performance Predictions for the Associated Oxidizer Technology Turbine Rig (OTTR)," United Technologies Pratt & Whitney SZL:38865.doc to Scientific Research Associates, Inc., April 19, 1993.

[19] American Institute of Aeronautics and Astronautics, *Assessment of Wind Tunnel Data Uncertainty*, AIAA Standard S-071, 1995.

[20] Advisory Group for Aerospace Research and Development, *Assessment of Wind Tunnel Data Uncertainty*, AGARD-AR-304, 1994.

[21] de Jong, F.J., Chan, Y-T., and Gibeling, H.J., "Design of ETO Propulsion Turbine Using CFD Analysis—Final Report," Scientific Research Associates, Inc., Contract No. NAS8-38865, Document No. R95-9084-F, April, 1995.

[22] Hudson, S.T., "Oxidizer Technology Turbine Rig (Model 551) Temperature and Pressure Rake Dynamic Calibration Posttest and Analysis Report," NASA/MSFC memo ED34(96-038), June 11, 1996.

[23] Hudson, S.T., "Oxidizer Technology Turbine Rig (Model 551) Three-hole Probe Calibration Report," MSFC memo ED34-98-0009, January 26, 1998.

[24] International Organization for Standardization, *Guide to the Expression of Uncertainty in Measurement*, ISO, ISBN 92-67-10188-9, 1993.

APPENDIX

Turbine Efficiency Uncertainty Code

```
C     Program Efficiency.FOR  Written February 1998 by Dr. Susan Hudson
C     and modified February 2001 by Boon Liang Heng.
C     This program calculates the uncertainty in turbine efficiency
C     calculated by both the thermodynamic and mechanical methods.
C     All correlation terms are considered.  The program was written
C     for the OTTR Baseline Test performance data.
C
C     DIMENSION ARRAYS
      IMPLICIT REAL*8 (A-H,O-Z)
      DIMENSION P01(720),P02(720),T01(720),T02(720),P2(720),ALPHA2(720)
      DIMENSION UP2(720),UA2(720),BA2A2(720,720)
      DIMENSION BP01A2(720),BP02A2(720),BP2A2(720)
      DIMENSION DP02TH(720),DT02TH(720),DP2TH(720),DA2TH(720)
      DIMENSION DP02P02TH(720,720),DT02T02TH(720,720),DP2P2TH(720,720)

      DIMENSION DA2A2TH(720,720),DP01P02TH(720),DP01P2TH(720)
      DIMENSION DP01A2TH(720),DP02P2TH(720,720),DP02A2TH(720,720)
      DIMENSION DT01T02TH(720),DP2A2TH(720,720)
      DIMENSION DP02ME(720),DP2ME(720),DA2ME(720)
      DIMENSION DP02P02ME(720,720),DP2P2ME(720,720)
      DIMENSION DA2A2ME(720,720),DP01P02ME(720),DP01P2ME(720)
      DIMENSION DP01A2ME(720),DP02P2ME(720,720),DP02A2ME(720,720)
      DIMENSION DP2A2ME(720,720)
      DIMENSION RP01(720),RP02(720),RT01(720),RT02(720),RP2(720)
      DIMENSION RALPHA2(720)
      REAL T01C,T02C,P01C,P02C,RT01C,RT02C,RP01C,RP02C
      REAL BT01C,BT02C,BP01C,BP02C
C
C     OPEN INPUT AND OUTPUT FILES
C
      OPEN(UNIT=10,FILE='effin_720C.TXT',STATUS='UNKNOWN')
      OPEN(UNIT=11,FILE='EFFOUT_720C.TXT',STATUS='UNKNOWN')
C
C     SET STEP SIZE
C
      READ(10,*) H
      WRITE(*,*) H
      WRITE(11,5)
5     FORMAT (1X,' This output is for EFFICIENCY.FOR'/)
```

```
C    CORRECTION DEFINITION FOR PROPERTIES
     T01C = 0.0000001
          T02C = 0.0000001
          P01C = 0.0000001
          P02C = 0.0000001
          BT01C = 0.0
          BT02C = 0.0
          BP01C = 0.0
          BP02C = 0.0
C
C         READ INPUT FILE
C
     READ(10,*) (P01(I),I=1,720)
     READ(10,*) (P02(I),I=1,720)
     READ(10,*) (T01(I),I=1,720)
     READ(10,*) (T02(I),I=1,720)
     READ(10,*) (P2(I),I=1,720)
     READ(10,*) (ALPHA2(I),I=1,720)
          READ(10,*) WDOT,TQ,RPM
          READ(10,*) PP01,BP01,PP02,BP02,PT01,BT01,UT02
          READ(10,*) (UP2(I),I=1,720)
          READ(10,*) (UA2(I),I=1,720)
          READ(10,*) UWDOT,PTQ,BTQ,PRPM,BRPM
          READ(10,*) BP01P01,BP02P02,BT01T01,BT02T02,BP2P2
          READ(10,*) BP01P02,BP01P2,BP02P2,BT01T02
C
C         INITIALIZE ALL CORRELATED BIAS TERMS BETWEEN PRESSURES
C         AND ALPHA2 TO ZERO.  ALSO INITIALIZE BA2A2 ARRAY TO ZERO.
C
          DO 100 I=1,720
            BP01A2(I)=0.0
            BP02A2(I)=0.0
            BP2A2(I)=0.0
            DO 110 J=1,720

          BA2A2(I,J)=0.0
110         CONTINUE
100       CONTINUE
C
C         SINCE BA2A2 IS A 720*720 ARRAY, BUT MOST VALUES ARE ZERO,
C         WILL ASSIGN VALUES HERE RATHER THAN USING INPUT FILE.
C         HAVE ALREADY INITIALIZED ARRAY TO ZERO ABOVE.
C
C         FOR COUNTERS 1 TO 144
          DO I=1,31
            DO J=1,31
              BA2A2(I,J)=0.0
            ENDDO
            DO J=140,144
              BA2A2(I,J)=0.0
            ENDDO
```

```
      ENDDO
      DO I=32,58
        DO J=32,58
          BA2A2(I,J)=0.0
        ENDDO
        DO J=104,130
          BA2A2(I,J)=0.0
        ENDDO
      ENDDO
      DO I=68,103
        DO J=68,103
          BA2A2(I,J)=0.0
        ENDDO
      ENDDO
      DO I=104,130
        DO J=104,130
          BA2A2(I,J)=0.0
        ENDDO
      ENDDO
      DO I=140,144
        DO J=140,144
          BA2A2(I,J)=0.0
        ENDDO
      ENDDO
C     FOR COUNTERS 145 TO 288
      DO I=145,175
        DO J=145,175
          BA2A2(I,J)=0.0
        ENDDO
        DO J=284,288
          BA2A2(I,J)=0.0
        ENDDO
      ENDDO
      DO I=176,202
        DO J=176,202
          BA2A2(I,J)=0.0
        ENDDO
        DO J=248,274
          BA2A2(I,J)=0.0
        ENDDO
      ENDDO
      DO I=212,247
        DO J=212,247
          BA2A2(I,J)=0.0
        ENDDO
      ENDDO
      DO I=248,274
        DO J=248,274
          BA2A2(I,J)=0.0
        ENDDO
      ENDDO
```

```
      DO I=284,288
        DO J=284,288
          BA2A2(I,J)=0.0
        ENDDO
      ENDDO
C     FOR COUNTERS 289 TO 432
      DO I=289,319
        DO J=289,319
          BA2A2(I,J)=0.0
        ENDDO
        DO J=428,432
          BA2A2(I,J)=0.0
        ENDDO
      ENDDO
      DO I=320,346
        DO J=320,346
          BA2A2(I,J)=0.0
        ENDDO
        DO J=392,418
          BA2A2(I,J)=0.0
        ENDDO
      ENDDO
      DO I=356,391
        DO J=356,391
          BA2A2(I,J)=0.0
        ENDDO
      ENDDO
      DO I=392,418
        DO J=392,418
          BA2A2(I,J)=0.0
        ENDDO
      ENDDO
      DO I=428,432
        DO J=428,432
          BA2A2(I,J)=0.0
        ENDDO
      ENDDO
C     FOR COUNTERS 433 TO 576
      DO I=433,463
        DO J=433,463
          BA2A2(I,J)=0.0
        ENDDO
        DO J=572,576
          BA2A2(I,J)=0.0
        ENDDO
      ENDDO
      DO I=464,490
        DO J=464,490
          BA2A2(I,J)=0.0
        ENDDO
        DO J=536,562
```

```
          BA2A2(I,J)=0.0
        ENDDO
      ENDDO
      DO I=500,535
        DO J=500,535
          BA2A2(I,J)=0.0
        ENDDO
      ENDDO
      DO I=536,562
        DO J=536,562
          BA2A2(I,J)=0.0
        ENDDO
      ENDDO
      DO I=572,576
        DO J=572,576
          BA2A2(I,J)=0.0
        ENDDO
      ENDDO
C     FOR COUNTERS 577 TO 720
      DO I=577,607
        DO J=577,607
          BA2A2(I,J)=0.0
        ENDDO
        DO J=716,720
          BA2A2(I,J)=0.0
        ENDDO
      ENDDO
      DO I=608,634
        DO J=608,634
          BA2A2(I,J)=0.0
        ENDDO
        DO J=680,706
          BA2A2(I,J)=0.0
        ENDDO
      ENDDO
      DO I=644,679
        DO J=644,679
          BA2A2(I,J)=0.0
        ENDDO
      ENDDO
      DO I=680,706
        DO J=680,706
          BA2A2(I,J)=0.0
        ENDDO
      ENDDO
      DO I=716,720
        DO J=716,720
          BA2A2(I,J)=0.0
        ENDDO
      ENDDO
```

```
C       CALL SUBROUTINE TO CALCULATE EFFICIENCY
C
        CALL EFF(P01,P02,T01,T02,P2,ALPHA2,WDOT,TQ,RPM,
     &T01C,T02C,P01C,P02C,P01AVG,P02AVG,T01AVG,T02AVG,
     &P2AVG,A2AVG,EFFTH,EFFME)
C
C       WRITE AVERAGE VALUES AND EFFICIENCY INPUT RESULTS TO OUTPUT
C       FILE
C
        WRITE(11,10)
10      FORMAT (1X,'EFFICIENCY RESULTS'/)
        WRITE(11,20)
20      FORMAT (1X,' P01  ',1X,' P02 ',1X,'  T01  ',1X,' T02  ',
        &1X,' WDOT  ',1X,' TQ ',1X,'   RPM  ',1X,'  P2 ',1X'   A2 ')
        WRITE(11,30)
30      FORMAT (1X,'------',1X,'------',1X,'------',1X,'------',
        &1X,'------',1X,'------',1X,'-------',1X'------',1X,'------')
        WRITE(11,40) P01AVG,P02AVG,T01AVG,T02AVG,WDOT,TQ,
        &RPM,P2AVG,A2AVG
40      FORMAT (6(1X,F6.2),1X,F7.2,2(1X,F6.2)/)
C
C       UNCERTAINTY CALCULATIONS
C
C       CALCULATE PARTIAL DERIVATIVES
C
C
C    CONCEPTUAL BIAS DERIVATIVES
C
     RT01C=T01C*(1.-H)
     DEL=RT01C-T01C
     CALL EFF(P01,P02,T01,T02,P2,ALPHA2,WDOT,TQ,RPM,
    &RT01C,T02C,P01C,P02C,P01AVG,P02AVG,T01AVG,T02AVG,
    &P2AVG,A2AVG,EFFTH2,EFFME2)
     RT01C=T01C*(1.+H)
     CALL EFF(P01,P02,T01,T02,P2,ALPHA2,WDOT,TQ,RPM,
    &RT01C,T02C,P01C,P02C,P01AVG,P02AVG,T01AVG,T02AVG,
    &P2AVG,A2AVG,EFFTH1,EFFME1)
     RT01C=T01C
        DT01CTH=(EFFTH2-EFFTH1)/(2.*DEL)
        DT01CME=(EFFME2-EFFME1)/(2.*DEL)

        RT02C=T02C*(1.-H)
     DEL=RT02C-T02C
     CALL EFF(P01,P02,T01,T02,P2,ALPHA2,WDOT,TQ,RPM,
    &T01C,RT02C,P01C,P02C,P01AVG,P02AVG,T01AVG,T02AVG,
    &P2AVG,A2AVG,EFFTH2,EFFME2)
     RT02C=T02C*(1.+H)
     CALL EFF(P01,P02,T01,T02,P2,ALPHA2,WDOT,TQ,RPM,
    &T01C,RT02C,P01C,P02C,P01AVG,P02AVG,T01AVG,T02AVG,
    &P2AVG,A2AVG,EFFTH1,EFFME1)
     RT02C=T02C
```

```
      DT02CTH=(EFFTH2-EFFTH1)/(2.*DEL)
      DT02CME=(EFFME2-EFFME1)/(2.*DEL)

      RP01C=P01C*(1.-H)
     DEL=RP01C-P01C
     CALL EFF(P01,P02,T01,T02,P2,ALPHA2,WDOT,TQ,RPM,
    &T01C,T02C,RP01C,P02C,P01AVG,P02AVG,T01AVG,T02AVG,
    &P2AVG,A2AVG,EFFTH2,EFFME2)
     RP01C=P01C*(1.+H)
     CALL EFF(P01,P02,T01,T02,P2,ALPHA2,WDOT,TQ,RPM,
    &T01C,T02C,RP01C,P02C,P01AVG,P02AVG,T01AVG,T02AVG,
    &P2AVG,A2AVG,EFFTH1,EFFME1)
     RP01C=P01C
      DP01CTH=(EFFTH2-EFFTH1)/(2.*DEL)
      DP01CME=(EFFME2-EFFME1)/(2.*DEL)

      RP02C=P02C*(1.-H)
     DEL=RP02C-P02C
     CALL EFF(P01,P02,T01,T02,P2,ALPHA2,WDOT,TQ,RPM,
    &T01C,T02C,P01C,RP02C,P01AVG,P02AVG,T01AVG,T02AVG,
    &P2AVG,A2AVG,EFFTH2,EFFME2)
     RP02C=P02C*(1.+H)
     CALL EFF(P01,P02,T01,T02,P2,ALPHA2,WDOT,TQ,RPM,
    &T01C,T02C,P01C,RP02C,P01AVG,P02AVG,T01AVG,T02AVG,
    &P2AVG,A2AVG,EFFTH1,EFFME1)
     RP02C=P02C
      DP02CTH=(EFFTH2-EFFTH1)/(2.*DEL)
      DP02CME=(EFFME2-EFFME1)/(2.*DEL)
C
C
C
      DO 112 I=1,720
       RP01(I)=P01(I)
       RT01(I)=T01(I)
       RP02(I)=P02(I)
       RT02(I)=T02(I)
       RP2(I)=P2(I)
       RALPHA2(I)=ALPHA2(I)
112   CONTINUE

     RP01(1)=P01(1)*(1.-H)
      DEL=RP01(1)-P01(1)
      CALL EFF(RP01,P02,T01,T02,P2,ALPHA2,WDOT,TQ,RPM,
    &T01C,T02C,P01C,P02C,P01AVG,P02AVG,T01AVG,T02AVG,
    &P2AVG,A2AVG,EFFTH2,EFFME2)
      RP01(1)=P01(1)*(1.+H)
      CALL EFF(RP01,P02,T01,T02,P2,ALPHA2,WDOT,TQ,RPM,
    &T01C,T02C,P01C,P02C,P01AVG,P02AVG,T01AVG,T02AVG,
    &P2AVG,A2AVG,EFFTH1,EFFME1)
      RP01(1)=P01(1)
      DP01TH=(EFFTH2-EFFTH1)/(2.*DEL)
```

```
      DP01ME=(EFFME2-EFFME1)/(2.*DEL)


      RT01(1)=T01(1)*(1.-H)
      DEL=RT01(1)-T01(1)
      CALL EFF(P01,P02,RT01,T02,P2,ALPHA2,WDOT,TQ,RPM,
&T01C,T02C,P01C,P02C,P01AVG,P02AVG,T01AVG,T02AVG,
&P2AVG,A2AVG,EFFTH2,EFFME2)
      RT01(1)=T01(1)*(1.+H)
      CALL EFF(P01,P02,RT01,T02,P2,ALPHA2,WDOT,TQ,RPM,
&T01C,T02C,P01C,P02C,P01AVG,P02AVG,T01AVG,T02AVG,
&P2AVG,A2AVG,EFFTH1,EFFME1)
      RT01(1)=T01(1)
      DT01TH=(EFFTH2-EFFTH1)/(2.*DEL)
      DT01ME=(EFFME2-EFFME1)/(2.*DEL)

      RWDOT=WDOT*(1.-H)
      DEL=RWDOT-WDOT
      CALL EFF(P01,P02,T01,T02,P2,ALPHA2,RWDOT,TQ,RPM,
      &T01C,T02C,P01C,P02C,P01AVG,P02AVG,T01AVG,T02AVG,
      &P2AVG,A2AVG,EFFTH2,EFFME2)
      RWDOT=WDOT*(1.+H)
      CALL EFF(P01,P02,T01,T02,P2,ALPHA2,RWDOT,TQ,RPM,
      &T01C,T02C,P01C,P02C,P01AVG,P02AVG,T01AVG,T02AVG,
      &P2AVG,A2AVG,EFFTH1,EFFME1)
      RWDOT=WDOT
      DWDOTME=(EFFME2-EFFME1)/(2.0*DEL)

      RTQ=TQ*(1.-H)
      DEL=RTQ-TQ
      CALL EFF(P01,P02,T01,T02,P2,ALPHA2,WDOT,RTQ,RPM,
      &T01C,T02C,P01C,P02C,P01AVG,P02AVG,T01AVG,T02AVG,
      &P2AVG,A2AVG,EFFTH2,EFFME2)
      RTQ=TQ*(1.+H)
      CALL EFF(P01,P02,T01,T02,P2,ALPHA2,WDOT,RTQ,RPM,
      &T01C,T02C,P01C,P02C,P01AVG,P02AVG,T01AVG,T02AVG,
      &P2AVG,A2AVG,EFFTH1,EFFME1)
      RTQ=TQ
      DTQME=(EFFME2-EFFME1)/(2.*DEL)

      RRPM=RPM*(1.-H)
      DEL=RRPM-RPM
      CALL EFF(P01,P02,T01,T02,P2,ALPHA2,WDOT,TQ,RRPM,
      &T01C,T02C,P01C,P02C,P01AVG,P02AVG,T01AVG,T02AVG,
      &P2AVG,A2AVG,EFFTH2,EFFME2)
      RRPM=RPM*(1.+H)
      CALL EFF(P01,P02,T01,T02,P2,ALPHA2,WDOT,TQ,RRPM,
      &T01C,T02C,P01C,P02C,P01AVG,P02AVG,T01AVG,T02AVG,
      &P2AVG,A2AVG,EFFTH1,EFFME1)
      RRPM=RPM
      DRPMME=(EFFME2-EFFME1)/(2.*DEL)
```

```
DO 120 I=1,720

RP02(I)=P02(I)*(1.-H)
DEL=RP02(I)-P02(I)
CALL EFF(P01,RP02,T01,T02,P2,ALPHA2,WDOT,TQ,RPM,
&  T01C,T02C,P01C,P02C,P01AVG,P02AVG,T01AVG,T02AVG,
&  P2AVG,A2AVG,EFFTH2,EFFME2)
RP02(I)=P02(I)*(1.+H)
CALL EFF(P01,RP02,T01,T02,P2,ALPHA2,WDOT,TQ,RPM,
&  T01C,T02C,P01C,P02C,P01AVG,P02AVG,T01AVG,T02AVG,
&  P2AVG,A2AVG,EFFTH1,EFFME1)
RP02(I)=P02(I)
DP02TH(I)=(EFFTH2-EFFTH1)/(2.*DEL)
DP02ME(I)=(EFFME2-EFFME1)/(2.*DEL)

RT02(I)=T02(I)*(1.-H)
DEL=RT02(I)-T02(I)
CALL EFF(P01,P02,T01,RT02,P2,ALPHA2,WDOT,TQ,RPM,
&  T01C,T02C,P01C,P02C,P01AVG,P02AVG,T01AVG,T02AVG,
&  P2AVG,A2AVG,EFFTH2,EFFME2)
RT02(I)=T02(I)*(1.+H)
CALL EFF(P01,P02,T01,RT02,P2,ALPHA2,WDOT,TQ,RPM,
&  T01C,T02C,P01C,P02C,P01AVG,P02AVG,T01AVG,T02AVG,
&  P2AVG,A2AVG,EFFTH1,EFFME1)
RT02(I)=T02(I)
DT02TH(I)=(EFFTH2-EFFTH1)/(2.*DEL)

RP2(I)=P2(I)*(1.-H)
DEL=RP2(I)-P2(I)
CALL EFF(P01,P02,T01,T02,RP2,ALPHA2,WDOT,TQ,RPM,
&  T01C,T02C,P01C,P02C,P01AVG,P02AVG,T01AVG,T02AVG,
&  P2AVG,A2AVG,EFFTH2,EFFME2)
RP2(I)=P2(I)*(1.+H)
CALL EFF(P01,P02,T01,T02,RP2,ALPHA2,WDOT,TQ,RPM,
&  T01C,T02C,P01C,P02C,P01AVG,P02AVG,T01AVG,T02AVG,
&  P2AVG,A2AVG,EFFTH1,EFFME1)
RP2(I)=P2(I)
DP2TH(I)=(EFFTH2-EFFTH1)/(2.*DEL)
DP2ME(I)=(EFFME2-EFFME1)/(2.*DEL)

RALPHA2(I)=ALPHA2(I)*(1.-H)
DEL=RALPHA2(I)-ALPHA2(I)
CALL EFF(P01,P02,T01,T02,P2,RALPHA2,WDOT,TQ,RPM,
&  T01C,T02C,P01C,P02C,P01AVG,P02AVG,T01AVG,T02AVG,
&  P2AVG,A2AVG,EFFTH2,EFFME2)
RALPHA2(I)=ALPHA2(I)*(1.+H)
CALL EFF(P01,P02,T01,T02,P2,RALPHA2,WDOT,TQ,RPM,
&  T01C,T02C,P01C,P02C,P01AVG,P02AVG,T01AVG,T02AVG,
&  P2AVG,A2AVG,EFFTH1,EFFME1)
RALPHA2(I)=ALPHA2(I)
DA2TH(I)=(EFFTH2-EFFTH1)/(2.*DEL)
```

```
      DA2ME(I)=(EFFME2-EFFME1)/(2.*DEL)

120   CONTINUE

      DP01P01TH=DP01TH*DP01TH
      DP01P01ME=DP01ME*DP01ME
      DT01T01TH=DT01TH*DT01TH
      DT01T01ME=DT01ME*DT01ME
C
C   CONCEPTUAL DERIVATIVE SQUARED
C
      DP01CP01CTH=DP01CTH*DP01CTH
      DP01CP01CME=DP01CME*DP01CME
      DP02CP02CTH=DP02CTH*DP02CTH
      DP02CP02CME=DP02CME*DP02CME
      DT01CT01CTH=DT01CTH*DT01CTH
      DT01CT01CME=DT01CME*DT01CME
      DT02CT02CTH=DT02CTH*DT02CTH
      DT02CT02CME=DT02CME*DT02CME
      WRITE(*,*) DP01CP01CTH, DP01CP01CME
C

      DO 130 I=1,719
        DO 140 J=I+1,720
          DP02P02TH(I,J)=DP02TH(I)*DP02TH(J)
          DP02P02ME(I,J)=DP02ME(I)*DP02ME(J)
          DT02T02TH(I,J)=DT02TH(I)*DT02TH(J)
          DP2P2TH(I,J)=DP2TH(I)*DP2TH(J)
          DP2P2ME(I,J)=DP2ME(I)*DP2ME(J)
          DA2A2TH(I,J)=DA2TH(I)*DA2TH(J)
          DA2A2ME(I,J)=DA2ME(I)*DA2ME(J)
140     CONTINUE
130   CONTINUE

      DO 150 I=1,720
        DP01P02TH(I)=DP01TH*DP02TH(I)
        DP01P02ME(I)=DP01ME*DP02ME(I)
        DP01P2TH(I)=DP01TH*DP2TH(I)
        DP01P2ME(I)=DP01ME*DP2ME(I)
        DP01A2TH(I)=DP01TH*DA2TH(I)
        DP01A2ME(I)=DP01ME*DA2ME(I)
        DT01T02TH(I)=DT01TH*DT02TH(I)
        DO 160 J=1,720
          DP02P2TH(I,J)=DP02TH(I)*DP2TH(J)
          DP02P2ME(I,J)=DP02ME(I)*DP2ME(J)
          DP02A2TH(I,J)=DP02TH(I)*DA2TH(J)
          DP02A2ME(I,J)=DP02ME(I)*DA2ME(J)
          DP2A2TH(I,J)=DP2TH(I)*DA2TH(J)
          DP2A2ME(I,J)=DP2ME(I)*DA2ME(J)
160     CONTINUE
150   CONTINUE
```

```
C
C       CALCULATE TERMS FOR EFFICIENCY UNCERTAINTY EQUATION
C
C       THERMODYNAMIC METHOD
C
C       TERMS WITH NO SUMMATIONS
C
        TTH1=720.*(DP01TH*PP01)**2
        TTH3=720.*(DT01TH*PT01)**2
        TTH7=720.*(DP01TH*BP01)**2
        TTH9=720.*(DT01TH*BT01)**2
        TTH13=2.*258121*DP01P01TH*BP01P01
        TTH15=2.*258121*DT01T01TH*BT01T01
C
C   CONCEPTUAL BIAS TERMS
C
        TTH31=1.*(DP01CTH*BP01C)**2
        TTH32=1.*(DP02CTH*BP02C)**2
        TTH33=1.*(DT01CTH*BT01C)**2
        TTH34=1.*(DT02CTH*BT02C)**2
C
C
C       INITIALIZE TERMS WITH SUMMATIONS TO ZERO
C
        TTH2=0.
        TTH410=0.
        TTH511=0.
        TTH612=0.
        TTH8=0.
        TTH19=0.
        TTH20=0.
        TTH21=0.
        TTH24=0.
        TTH14=0.
        TTH16=0.
        TTH17=0.
        TTH18=0.
        TTH22=0.
        TTH23=0.
        TTH25=0.


        DO 170 I=1,720
          TTH2I=(DP02TH(I)*PP02)**2
          TTH410I=(DT02TH(I)*UT02)**2
          TTH511I=(DP2TH(I)*UP2(I))**2
          TTH612I=(DA2TH(I)*UA2(I))**2
          TTH8I=(DP02TH(I)*BP02)**2
          TTH19I=DP01P02TH(I)*BP01P02
          TTH20I=DP01P2TH(I)*BP01P2
          TTH21I=DP01A2TH(I)*BP01A2(I)
```

```
          TTH24I=DT01T02TH(I)*BT01T02
          TTH2=TTH2+TTH2I
          TTH410=TTH410+TTH410I
          TTH511=TTH511+TTH511I
          TTH612=TTH612+TTH612I
          TTH8=TTH8+TTH8I
          TTH19=TTH19+TTH19I
          TTH20=TTH20+TTH20I
          TTH21=TTH21+TTH21I
          TTH24=TTH24+TTH24I
170       CONTINUE
          TTH19=2.*720.*TTH19
          TTH20=2.*720.*TTH20
          TTH21=2.*720.*TTH21
          TTH24=2.*720.*TTH24


          DO 180 I=1,719
           DO 190 J=I+1,720
             TTH14IJ=DP02P02TH(I,J)*BP02P02
             TTH16IJ=DT02T02TH(I,J)*BT02T02
             TTH17IJ=DP2P2TH(I,J)*BP2P2
             TTH18IJ=DA2A2TH(I,J)*BA2A2(I,J)
             TTH14=TTH14+TTH14IJ
             TTH16=TTH16+TTH16IJ
             TTH17=TTH17+TTH17IJ
             TTH18=TTH18+TTH18IJ
190        CONTINUE
180       CONTINUE
          TTH14=2.*TTH14
          TTH16=2.*TTH16
          TTH17=2.*TTH17
          TTH18=2.*TTH18

          DO 200 I=1,720
           DO 210 J=1,720
             TTH22IJ=DP02P2TH(I,J)*BP02P2
             TTH23IJ=DP02A2TH(I,J)*BP02A2(J)
             TTH25IJ=DP2A2TH(I,J)*BP2A2(J)
             TTH22=TTH22+TTH22IJ
             TTH23=TTH23+TTH23IJ
             TTH25=TTH25+TTH25IJ
210        CONTINUE
200       CONTINUE
          TTH22=2.*TTH22
          TTH23=2.*TTH23
          TTH25=2.*TTH25

     UEFFTHSQ=TTH1+TTH3+TTH7+TTH9+TTH13+TTH15+TTH2+TTH410
    &+TTH511+TTH612+TTH8+TTH19+TTH20+TTH21+TTH24+TTH14
    &+TTH16+TTH17+TTH18+TTH22+TTH23+TTH25
```

```
     &+TTH31+TTH32+TTH33+TTH34
          UEFFTH=SQRT(UEFFTHSQ)

C
C         MECHANICAL METHOD
C
C         TERMS WITHOUT SUMMATIONS
C
          TME1=720.*(DP01ME*PP01)**2
          TME3=720.*(DT01ME*PT01)**2
          TME7=(DTQME*PTQ)**2
          TME8=(DRPMME*PRPM)**2
          TME9=720.*(DP01ME*BP01)**2
          TME11=720.*(DT01ME*BT01)**2
          TME15=(DTQME*BTQ)**2
          TME16=(DRPMME*BRPM)**2
          TME614=(DWDOTME*UWDOT)**2
          TME17=2.*258121*DP01P01ME*BP01P01
          TME19=2.*258121*DT01T01ME*BT01T01
C
C    CONCEPTUAL BIAS TERMS
C
          TME31=1.*(DP01CME*BP01C)**2
          TME32=1.*(DP02CME*BP02C)**2
          TME33=1.*(DT01CME*BT01C)**2
C
C
C         INITIALIZE TERMS WITH SUMMATIONS TO ZERO
C
          TME2=0.
          TME412=0.
          TME513=0.
          TME10=0.
          TME22=0.
          TME23=0.
          TME24=0.
          TME18=0.
          TME20=0.
          TME21=0.
          TME25=0.
          TME26=0.
          TME27=0.

          DO 220 I=1,720
            TME2I=(DP02ME(I)*PP02)**2
            TME412I=(DP2ME(I)*UP2(I))**2
            TME513I=(DA2ME(I)*UA2(I))**2
            TME10I=(DP02ME(I)*BP02)**2
            TME22I=DP01P02ME(I)*BP01P02
            TME23I=DP01P2ME(I)*BP01P2
            TME24I=DP01A2ME(I)*BP01A2(I)
```

```
          TME2=TME2+TME2I
          TME412=TME412+TME412I
          TME513=TME513+TME513I
          TME10=TME10+TME10I
          TME22=TME22+TME22I
          TME23=TME23+TME23I
          TME24=TME24+TME24I
220       CONTINUE
          TME22=2.*720.*TME22
          TME23=2.*720.*TME23
          TME24=2.*720.*TME24

          DO 230 I=1,719
            DO 240 J=I+1,720
              TME18IJ=DP02P02ME(I,J)*BP02P02
              TME20IJ=DP2P2ME(I,J)*BP2P2
              TME21IJ=DA2A2ME(I,J)*BA2A2(I,J)
              TME18=TME18+TME18IJ
              TME20=TME20+TME20IJ
              TME21=TME21+TME21IJ
240         CONTINUE
230       CONTINUE
          TME18=2.*TME18
          TME20=2.*TME20
          TME21=2.*TME21

          DO 250 I=1,720
            DO 260 J=1,720
              TME25IJ=DP02P2ME(I,J)*BP02P2
              TME26IJ=DP02A2ME(I,J)*BP02A2(J)
              TME27IJ=DP2A2ME(I,J)*BP2A2(J)
              TME25=TME25+TME25IJ
              TME26=TME26+TME26IJ
              TME27=TME27+TME27IJ
260         CONTINUE
250       CONTINUE
          TME25=2.*TME25
          TME26=2.*TME26
          TME27=2.*TME27

          UEFFMESQ=TME1+TME3+TME7+TME8+TME9+TME11+TME15
     &+TME16+TME614+TME17+TME19+TME2+TME412
     &+TME513+TME10+TME22+TME23+TME24+TME18+TME20
     &+TME21+TME25+TME26+TME27+TME31+TME32+TME33
          UEFFME=SQRT(UEFFMESQ)

C
C         WRITE EFFICIENCY AND UNCERTAINTY RESULTS TO OUTPUT FILE
C
          WRITE(11,50)
50        FORMAT (1X,'EFFTH ',1X,'UEFFTH',1X,'EFFME ',1X,'UEFFME')
```

```
      WRITE(11,60)
60    FORMAT (4(1X,'------'))
      WRITE(11,70) EFFTH,UEFFTH,EFFME,UEFFME
70    FORMAT (4(1X,F6.4)/)
      WRITE(11,80) TTH1,TTH2,TTH3,TTH7,TTH8,TTH9,TTH410,TTH511,TTH612,
     &TTH13,TTH14,TTH15,TTH16,TTH17,TTH18,TTH19,TTH20,TTH21,TTH22,
     &TTH23,TTH24,TTH25,TTH31,TTH32,TTH33,TTH34
80    FORMAT (1X,'TTH TERMS',/,22(1X,E11.5,/))
      WRITE(11,90) TME1,TME2,TME3,TME7,TME8,TME9,TME10,TME11,
     &TME412,TME513,TME614,TME15,TME16,TME17,TME18,TME19,TME20,
     &TME21,TME22,TME23,TME24,TME25,TME26,TME27,TME31,TME32,
     &TME33
90    FORMAT(1X,'TME TERMS',/,24(1X,E11.5,/))
    END

C
C     SUBROUTINE TO CALCULATE EFFICIENCY
C
      SUBROUTINE EFF(P01,P02,T01,T02,P2,ALPHA2,WDOT,TQ,RPM,
     &T01C,T02C,P01C,P02C,P01AVG,P02AVG,T01AVG,T02AVG,P2AVG,
     &A2AVG,EFFTH,EFFME)
      IMPLICIT REAL*8 (A-H,O-Z)
      DIMENSION P01(720),P02(720),T01(720),T02(720),P2(720),
     &ALPHA2(720),W(720),SPP(720),SPT(720),SPP2(720),SPA2(720)
      REAL MACH
      REAL T01C,T02C,P01C,P02C
C
C
C     DEFINE CONSTANTS
      PI=3.141593
      GAM=1.4
      CONK=PI/30.
      CONJ=778.3
      CONCP=0.24
      R=53.35
      GC=32.174
C
C     INITIALIZE SUMS FOR INLET AREA AVERAGES TO ZERO
      SUMP011=0.0
      SUMP012=0.0
      SUMP013=0.0
      SUMP014=0.0
      SUMP015=0.0
      SUMT011=0.0
      SUMT012=0.0
      SUMT013=0.0
      SUMT014=0.0
      SUMT015=0.0
C
C     CALCULATE TURBINE INLET AREA AVERAGE VALUES
      DO 10 I=1,144
```

```
      SUMP011=SUMP011+P01(I)

      SUMT011=SUMT011+T01(I)
10    CONTINUE
      SUMP011=SUMP011/144.
      SUMT011=SUMT011/144.
      DO 20 I=145,288

      SUMP012=SUMP012+P01(I)

      SUMT012=SUMT012+T01(I)
20    CONTINUE
      SUMP012=SUMP012/144.
      SUMT012=SUMT012/144.
      DO 30 I=289,432

      SUMP013=SUMP013+P01(I)

      SUMT013=SUMT013+T01(I)
30    CONTINUE
      SUMP013=SUMP013/144.
      SUMT013=SUMT013/144.
      DO 40 I=433,576

      SUMP014=SUMP014+P01(I)

      SUMT014=SUMT014+T01(I)
40    CONTINUE
      SUMP014=SUMP014/144.
      SUMT014=SUMT014/144.
      DO 50 I=577,720

      SUMP015=SUMP015+P01(I)

      SUMT015=SUMT015+T01(I)
50    CONTINUE
      SUMP015=SUMP015/144.
      SUMT015=SUMT015/144.
      P01AVG=(SUMP011+SUMP012+SUMP013+SUMP014+SUMP015)/5.
      T01AVG=(SUMT011+SUMT012+SUMT013+SUMT014+SUMT015)/5.
C
C     CALCULATE TURBINE EXIT MASS AVERAGE VALUES
      WTOTAL=0.0
      DO 60 I=1,720
        TERM1=((P02(I)/P2(I))**((GAM-1.)/GAM))-1.
        MACH=SQRT((2./(GAM-1.))*TERM1)
        B=1.+((GAM-1.)/2.)*MACH**2
        TERM2=0.0545*COS(ALPHA2(I)*PI/180.)*P02(I)
        TERM3=SQRT((GC*GAM)/(R*T02(I)))
        W(I)=TERM2*TERM3*MACH*B**((GAM+1.)/(2.*(1.-GAM)))
```

```
        WTOTAL=WTOTAL+W(I)
60      CONTINUE
        DO 70 I=1,720
          SPP(I)=0.
          SPT(I)=0.
          SPP2(I)=0.
          SPA2(I)=0.
70      CONTINUE

        DO 80 I=1,720
        SPP(I)=P02(I)*W(I)
        SPT(I)=T02(I)*W(I)
          SPP2(I)=P2(I)*W(I)
          SPA2(I)=ALPHA2(I)*W(I)
80      CONTINUE
        SPPTOTAL=0.
        SPTTOTAL=0.
        SPP2TOTAL=0.
        SPA2TOTAL=0.
        DO 90 I=1,720
          SPPTOTAL=SPPTOTAL+SPP(I)
          SPTTOTAL=SPTTOTAL+SPT(I)
          SPP2TOTAL=SPP2TOTAL+SPP2(I)
          SPA2TOTAL=SPA2TOTAL+SPA2(I)
90      CONTINUE
        P02AVG=SPPTOTAL/WTOTAL
        T02AVG=SPTTOTAL/WTOTAL
        P2AVG=SPP2TOTAL/WTOTAL
        A2AVG=SPA2TOTAL/WTOTAL
C
C       CALCULATE EFFICIENCY
        PTERM=1.-(((P02AVG+P02C)/(P01AVG+P01C))**((GAM-1.)/GAM))
        ETHNUM=((T01AVG+T01C)-(T02AVG+T02C))
        ETHDEN=(T01AVG+T01C)*PTERM
        EFFTH=ETHNUM/ETHDEN
        EMENUM=CONK*TQ*RPM
        EMEDEN=CONJ*CONCP*WDOT*(T01AVG+T01C)*PTERM
        EFFME=EMENUM/EMEDEN
C
        RETURN
        END
```